Optimization of a cross-reactivity-free proteomic platform toward neurological biomarker analysis

Woo Jong Rho

Department of Biomedical Engineering

Integrated Program in Neuroscience

McGill University

Montreal, Canada

February 2020

A thesis submitted to McGill University in partial fulfillment

of the requirements of the degree of

Master of Science

Table of Contents

List of Figures

List of Tables

Acknowledgments

I would like to thank everyone who has contributed to this thesis. First and foremost, I would like to thank my MSc supervisor, Prof. David Juncker, who has given me the opportunity to work in his lab. Having graduated from an undergraduate degree in Biochemistry, I entered his lab without any knowledge of technology development for biomedical applications, but I was encouraged to push my boundaries and learn all that I could about new topics and ideas and become proud of what I was able to accomplish. Thank you for your support, guidance, and feedback, David—it broadened my perspective of academic research and gave me clarity as to what I would like to pursue in the future.

Secondly, I would like to thank Dr. Andy Ng for his enduring support since the beginning of my project, which persisted all the way through to the editing process of the written document itself. Andy was an essential pillar in the lab who assisted me in brainstorming and developing new ideas, analyzing data, answering general lab-life and administrative questions, as well as offering feedback whenever I required.

I would also like to thank the CLAMP team in the DJ Group: Milad Dagher, Jeff Munzar, Jinglin Kong, and Arya Tavakoli. You all supported me throughout the entirety of my thesis, offered me your friendship, and were always willing to lend a helping hand for experimental planning, operation, and analysis. You have helped me to mature my thinking process and develop my skills for generating new ideas and critically analyzing research, and for that I am extremely grateful. I would also like to give a special thank-you to Dr. Jeff Munzar for his remarkable assistance during my writing period. Despite being incredibly busy with an infinite list of To-Do's, you always made time to help me when I needed it. Thank you very so much for making me a priority during those difficult times!

Along with David, Andy, and the CLAMP team, I would like to deeply thank the other members of the DJ Group for their help, support, and friendship over the years. Special thanks to Edward, Alia, Rosalie, Molly, and Zijie—thank you for all the laughs, new ideas, and good food over the last few years.

I would like to acknowledge the support from the Natural Sciences and Engineering Research Council of Canada (NSERC) which funded part of the research presented in this thesis. I would also like to acknowledge the Max E. Binz Fellowship awarded by the Faculty of Medicine that also helped to financially support me during the course of my MSc.

Finally, I would like to give a huge thank-you to my friends and family: to my father, for teaching me the concept of scientific thinking and what it means to be curious from such an early age; to my mother and brother, for their continued support through every chapter in my life; to Kieran, Will, and Cody, for always lending an ear and keeping me sane during the hard times (Who's Sildar again? – FR); and finally, to Jaclyn, for her everlasting support during all stages of my thesis and my life beyond, as well as her huge contributions during the stressful writing and editing process.

Contribution of Authors

Some experiments reported in this thesis were assisted by several members of the CLAMP team in the Juncker lab.

The experiments for “4.1.1 | DNA and Antibody Sticking” were planned, performed, and analyzed by Woo Jong Rho. The optimization of the hook oligo for this set of experiments received assistance from Dr. Andy Ng and Dr. Jeffrey Munzar.

The experiments for “4.1.2 | Effects of Prolonged Cold Storage” were planned, performed, and analyzed by Woo Jong Rho.

The experiments for “4.2 | Assay Parameter Optimizations” were planned by Woo Jong Rho, Dr. Jinglin Kong, and Dr. Milad Dagher; performed by Woo Jong Rho and Dr. Jinglin Kong; and analyzed by Woo Jong Rho and Dr. Jinglin Kong.

Finally, the experiments for “4.3 | Optimizing Analysis of Complex Samples” were planned by Woo Jong Rho, Dr. Jinglin Kong, and Dr. Milad Dagher; performed by Woo Jong Rho, Dr. Jinglin Kong, and Dr. Milad Dagher; and analyzed by Woo Jong Rho, Dr. Jinglin Kong, and Dr. Milad Dagher.

Abstract

Proteins are macromolecules that are essential to many biological processes, and the pivotal role of proteins as effectors in the cellular environment makes them central to understanding human disease. For example, some of the most common neurological diseases, including Alzheimer's disease, Parkinson's disease, and multiple sclerosis, are believed to be mediated by dysregulated and/or mutated proteins. As such, the measurement of proteins, and indeed the development of protein-based biomarkers, holds great promise for the diagnosis, monitoring, and treatment of neurological diseases. Unfortunately, current gold standard techniques for protein analysis, namely sandwich immunoassays (*i.e.* ELISA) and mass spectrometry, suffer from a distinct tradeoff between sensitivity and multiplexing. Due to this, immunoassays are largely limited to measuring proteins one-at-a-time, while mass spectrometry may lack sensitivity to measure lowly abundant proteins. As such, the development of new technologies that can profile many proteins sensitively in a single sample, ideally at low cost, could transform the state of neurological biomarker discovery. Recently, a new format of sandwich immunoassay was developed in our lab for the measurement of multiple proteins in a single assay, termed the Colocalization-by-Linkage Assay on MicroParticles (CLAMP). The CLAMP platform utilizes DNA oligonucleotides as antibody tethers to colocalize antibody pairs on single microparticles (MPs) prior to antigen capture. This design enables ELISA-like performance without the possibly of mismatched antibody pairs interacting, and hence eliminating antibody cross-reactivity. Previously, CLAMP was optimized for non-physiological buffers. However, the optimization of the CLAMP platform for profiling neurological samples remains to be established.

Here, the CLAMP platform was optimized to accurately measure proteins in relevant clinical samples. Successive optimization strategies were pursued, including optimizing (1) CLAMP fabrication and assay workflows to minimize non-specific binding of CLAMP constituents, (2) the antibody-DNA ratio in conjugation, DNA density on the MP surface, and the duration of sample incubation to ensure a high fluorescent signal whilst minimizing background, and (3) a buffer that sufficiently imitates the complexity of blood plasma so as to generate accurate standard curves for sample analysis. First, non-specific binding events were minimized by testing the effects of DNA and antibody sticking on the MP surface during various stages of CLAMP fabrication. Following this, the effect of long-term storage on the stability and non-specific binding of CLAMPs was

tested. Second, the antibody-oligonucleotide conjugation ratio, surface densities of CLAMP components, and duration of sample incubation were optimized for low background signal and maximal fluorescent signal. This was done by first creating antibody-oligo conjugates with varying levels of oligos to produce antibody conjugates with low, medium, and high valency of oligonucleotides. Afterwards, CLAMPs were fabricated with varying levels of DNA on the surface and antibody-oligo conjugate valencies, in which the performance of the CLAMPs were tested with replicated standard curves. Lastly, a suitable buffer that imitated the complexity of human plasma sample matrix, termed a mimic buffer, was developed and validated using spike-in and recovery testing. This optimization facilitated the CLAMP platform to be fit-for-purpose for the accurate measurement of blood plasma samples. Building on the impact that other high throughput protein measurement platforms have had on neuroscience, the optimized CLAMP platform developed here may help expedite neurological biomarker discovery and validation, and thereby increase the number of promising candidate neurological biomarkers that make it the approval stage and ultimately into the clinic.

Résumé

Les protéines sont des macromolécules indispensables au bon fonctionnement de nombreux processus biologiques. En tant que principales effectrices de l'environnement cellulaire, elles sont essentielles pour comprendre les maladies humaines. Par exemple, certaines des maladies neurologiques les plus communes, dont la maladie d'Alzheimer, la maladie de Parkinson et la sclérose en plaques, seraient liées à des protéines dérégulées ou mutées. De ce fait, la mesure des protéines et le développement de biomarqueurs protéiques sont très prometteurs pour le diagnostic, le suivi et le traitement des maladies neurologiques. Malheureusement, les techniques de référence pour l'analyse des protéines, à savoir les immunoessais en sandwich (ELISA) et la spectrométrie de masse, doivent composer avec un important compromis entre sensibilité et multiplexage. Pour cette raison, les immunoessais ne peuvent généralement mesurer qu'une seule protéine à la fois, tandis que la spectrométrie de masse peut s'avérer insuffisamment sensible pour mesurer les protéines les moins abondantes. Ainsi, le développement de nouvelles technologies pouvant mesurer de nombreuses protéines dans un même échantillon, avec une sensibilité élevée et idéalement à faible coût, pourrait transformer le paysage de la recherche de biomarqueurs neurologiques. Récemment, une nouvelle implémentation de l'immunoessai en sandwich, nommée Essai de Colocalisation par Liaison sur Microparticules (*Colocalization-by-Linkage Assay on MicroParticles, CLAMP*) a été développée par notre laboratoire afin de mesurer de nombreuses protéines en un seul test. CLAMP repose sur l'utilisation d'oligonucléotides d'ADN comme ancrages, de sorte que les paires d'anticorps soient colocalisées à la surface des microparticules (MPs) lors de la détection des antigènes. Ce concept permet de récapituler la performance des immunoessais de type ELISA tout en éliminant l'interaction entre anticorps dépareillés, minimisant ainsi les problèmes de réactivité croisée. Précédemment, CLAMP a été optimisé pour usage avec des tampons non physiologiques. Cependant, l'utilisation de CLAMP pour mesurer des échantillons neurologiques reste à établir.

Nous présentons ici l'optimisation de CLAMP afin de mesurer précisément les protéines d'échantillons cliniques pertinents. Plusieurs stratégies d'optimisation ont été explorées successivement, dont l'optimisation (1) du processus de fabrication et du protocole d'utilisation de CLAMP pour minimiser les interactions non spécifiques entre les éléments constitutifs de la plateforme; (2) du ratio entre les quantités d'anticorps et d'ADN utilisées lors de la conjugaison,

de la densité d'ADN à la surface des MPs et du le temps d'incubation requis pour obtenir un signal fluorescent élevé tout en minimisant le bruit de fond; et (3) d'une solution tampon récapitulant de manière suffisante la complexité du plasma sanguin afin de générer des courbes d'étalonnage précises pour l'analyse d'échantillons. Tout d'abord, pour minimiser les événements de liaison non spécifiques, l'adhérence de l'ADN et des anticorps à la surface des MPs a été testée au cours des différentes étapes de fabrication de CLAMP. Ensuite, le ratio entre les quantités d'anticorps et d'oligonucléotides utilisées lors de la conjugaison, la densité de surface des composantes de CLAMP, et le temps d'incubation de l'échantillon ont été optimisés pour minimiser le bruit de fond et maximiser le signal fluorescent. Pour ce faire, des conjugués anticorps-oligo ont d'abord été créés en utilisant des quantités variables d'oligos afin de produire des conjugués comprenant une valence d'oligonuclétides faible, moyenne ou élevée. Par la suite, plusieurs versions de CLAMP incorporant des variations dans la quantité d'ADN superficiel et la valence des conjugués anticorps-oligo ont été fabriquées, puis testées pour leur performance à l'aide de courbes d'échantillonnage répliquées. Enfin, une solution tampon simulant la complexité de la matrice biologique d'un échantillon de plasma humain, nommée tampon mimétique, a été développée et validée au moyen de tests d'inoculation et de récupération. Ce processus d'optimisation a facilité l'adaptation de la plateforme CLAMP à l'usage prévu de mesure précise d'échantillons de plasma sanguin. Étant donné l'impact que d'autres modalités de mesure de protéines à grande capacité ont eu sur les neurosciences, la plateforme CLAMP optimisée ici a le potentiel d'accélérer la découverte et la validation de biomarqueurs neurologiques, augmentant de ce fait le nombre de marqueurs candidats prometteurs se rendant aux stades d'approbation et d'usage en clinique.

1 | Introduction

1.1 Background

Proteins are macromolecules essential for the regulation of biological pathways such as the cell cycle, DNA replication, cellular signaling, molecular transportation, and structural support. In many pathologies, subsets of proteins are deregulated, thereby significantly altering their effective concentrations from an individual's normal levels[1]. This deregulation makes proteins very useful as measurable molecular targets, or *biomarkers*, for clinicians to determine the disease status of a patient. Biomarker detection must be highly accurate and reliable to be useful in the understanding of disease onset and progression[2]. Existing biomarkers such as MUC-1 and carcinoembryonic antigen (CEA) are examples of protein-based biomarkers that have been approved by the Food and Drug Administration (FDA) for the monitoring and treatment of breast cancer[3].

Protein-based biomarkers can offer real-time analysis of a patient's disease state. This aspect is missing in genomic-based analyses since genes cannot report when the disease is active or will become active. Especially in diseases which have overlapping phenotypes, the measurement of protein-based biomarkers can reduce the time spent on diagnosis and speed up treatment plans. For example, kidney diseases can be very difficult to detect and diagnose, and because most people have two kidneys, the healthy one could make up any defiencies the other may have. However, this results in the impaired kidney accumulating the damage unnoticed. Furthermore, certain types of kidney disease, such as acute intestinal nephritis, require a biopsy for accurate diagnosis, an invasive technique which may result in further complications. Thus, the measurement of protein-based biomarkers can aide existing methods to expedite and simplify the process of disease detection and diagnosis[4].

With regards to the role of proteins as biomarkers in neuroscience, many neurological diseases include the inflammation of nervous tissue (neuroinflammation) and the degeneration of cells in the brain (neurodegeneration)[5-7]. Sharing these similar mechanisms, the cell types and inflammatory mediators that regulate these processes can be mutual between many of the diseases, however the outcome of these pathways can vary significantly resulting in ambiguity of which biomarkers are indicative of disease[7, 8]. Due to the vast number of proteins belonging to these processes, substantial focus has been placed on measuring many proteins simultaneously

(multiplexing) to rapidly determine which of them can be used as clinical biomarkers for their respective diseases.

Currently, protein biomarkers are expected to play a core role in the broader push for precision medicine to better assess a patient's health status. Precision medicine is a model of health care that considers individual variability in genetics and environment. The objective of precision medicine is to identify the best treatment for each patient, *i.e.* the treatment that will maximize efficacy while minimizing adverse side effects (**Fig. 1.1-1**)[3]. Whereas our current medical system predominantly utilizes a "one-size-fits-all" approach, ideally an individual's unique background would be considered when selecting a course of treatment. To establish a better system of health care, efforts are underway to shift our clinical paradigms toward precision medicine.

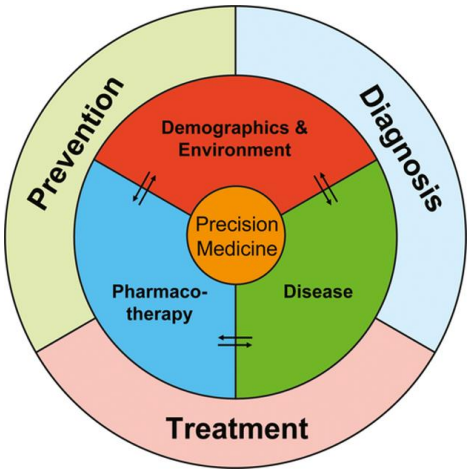

Figure 1.1 | Factors encompassing precision medicine. Precision medicine aims to cover all the different phases of health care: prevention, diagnosis, and treatment. Furthermore, precision medicine aims to tailor treatment to the patient, in which the factors that differentiate the patients with the same disease are categorized into three categories: demographics and environment, which include age, sex, lifestyle, and ethnicity; pharmacotherapy, which involves the variables that influence the drug's efficacy and safety for the patient; and disease, which includes the patient's individual differences in their biological disease processes, typically involving both genomics and proteomics. Reproduced from ref.[9] with permission from the John Wiley and Sons, copyright 2019.

A precision medicine approach might be particularly beneficial to the treatment of neurological diseases to generate unique health profiles of the patients. These profiles can be used to expedite early diagnosis, establish an accurate prognosis, and to tailor an effective treatment plan to the

individual's unique background. In neurological diseases and disorders, such as major depressive disorder, there are often many drugs prescribed to the patient to control the symptoms of their disease. However, there currently lacks a method to stratify which patient will respond best to a given drug, neglecting to account many factors that are individually variable, and thus resulting in the patient consuming drugs that may have poor efficacy and adverse side effects[10]. Furthermore, neurodegenerative disorders, such as Parkinson's Disease, can present variable clinical features amongst patients with the same disease. Due to this, the traditional "one-size-fits-all" approach of prescribing drugs is unlikely to work, in which the prescribed medicine may result in adverse side effects, further disabling the patient. In this context, the development of a precision medicine approach can greatly benefit the current model of health care by aiding the identification of the preclinical stages of disease, making differential diagnoses, and providing optimal treatments at a timely manner. Furthermore, the precision medicine approach has potential to provide these treatments earlier on, as opposed to current treatments which are typically applied at the later stages of disease[11].

However, very few biomarkers have been approved by the Food and Drug Administration (FDA) for neurological applications to date. Currently, the path from biomarker discovery and validation to FDA approval is very time-consuming, laborious, and costly due to the requirement of reproducibility, superior clinical significance of existing biomarkers, and extensive clinical trials[12]. Failure of a candidate biomarker to achieve FDA-approval can be attributed to one of three reasons, highlighted in **Figure 1.2**. First, in rare cases, candidate biomarkers may have emerged from fraudulent data. Second, candidate biomarkers that have been appropriately validated may fail to provide useful information to clinicians or have insufficient predicative ability. Lastly, candidate biomarkers that initially seemed promising may have shortcomings during discovery or validation stages, thereby eliminating them from further consideration[13]. While major investments have been made from both academia and industry, approximately only 115 unique proteins, excluding autoantibodies and posttranslational modifications, have been approved to date, with 1.5 new proteins projected to be added each year[14, 15].

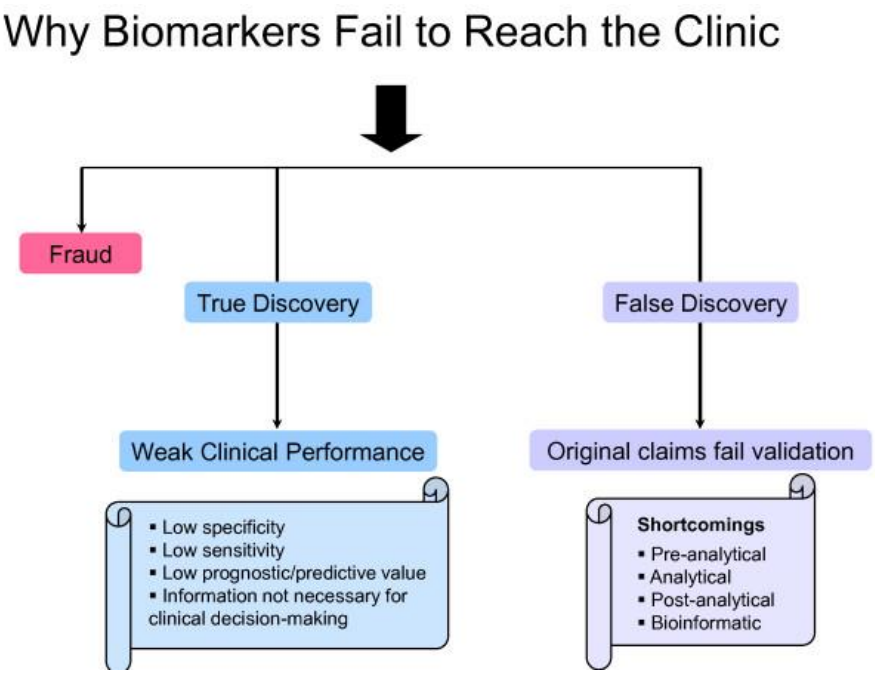

Figure 1.2 | Summary of biomarker failure to reach clinical settings. Candidate biomarkers under the "Fraud" category fail due to being reported in fraudulent findings. "True Discovery" biomarkers typically completed their discovery and validation stages but fail from their lack of clinical significance. Finally, "false discovery" biomarkers were thought to be promising initially, however failed the discovery or validation stage, resulting in their failure. Reproduced from ref. [13] under CC BY 2.0.

A platform for protein measurement that is affordable, multiplexable, with gold standard sensitivity would expedite the process of biomarker discovery and validation to advance candidate proteins to the approval stage more readily. This platform could greatly transform current methods of neurological health care, by supplementing current diagnostic tests with rich additional information about the patient. In the case of unsatisfactory candidate markers, more sensitive and accurate protein measurement technologies could help researchers to detect poor target viability earlier on in the discovery process, reducing the amount of time and resources lost. On the other hand, if the candidate biomarker is found to have sufficient performance, both the discovery and validation phases could be conducted more rapidly and with higher reproducibility, thereby speeding up the process towards the approval stage. However, current platforms for protein measurement are not fully equipped for reliable and cost-effective establishment of a panel of candidate biomarkers.

Commercially available methods of protein detection are often hindered by two key challenges as they attempt to measure their intended target(s). The first challenge is sustaining high analytical sensitivity when measuring low abundance proteins in complex samples such as blood plasma. Since many candidate biomarkers are only present at very low concentrations, the method of protein measurement must have a sufficient limit of detection to measure the target quantitatively. Additionally, complex samples with extremely high total protein concentrations can confound the detection of the protein target due to conserved domains across protein families[16-18]. In fact, due to the low analytical sensitivity of most existing methods of protein measurement, it is estimated that only 10% of proteins in blood plasma have been quantified[19]. Typically, enzyme-linked immunosorbent assays (ELISAs), the current gold standard for protein measurement, work well to deliver high sensitivity in single protein measurements. Challenges of sensitivity for various immunoassay technologies, and for different sample types, are discussed in more detail in **Chapter 2.3.1.**

The second challenge involves developing the protein measurement tool to be compatible with multiplexing. Mass Spectrometry can simultaneously measure many proteins at once; however, it has lower analytical sensitivity compared to the ELISA. For clinical applications or biomedical research, mass spectrometry can prove inadequate for the measurement of low abundance proteins. For sandwich immunoassays, like ELISAs, multiplexed measurements are constrained by cross-reactivity that hinder its reproducibility and accuracy[2]. Multiplexed sandwich assays (MSAs) thus require complex optimizations to increase the number of targets that can be simultaneously measured, although this complicates the feasibility of their development. Cross-reactivity will be further discussed in **Chapter 2.3.2**, detailing scenarios of how cross-reactivity affects different assay formats.

In an effort to develop a technology that satisfies the dual challenge of being sensitive and multiplexable, an emerging platform was recently conceived to achieve ELISA-level sensitivity and multiplex compatibility without sacrificing either, termed the Colocalization-by-Linkage Assay on MicroParticles (CLAMP) platform. Briefly, the CLAMP platform overcomes cross-reactivity from multiplexing by eliminating the possible interactions between different target affinity binders. In typical MSAs, when detection antibodies are mixed in the solution, the number of possible cross-reactivity events increases exponentially with the number of protein targets. The

CLAMP platform physically separates the detection antibodies for each protein target by colocalizing it onto the microparticle (MP), which effectively makes each CLAMP analogous to a single ELISA (**Fig. 1.3**). This design facilitates the measurement of many protein targets by allocating a specific CLAMP to each target and mixing them together in a single sample. The CLAMP platform is described in more detail in **Chapter 2.5.2.5**.

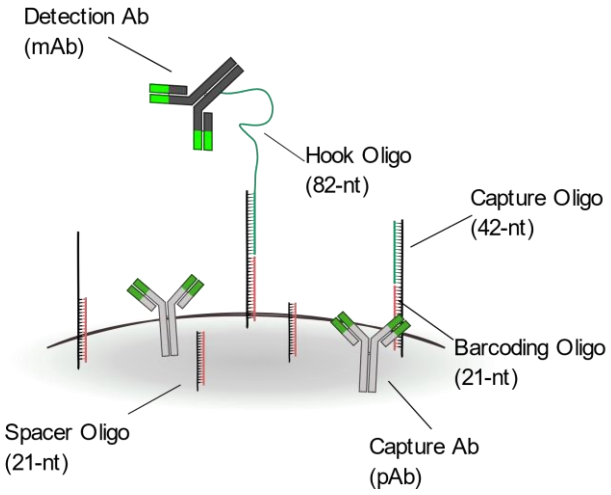

Figure 1.3 | CLAMP Composition. Polyclonal biotinylated capture antibodies (light gray), biotinylated capture oligos, and spacer oligos are immobilized onto the MP surface via biotin-streptavidin interactions. The spacer oligo lacks the sequence to bind to the hook oligo, functioning only to barcode the bead and control the density of capture oligos on the surface. A monoclonal detection antibody (dark gray) is tethered onto the hook oligo and is bound to the bead with hybridization onto the capture oligo. Lastly, the barcoding oligos binds complementarily to the capture and spacer oligos to create the unique fluorescent emission spectra for each CLAMP target. Reproduced from ref. [20] with permission from author, copyright 2018.

1.2 Thesis Objectives

Previous experiments have demonstrated the advantages of the CLAMP platform, especially the ability of CLAMP to overcome cross-reactivity. In order to further improve the performance of the CLAMP platform, including sensitivity, precision, and reproducibility, optimization of CLAMP fabrication and of the assay workflow were required.

The goal of this thesis was to further optimize the CLAMP platform so as to make it suitable for use with clinical samples and larger scale biomarker discovery efforts. The main challenges that were overcome included: (a) designing CLAMPs with maximized signal generation, whilst also minimizing background signal; (b) fine-tuning the duration of sample incubation during CLAMP assays to reduce non-specific binding events from the DNA, antibodies, or that could potentially generate false positive signals; and (c) identifying an accurate mimic buffer to imitate the unique background signal of blood plasma, and thereby make CLAMP amenable to testing clinical samples.

First, the CLAMP fabrication protocol was optimized. This included optimizing (A) the conditions for the conjugation of the hook oligo to the detection antibody, (B) the density of oligonucleotides (oligos) and capture antibodies on the MP surface, and (C) the concentration of the tethered antibodies to be pulled-down onto the MP surface. These optimizations were performed to ensure the different target CLAMPs were resource-efficient in their fabrication, had minimal potential to generate false positive signals, and generate a high detectable signal while minimizing background.

Second, the various aspects of the assay procedure were optimized. This included optimizing (A) any DNA or antibody sticking effects from the CLAMP constituents, (B) the storage conditions of the CLAMP, and (C) the duration of sample incubation. These optimizations were essential to minimize the effects of any DNA-, protein-, or antibody-sticking from the constituents of the CLAMPs or of the sample. These optimizations were accomplished so that the CLAMP platform could be further scaled up to accommodate an increased pool of targets.

Lastly, to achieve compatibility with patient samples, the ability to mimic the properties of complex sample matrices, such as blood and CSF, was necessary. To optimize a mimic buffer specifically for blood plasma, many candidate buffers were first screened according to their background signal and compared to diluted human blood plasma. Upon isolating the buffer compositions that most closely matched the blood plasma, the buffers were tested for their accuracy to the blood plasma through spike-in and recovery experiments, in which the buffer closest to 100% was selected. Identification of a suitable mimic buffer is necessary to generate the standard curves that will be the basis for patient sample quantification, a critical step in accurate protein measurement.

1.3 Thesis Outline

Chapter 2 presents a review of the literature that describes the potential application of MSAs in neuroscience, common methods of protein measurement, how cross-reactivity behaves in different immunoassay formats, and the technological advances in protein immunoassays that overcome the current limits of sensitivity and cross-reactivity.

Chapter 3 presents the materials and methods section which will outline the fabrication process and assay workflow of the CLAMP platform. Furthermore, details of optimizing the following parameters will be described: (A) DNA- and antibody-sticking, (B) prolonged cold storage, (C) CLAMP assay and fabrication workflows, and (D) mimic buffer for human blood plasma.

Chapter 4 presents the results section which will show the outcomes of the optimizations described in the materials and methods section. Briefly, bar graphs of the sticking data will be depicted, along with oligo optimizations. Furthermore, standard curves will be presented for different protein targets, and the developments from the assay and fabrication workflow optimizations shown. Lastly, the spike-in and recovery plots will be shown, depicting which among the mimic buffer candidates was selected for human blood plasma.

Chapter 5 presents the discussion of results and provides justification of the methods used, as well as insight into how these may be improved upon in the future. Specifically, the ramifications of the findings are examined in greater detail, and interpretation and rationalization of erroneous outcomes are explored.

Chapter 6 presents a brief conclusion of the thesis, summarizing the optimizations performed and framing these results in the context of translational medicine and biomarker discovery.

2 | Literature Review

2.1 Biomarkers in Neuroscience

Alzheimer's Disease (AD) and Parkinson's Disease (PD) are the two most common neurodegenerative diseases. Worldwide, nearly 44 million people have been diagnosed with AD or a related dementia, and nearly 10 million people have been diagnosed with PD[21]. Each of these diseases have a myriad of candidate protein biomarkers that are currently under investigation to support and improve patient care and treatment. Descriptions for AD and PD, detailing hallmarks of disease and their respective candidate biomarkers, will be further described below[22].

Alzheimer's disease is the most common neurodegenerative disease and cause of dementia worldwide. Currently, it is estimated to have a 2-25% prevalence from the seventh to ninth decade of life[23, 24]. As there continues to be a global shift to longer life expectancy, this figure is projected to triple by 2050 as current treatments focus mainly on relieving the symptoms of disease, rather than treating the underlying causes[25]. AD is a chronic progressive disease characterized by distinct neuropathological hallmarks and three primary groups of symptoms[21]. The neuropathological hallmarks of AD include the formation of extracellular plaques and intracellular neurofibrillary tangles in the brain. Symptoms of AD fall under three groups: (1) cognitive dysfunction, (2) non-cognitive symptoms, and (3) difficulty with daily activities. Cognitive dysfunction involves the loss of higher-level planning, such as memory loss, language difficulties, executive dysfunction, and the loss of coordination skills. Non-cognitive symptoms involve behavioral or psychological symptoms, such as personality changes, aggression, depression, hallucinations, and delusions[26, 27]. Finally, the last group of symptoms involves difficulty performing daily activities, such as driving, dressing, and eating unaided[28].

Parkinson's disease is the second most common neurodegenerative disease, and is clinically exhibited by a triad of cardinal motor symptoms: rigidity, bradykinesia, and tremors[29]. Furthermore, PD is a heterogenous disease as rigidity and bradykinesia are the major issues in some patients, while tremors are more prevalent in others. PD is caused by the degeneration of neural connections in dopaminergic neurons and the formation of protein aggregates in nerve cells, termed Lewy bodies[21]. As the dopaminergic neurons are destroyed, the motor-related and pre-motor symptoms of PD, such as sleep disorders, depression, and cognitive disturbances, emerge

and worsen over time[23, 30]. Currently, dopamine-replacement therapy is used to alleviate the symptoms of the disease; however, fails to slow or stop the disease from progressing. Moreover, the side-effects of the therapy can induce involuntary body movements and other motor complications, intensifying the patient's overall disability.

In neurological disease research, blood and cerebral spinal fluid (CSF) are commonly the sample-types selected to investigate disease pathogenesis. For AD, some of the current protein markers that are being investigated in CSF include: total-tau (T-tau), phosphorylated-tau (P-tau), neurofilament light protein (Nfl), amyloid β-40 (Aβ-40), and amyloid β-42 (Aβ-42). Currently, amyloid β is one of the most important candidate biomarkers for AD since its levels correlate with plaque pathologies, a hallmark of AD. For the other candidate markers, T-tau levels correlates with neuroaxonal degeneration intensity, P-tau correlates with tangle pathology, and the levels of Nfl are representative of axonal injury[23, 31-33]. These same candidate biomarkers can also be present in blood plasma, however they are generally found at very low concentrations, making their accurate detection difficult. Currently in AD research, a large number of candidate biomarkers are being measured in blood plasma to correlate their levels to the measurements performed in CSF[34]. However, it was found that plasma measurements were prone to more variability and have also been difficult to validate with sufficient accuracy, sensitivity, and specificity.

For PD, protein biomarkers are useful for early diagnosis, prognosis, detection of patients at greater risk, predicting response to therapy, and differentiation of PD from Parkinsonism. Some proteins that are currently under investigation as candidate biomarkers include α-synuclein, orexin, glial fibrillary acidic protein (GFAP), proteasomes, dopamine, dopamine receptors, Apolipoprotein A1 (ApoA1)[23, 35-38]. These proteins range from the constituents of Lewy bodies, hormones expressed in neurons, cytoskeletal proteins, to entire enzyme complexes. Generally, these proteins are found in CSF, although α-synuclein has also been reportedly found in blood and saliva[36]. Currently, focus is being shifted to metabolomic biomarkers in conjunction with α-synuclein and some other candidate biomarkers to acquire a better appreciation for the disease profile of PD and to further the understanding of this disease and its progression.

As described above, AD and PD have many candidate biomarkers that could help identify the disease state of the patient. The discovery and validation stages of biomarkers, as well as processes of drug development and testing, can be greatly accelerated through the accurate and

simultaneous measurement of many proteins. Additionally, with these means of protein measurement, the best course of action to identify, prevent, and cure diseases could be more-readily established and tested. However, to reach this goal, costs, sample consumption, and assay performances must first be feasible, and the major issue of cross-reactivity must be eliminated so that the associated false-positive signals cannot create inaccuracies and confusion in the protein measurements. In order to measure these markers and support the advancement of patient care and treatment, it is critical that methods of protein measurement are developed that are both capable of being multiplexed and retain the gold-standard sensitivity of single-plex ELISAs. Thus, specific focus on eliminating the issue of cross-reactivity in sandwich immunoassays can achieve this, providing a method of protein measurement that can be easily used in clinical settings and provide a tool to supplement current genomic efforts towards a precision medicine approach.

2.2 Common Methods for Protein Measurement

In this section, we will review common methods of protein measurement and detection, which include gel electrophoresis (1D and 2D), western blotting, mass spectrometry, and affinity-based immunoassays. Among these, there are traditional methods that separate out proteins in a gel matrix, others that measure the mass of protein fragments to predict the identities of proteins in a sample, and finally some methods that detect their target protein using antibodies typically in microtiter wells or microarrays.

2.2.1 Gel Electrophoresis

Gel electrophoresis is one of the simplest methods of protein measurement. In traditional gel electrophoresis (1D), an electrical field is applied to drive proteins to migrate through a porous gel matrix to achieve protein separation, highlighted in **Figure 2.1**.

Most commonly for separating proteins, this is typically performed in the presence of a detergent and under denaturing and reducing conditions. Commonly, sodium dodecyl sulfate (SDS) is used as a detergent, and under denaturing and reducing conditions, usually from heat treatment and β-mercaptoethanol or dithiothreitol (DTT) respectively, the proteins are denatured and coated in a negative charge proportional to their amino acid chain length. This treatment abolishes native protein conformation and linearizes the proteins. Once the electrical field is applied, the

negatively-charged, linearized proteins migrate through the gel matrix toward the positive electrode; smaller proteins travel more easily through the matrix and therefore migrate further than larger proteins[39]. This type of gel electrophoresis is termed SDS-polyacrylamide gel electrophoresis, or SDS-PAGE.

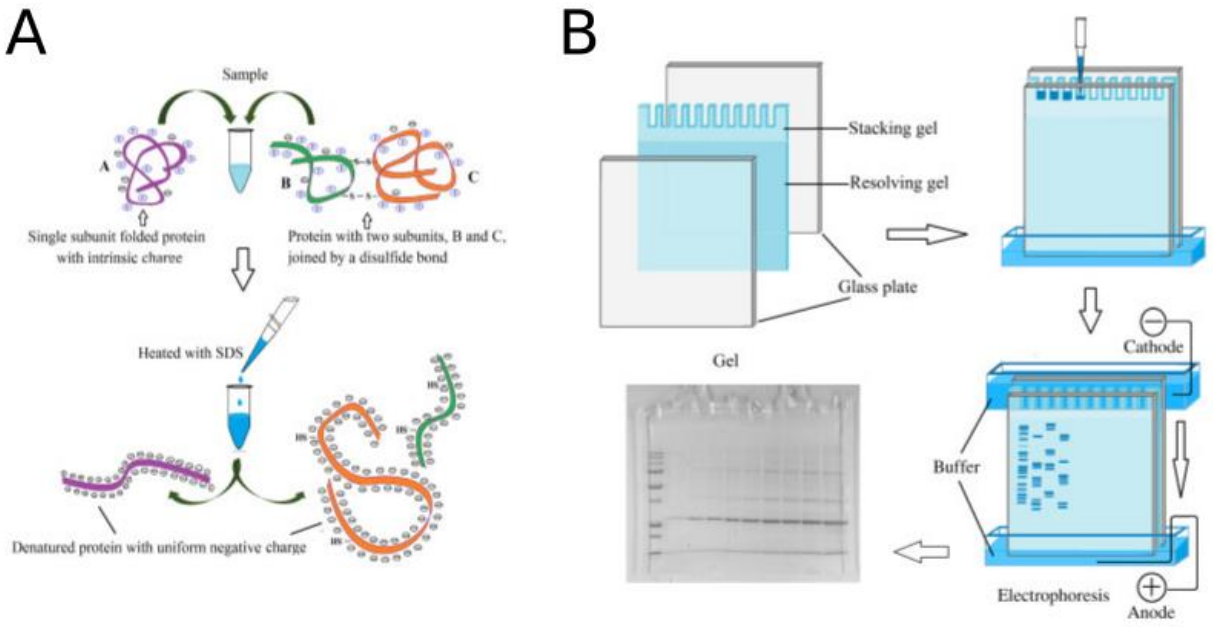

Figure 2.1 | SDS-PAGE Workflow. (A) A depiction of the sample made of two components: (a) single subunit protein, (b) two-subunit protein joined by a disulfide bond. With addition of SDS in denaturing and reducing conditions, the proteins are denatured and coated in a negative charge that is proportional with their amino acid chain length. **(B)** The polyacrylamide gel is prepared, the sample is added into each respective well, and the current passed. The negatively charged proteins run towards the positive end, in which the smaller proteins will migrate further down the gel. Reproduced from ref. [40] with permission from Elsevier, copyright 2018.

However, gel electrophoresis can also be performed using native, non-denaturing conditions. In native conditions, SDS is not used, and thus the separation of the proteins will rely on their inherent charge, which depends on the primary amino acid sequence of the protein and the pH of the running buffer during electrophoresis[39]. This method typically requires optimization of the separation conditions for the respective proteins, in which the process can begin with a normal protein gel protocol comprising of only the separation gel, the sample, and the gel electrophoresis buffer. Alternative protocols such as the "blue native" PAGE uses Coomassie Brilliant Blue to bind to

proteins and give the resulting complexes a negative charge. In this case, Coomassie Brilliant Blue plays a similar role to SDS in SDS-PAGE by tagging protein complexes with negative charges. However, certain protein complexes have a risk to be disrupted from Coomassie Brilliant Blue, and thus would also require optimizations.

To separate and distinguish proteins of similar sizes, gel electrophoresis can be performed in 2-dimensions, highlighted in **Figure 2.2**. In 2D gel electrophoresis, the protein sample must first be solubilized in a solution. Typically, this is performed in a solution of low ionic strength to prevent any changes to the size or charge of the protein, however, the solution used may require sample-specific optimizations to avoid issues of sample bias towards abundant proteins and interference with proceeding procedures. Additionally, the solubilized sample can first be depleted of abundant proteins and reduced in its complexity if necessary. The first dimension of separation involves the electrophoretic separation of proteins based on their isoelectric point, the pH at which proteins carry no net charge[40]. Generally, this is performed in an immobilized pH gradient strip using isoelectric focusing (IEF), under conditions to either denature and solubilize the proteins for proteomic analysis or maintain the native conformation for protein detection. Following IEF, SDS-PAGE is used to separate the proteins based on their molecular mass. The gel is then imaged using protein stains and analyzed using various software to determine the relative concentration patterns of the protein bands and calculate concentrations.

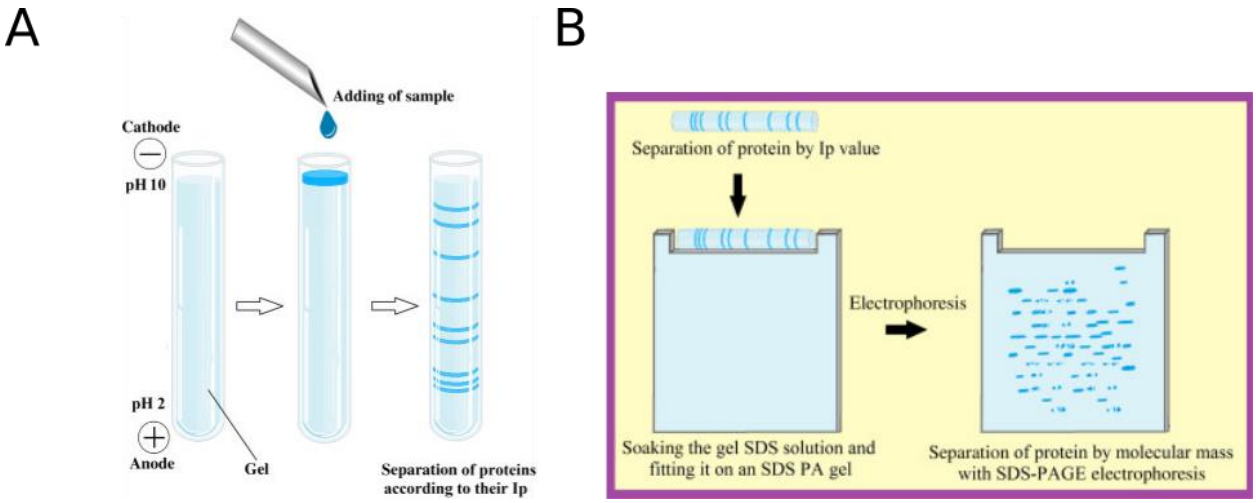

Figure 2.2 | 2-D Gel Electrophoresis Workflow. (A) Isoelectric focusing of the proteins. **(B)** Workflow of 2-D gel electrophoresis, in which proteins are first separated based on its isoelectric point, and then separated based on size. Reproduced from ref. [40] with permission from Elsevier, copyright 2018.

Whereas the 1D protocol separate proteins according to size in one dimension, the 2D protocol first separates the proteins based on their isoelectric point and then separates them by size, making it possible to distinguish proteins of similar size or charge from one-another. Furthermore, 2D electrophoresis is often used in protein expression experiments, as the presence of protein bands can be used to assess differential protein expression qualitatively, and spot intensity may cautiously be used to quantify relative expression differences[41, 42]. The greatest disadvantages of gel electrophoresis are that it cannot be used for reliable protein quantitation and that it lacks specificity. It is also limited in the number and types of proteins that are detectable, has difficulty resolving poorly abundant proteins, and lacks reproducibility; however, the low cost and time commitment associated with this technique make it a viable option when quantitation is not necessary.

2.2.2 Western Blot

Western blotting is a technique used to identify specific proteins from a sample, typically extracted from tissues or cells, highlighted in **Figure 2.3**. Western blotting utilizes three key parameters to separate and identify the target proteins: (1) separation by size, (2) transfer to a solid support/membrane, and (3) labeling the target protein with primary and secondary antibodies for visualization[43].

Western blotting first separates the sample based on the size of the proteins via gel electrophoresis, and then transfers the proteins onto a solid support membrane where the proteins are probed with antibodies. Primary antibodies are first used to bind the proteins of interest, and then incubated with secondary antibodies which bind onto the primary antibodies to generate a fluorescent signal[43]. If an enzyme is used to generate a signal instead of a fluorophore, the signal is generated upon incubation with the enzyme's substrate. The washing steps between the two antibody incubations and after the secondary incubation removes the unbound antibodies from solution, so that a signal is only generated based on the formation of a complete protein-primary-secondary immunocomplex. The intensity of this band can be compared to standards run in parallel on the gel to semi-quantitatively estimate of the amount of protein that is present.

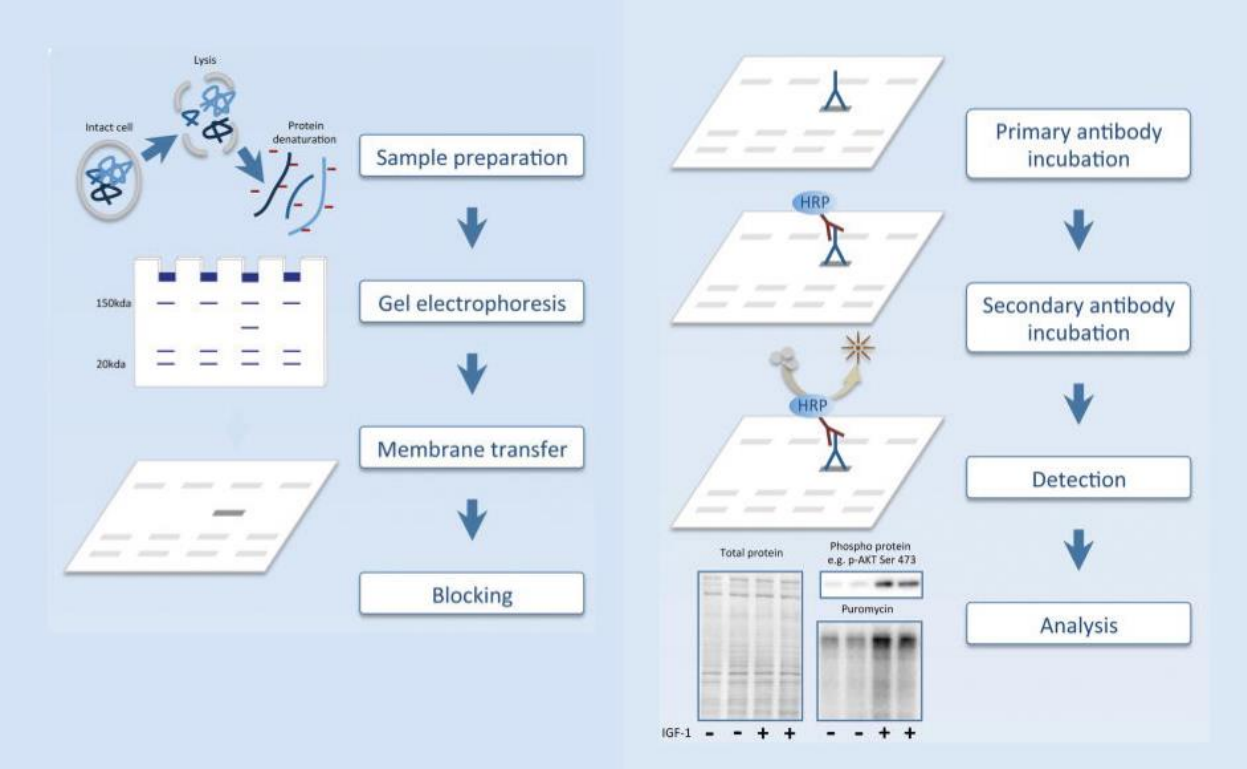

Figure 2.3 | Western Blot Workflow. The western blot protocol begins with standard gel electrophoresis to separate the proteins based on size. The gel is transferred onto a membrane and blocked to prevent non-specific interactions. Afterward, the primary antibody is incubated to bind to its target of interest, followed by a secondary antibody incubation to generate a readable signal. The signal is detected and subsequently analyzed. Adapted from ref. [44] under CC BY 4.0.

The major advantage of western blotting over other methods of detection is that by probing with affinity binders, not only is the protein detected, but information about its molecular size is collected to verify that the correct protein has been captured. Furthermore, this technology is simple to use, has many established standard operating protocols (SOPs) and reagent kits available, and does not require complex instrumentation. Although the procedure for western blotting is simple and straightforward, the protocol is very lengthy, and thus technically demanding. Due to this, commonly made mistakes, such as incubating an insufficient amount of primary antibody, can produce unusable results[45]. Furthermore, another limitation is that a primary antibody for the specific target must be readily available for blotting to be possible. The availability of a specific

antibody can be especially limiting when attempting to detect post-translational modifications, as the primary antibody will need to specific to those residues.

2.2.3 Mass Spectrometry

Another popular method of characterizing proteins is mass spectrometry (MS). Comprehensive reviews on the basics of mass spectrometry and its use for proteomic analysis are referenced for more detailed information[46-48].

Briefly, mass spectrometry is a comprehensive tool that allows for the mass analysis of proteins, highlighted in **Figure 2.4**. Typically, proteomic analysis with MS is divided into three categories based on whether the samples are first digested (traditional bottom-up proteomic analysis), selectively digested (middle-down proteomic analysis), or if the sample is analyzed in its undigested form (top-down proteomic analysis)[48]. Generally, in the case of bottom-up proteomic analysis, the sample is first digested and denatured, and then subsequently separated and analyzed via liquid chromatography mass-spectrometry (LC-MS). The bottom-up approach indirectly measures the proteins from their protease-degraded peptides, in which that generated data is compared with mass spectra in a protein database for identification. In the case of top-down proteomic analysis, intact proteins are measured, allowing for measurements of post-translational modifications and protein isoform determination. Finally, a combination of the bottom-up and top-down approaches, the middle-down approach analyzes larger peptide fragments than the bottom-up reducing the redundancy of peptides measured. Furthermore, with the measurement of larger peptide fragments, post-translational modifications can potentially be measured without the added difficulty of protein fractionation, ionization, and fragmentation that is associated with the top-down approach[48].

To conduct mass analysis on the sample proteins, the target must first be ionized to shift the target into a gaseous phase while minimizing degradation. Soft ionization, a type of ionization that does not significantly degrade the sample, is typically performed through matrix-assisted laser desorption ionization (MALDI) or electrospray ionization (ESI)[49, 50]. After ionization, the target ions move through an electric field, which causes them to accelerate so that the ions separate based on their charge—the greater the charge on the ion, the faster it will accelerate. The accelerated ions then move through a magnetic field, arcing their trajectory such that lighter and more positively charged ions will arc more, resulting in a spectrum of ion trajectories arranged by mass and charge.

An electrical detector records the generated spectrum and the data is used to reconstruct the fragment peptide sequences to ultimately resolve the identity of the source protein[51].

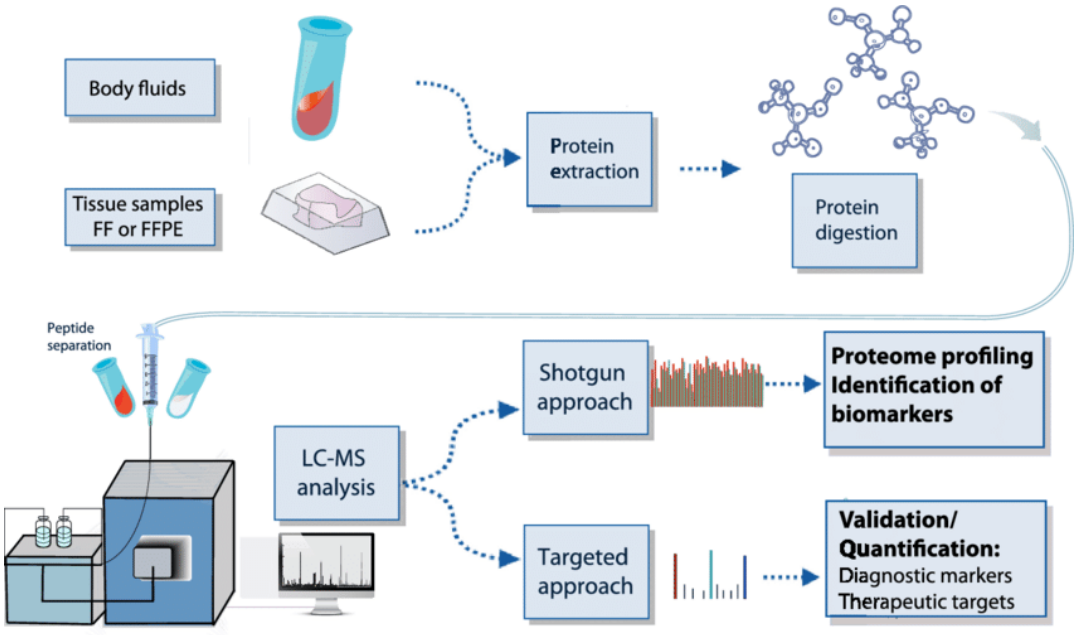

Figure 2.4 | Mass Spectrometry Workflow. Proteins are first extracted from the sample, and subsequently digested into peptides. In this example, the peptides are first separated with liquid chromatography and subsequently measured via mass spectrometry. FF, fresh frozen; FFPE, formalin-fixed paraffin-embedded; LC, liquid chromatography. Reproduced from ref.[52] with permission from Elsevier, copyright 2017.

In a recent publication, isobaric tags for relative and absolute quantitation (iTRAQ) 4-plex was used to detect and quantify >4,500 proteins per patient sample with two or more peptides per protein. Furthermore, to increase throughput, tandem mass tag (TMT) reagents were used to multiplex at 10-plex. However, increasing the throughput led to a decrease in the number of proteins quantified to approximately 600 proteins per patient sample[53]. Generally, some challenges of using mass spectrometry include the high cost required to maintain the specialized equipment and machinery, and the relative bias against the detection of small proteins. Furthermore, if all the high abundance proteins were not removed during sample preparation, detection of the less abundant target proteins can be obstructed[54].

2.2.4 Affinity-Based Immunoassays

The most commonly used methods for protein quantification are affinity-based immunoassays. Affinity-based immunoassays apply affinity binders (*i.e., antibodies*) to specifically bind to a protein of interest. Once binding occurs, the signal is recorded as a measure of these specific binding events[55]. Instead of detecting all proteins in the sample, as in the instances of gel electrophoresis and MS, the experimental design must consider which proteins to target with affinity-binders. Since the researcher can choose which proteins to target, affinity-based assays are a valuable tool for targeted or follow-up studies to determine the concentration of specific analytes. The advantages of this method of protein detection are its high sensitivity in the pg/mL range, broad dynamic range, and relative ease of use. However, affinity-based immunoassays are also limited from its reliance of suitable affinity binders that can reliably detect its matched protein at low concentrations[56]. Affinity-based immunoassays can typically be broken into four different formats depending on the type of experiment the researcher wants to perform: direct, indirect, sandwich, and competitive immunoassays. The simplest types of affinity-based immunoassays are the direct and indirect types, which only utilizes a single affinity binder to recognize and bind to its specific protein. These formats are highlighted in **Figure 2.5 A, B**.

In direct immunoassays, proteins from the sample are first attached or coated onto a solid surface (*i.e., magnetic beads, glass slide, 96-well plate).* The solid surface is subsequently washed and blocked to remove unbound proteins and block non-specific binding respectively. The protein coated surface is then incubated with its matching primary antibody, which is subsequently washed to remove any unbound excess of antibodies. The signal of the bound antibodies is then measured to determine the concentration of the protein target that coats the surface. Indirect immunoassays are very similar to direct immunoassays but has an additional step of incubating secondary antibodies after washing the unbound primary antibodies. In this case, the signal of the bound primary antibodies arises from the binding of the secondary onto the primary antibody. The two-step antibody detection of indirect immunoassays supports more sensitive detection of low-abundance proteins since the secondary antibody can amplify the signal generated from the antigen-primary antibody immunocomplex. Furthermore, indirect immunoassays allow for one secondary antibody to be used with a variety of different primary antibodies if they were produced

from the same animal species, saving on costs to attach a fluorescent label to each primary antibody.

As both the direct and indirect method relies on a single affinity-binding event between the protein and the antibody to generate a signal, a significant limitation is the issue of sample-driven cross-reactivity between the analyte and the binder. In these cases, the primary antibody has the potential to bind non-specifically to another protein and generate a false positive signal whether directly through the primary antibody, or indirectly from binding of a secondary antibody onto the non-specifically bound primary[57].

To mitigate the effects of sample-driven cross-reactivity in single-binder assays, a dual-binder (sandwich) assay is performed. The sandwich immunoassay is very similar to the single-binder assay, but it has an additional level of specificity conferred by a second high-affinity binder that targets a different epitope of the protein (**Fig. 2.5 C**). The addition of another specific affinity binder reduces the number of cross-reactivity events that are detected due to low probability that two off-target binding events will occur in tandem. This method of detection reduces the occurrence of false positive signals as the fluorescent signal will only be detected from a successfully formed immunocomplex. Sandwich immunoassays offer both high sensitivity from the high-affinity antibodies and high specificity from the double recognition of different epitopes on the protein[58]; however, it can be challenging to find suitable paired high-affinity binders that bind to separate, non-interfering epitopes on the target protein.

Typically, in sandwich immunoassays, primary antibodies against the protein of interest are immobilized onto a solid surface. The solid surface is washed and blocked to remove unbound antibodies and block the surface from non-specific binding. The sample is incubated to facilitate specific binding to the primary "capture" antibody. The solid surface is then washed to remove any non-cognate binding and a second "detection" antibody, that is typically tagged with a signal generating molecule, is incubated to specifically bind the target protein at a separate non-interfering epitope. After washing the excess detection antibodies away, the signal is subsequently measured and quantified[56].

Lastly, the competitive format measures the concentration of the target of interest by detecting the signal generated from the interference of a reference antigen (**Fig. 2.5 D**). Any of the previous formats can be altered into a competitive format, and is typically used when working with crude

samples, as minimal sample processing is necessary. Essentially, a reference antigen is first coated on a solid surface, which is then washed and blocked. Meanwhile, the sample is incubated with an excess of antibodies specific to the target of interest. During the incubation, target-specific antibodies that are tagged with a signal generating molecule will bind to the target protein and, depending on the amount of target protein in the sample, a varying number of tagged antibodies will remain free in solution. Afterwards, the sample is incubated with the solid surface and any previously unbound tagged antibodies can bind to the reference antigen coated on the surface. After subsequent washing to the eliminate the target-bound antibodies, the signal generated by the antibodies bound to the reference antigen is measured, which is inversely correlated with the amount of the target protein in the sample. In other words, the higher the amount of target protein in the sample, the fewer tagged antibodies there would be that are available to bind the reference antigen on the surface.

In each of these formats, a suitable signal must be measured to detect the presence of antibody-protein binding events to calculate the protein's concentration within the sample. When immunoassays were first developed, radioactively labeled isotopes were used to label antibodies to detect their respective proteins[59]. Radioimmunoassays (RIAs) were first used in the 1960s to detect and measure the endogenous concentration of insulin. In 1971, a modification of the RIA conjugation protocol was made to conjugate enzymes rather than radioactive isotopes onto antibodies and antigens. The new "enzyme immunoassay" (EIA), or "enzyme linked immunosorbent assay" (ELISA), proved to be much safer for use, as working with radioactive isotopes poses a potential health risk to the researcher, and changed the previous radioactive signal to a colorimetric one, in which a change in color was observed when the enzyme (*i.e., horseradish peroxidase*) reacted with a substrate *(i.e., ABTS)*[56, 60]. Newer forms of ELISA do not necessarily rely on an enzyme to produce a signal and may instead rely on fluorescent reporters or incorporate electrochemiluminescence to generate a signal. These newer methods of signal generation may influence the assay's availability for multiplexing and signal amplification, allow for improved analytical sensitivity, and decrease the background signal.

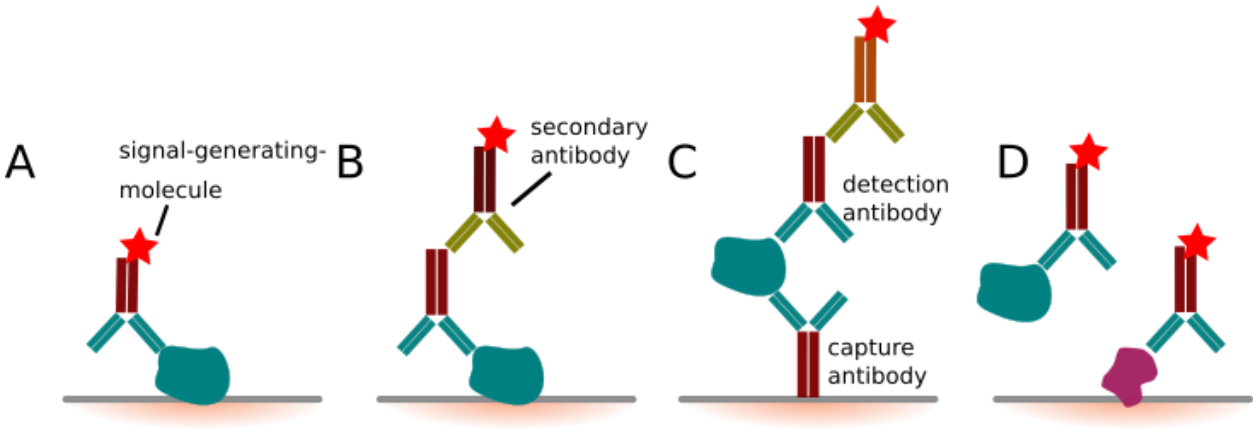

Figure 2.5 | Four Types of Affinity-Based Immunoassays. (A) A direct affinity-based immunoassay in which an antigen against a targeted antibody is immobilized on a solid surface. The antibody tagged with a signal-generating-molecule binds specifically to the antigen to generate a detectable signal. **(B)** An indirect affinity-based immunoassay in which the targeted antibody binds to the immobilized antigen. As opposed to the specifically bound primary antibody directly generating a signal, a secondary antibody that is prelabeled with a signal-generating-molecule binds to the targeted antibody and generates a detectable signal. **(C)** A sandwich affinity-based immunoassay in which an immobilized capture antibody binds to its specific targeted protein and a detection antibody subsequently binds to separate epitope on the target protein. The detection antibody may be labeled with the signal-generating-molecule or a secondary antibody with the molecule can be introduced to generate a detectable signal as shown. **(D)** A competitive affinity-based immunoassay first incubates an excess of target-specific antibodies tagged with a signal-generating molecule with the sample to facilitate specific binding complexes. The antibody-mixed sample is added to a solid surface spotted with reference proteins (pink) that bind to the tagged antibodies. After incubation, the solid surface is washed to remove any of the target protein-antibody complexes from generating a detectable signal. The amount of labeled antibody that binds to the reference antigen and thus generates a detectable signal is inverse to the amount of antigen present in the sample.

An approach that utilizes the immunoassay format to detect and characterize proteins in a highly parallel and high-throughput way is the protein microarray. Microarrays have been used to develop and further methods of drug development, disease diagnosis, biochemical pathway mapping, protein interaction analysis, and many more[61]. The three major formats for protein microarrays are analytical, functional, and reverse-phase[62, 63]. Analytical protein microarrays, also known as antibody microarrays, are essentially single binder or dual binder immunoassays that can be performed in parallel on the solid surface by introducing different targeted antibody pairs (**Fig. 2.6**

A). However, there is a limit to the amount of protein targets that can be measured simultaneously through this method due to the issue of cross-reactivity. Analytical microarrays are generally used for the purposes of protein detection.

Functional protein microarrays spot large amounts of purified proteins on a solid surface to identify the biochemical properties of the proteins, such as protein-protein, protein-DNA, protein-RNA, protein-drug, binding patterns, and a variety of other properties. Instead of using recombinant proteins that may be used in analytical arrays, functional microarrays typically utilize the full functional protein to enable their normal functionality. A few applications of functional protein microarrays are highlighted in **Figure 2.6 B**.

Finally, reverse-phase protein microarrays do the opposite of the other two types by spotting the sample (*i.e., tissue or cell lysate*) onto the solid surface (**Fig. 2.6 C**). This format of protein microarray allows for the analysis of different samples by incubating different probes to identify the proteins in the sample[64]. This technology was first developed to monitor histological changes in prostate cancer patients and identified the phosphorylation statuses of some of the proteins involved. Presently, this technology is used in many different fields of research, with specific clinical focus to study deregulated cell signaling networks in cancer tissues[65].

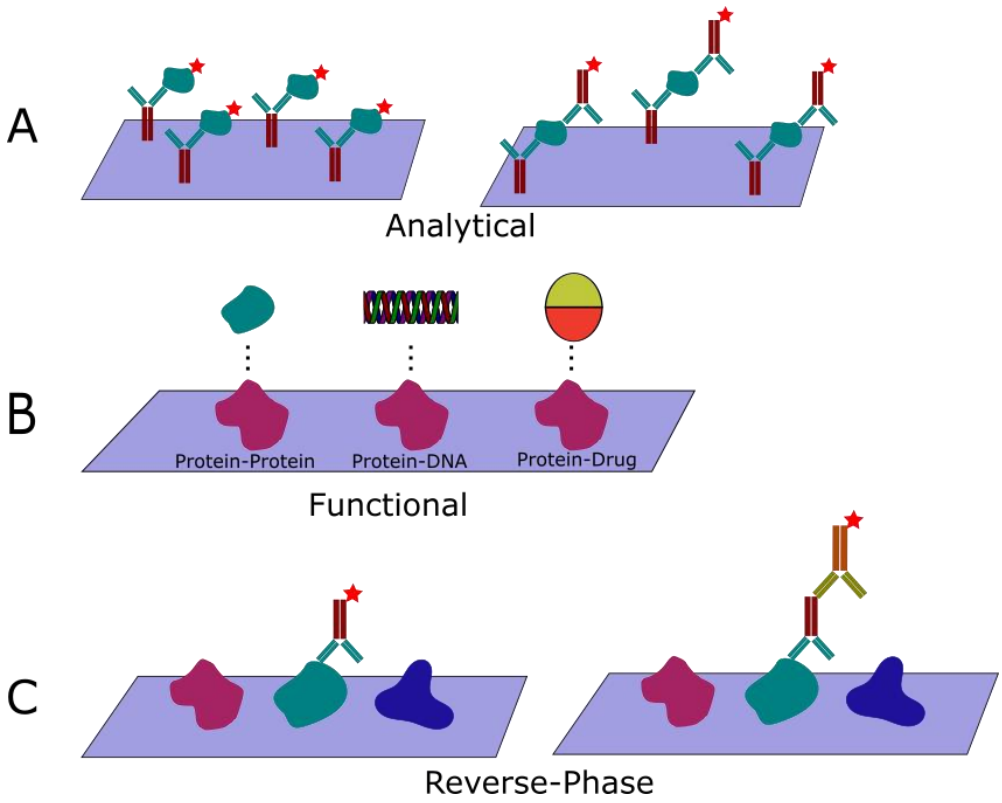

Figure 2.6 | Types of Protein Microarrays. (A) Analytical microarray depicting single-binder format on the left and dual-binder (sandwich) format on the right for one protein. This type of microarray is typically used for protein detection and has the potential to be multiplexed by incorporating antibodies for different protein targets. **(B)** Functional microarray showing three potential uses for this format: identifying protein-protein interactions (left), protein-DNA interactions (middle), and protein-drug interactions (right). This format of protein microarray is typically performed by spotting a purified protein onto a solid surface and then identifying its different properties and interactions. **(C)** Reverse-phase protein microarray depicting a single binder signal readout (left), or a secondary binder signal readout (right). This format is performed by immobilizing sample proteins onto a solid surface to analyze its protein composition.

2.3 Challenges of Developing Quantitative Immunoassays

2.3.1 Assay Sensitivity

High analytical sensitivity is attributed to being able to quantitatively measure low concentrations of protein analyte[66]. Most commonly, the limit of sensitivity is determined by assaying a zero "blank" calibrator sample repeatedly and calculating the concentration 2-3 standard deviations

above that mean. This is termed *analytical sensitivity*. However, the values of analytical sensitivity may not be reliable, as the precision of values at this concentration may be very poor and below acceptable levels. Due to this, *functional sensitivity* can be measured, which is defined as the lowest concentration in the assay for which the coefficient of variation (CV) is below a certain percentage[66]. The percentage is determined based on the type of protein assay being evaluated and is generally stated with the concentration of functional sensitivity. However, since the derivation of functional sensitivity is typically complicated, requiring justification of how the % CV was selected, it is more likely that analytical sensitivity is reported and quoted as the "sensitivity" of a given protein assay.

Sensitivity can further be expressed in terms of the *limit of detection (LOD)* and the *limit of quantification (LOQ)*[67, 68]. A schematic of a standard calibration curve is depicted in **Figure 2.7**, highlighting the differences between the LOD and LOQ.

The LOD is similar in concept to the analytical sensitivity, representing the lowest analyte concentration at which the concentration of the protein can be reliably distinguished from the background signal, and thus the detection of the protein feasible. In other words, a sufficient amount of protein analyte must be present in the sample to produce a signal that can be reliably distinguished from the background signal. Typically, 20 replicates of the blank are performed to determine the mean value and SD of the background signal, with an assumption that if protein analytes are present in the sample, they will produce a signal greater than the background signal observed[68]. The LOD is calculated using equation (1):

$$LOD = Mean_{blank} + 3\ (SD_{blank})$$

The LOQ is similar in concept to functional sensitivity and is the lowest analyte concentration at which the concentration of the protein can be reliably distinguished from the background signal, while also satisfying predefined goals for bias and imprecision. The calculation for LOQ is achieved using equation (1) with the added criteria of achieving a predetermined %CV (*i.e.* CV = 20%). The value of LOQ can be equivalent to the LOD or much greater but cannot be lower than the LOD. For example, if the observed LOD meet the requirements for error and imprecision of the analyte, then LOD = LOQ. However, if the LOD do not meet these requirements, a higher protein concentration must be tested to determine the LOQ. Furthermore, LOQ can be split into the lower limit of quantification (LLOQ) and the upper limit of quantification (ULOQ)[69]. The

LLOQ represents the lowest analyte concentration on the standard calibration curve where the response is reproducible and satisfies the criteria for bias and imprecision. Similarly, the ULOQ represents the highest analyte concentration on the standard calibration curve which is reproducible and satisfies the predefined goals of bias and imprecision. In practice, the LOQ sets the goals of precision and accuracy within 15-20% of the CV and the concentration, respectively.

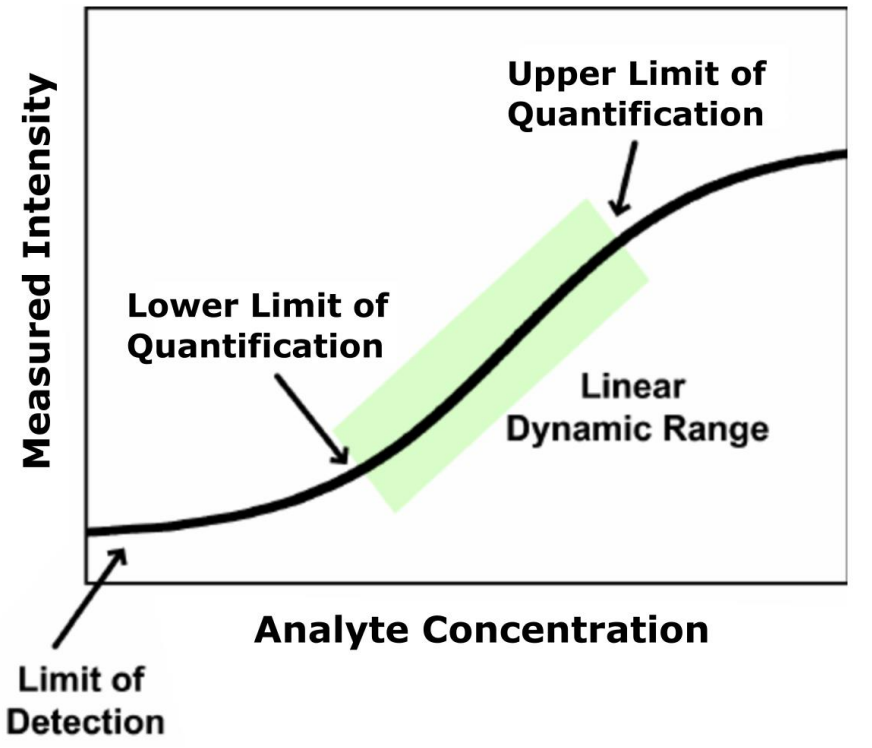

Figure 2.7 | Standard Curve Depicting the Limits of Detection and Quantification. The standard curve typically depicts measured fluorescence intensity on the y-axis and the analyte concentration on the x-axis. The LOD is shown depicting the lowest concentration which can be reliably distinguished from the background signal. Additionally, the lower and upper limits of quantification (LLOQ and ULOQ) represent the lowest and highest analyte concentration in which the signal is reproducible and satisfies the pre-determined criteria for bias and imprecision. The linear dynamic range highlighted in green between the LLOQ and ULOQ represents the region of the standard curve which is linear and most sensitive. This region is the optimal range for quantitative measurements of protein concentrations. Reproduced from ref.[70] under CC BY 3.0.

2.3.2 Cross-Reactivity in Different Assay Formats

One fundamental problem of immunoassays is cross-reactivity. Cross-reactivity is the result of binding of the affinity-binder to off-target molecules due to its similarity to the analyte. The most concerning issue of cross-reactivity arises from the fact that the signals generated from cross-reactive events fail to be distinguished from a signal generated via specific immunocomplex formation[57].Cross reactivity can be split in two groups which will be further described below: (A) sample-driven cross-reactivity and (B) reagent-driven cross-reactivity.

We define *sample-driven cross-reactivity* to be the cross-reactive events that occur between non-cognate proteins and the other proteins or affinity binders following sample incubation[57]. These interactions could include off-target proteins from the sample binding to the (A) affinity binder, (B) target protein bound to affinity binder, and (C) solid surface. These sample-driven cross-reactive events can generate false positive signals when only a single cross-reactive event is required—specifically, in single-binder immunoassays (**Fig. 2.8 A, B**). Dual-binder, or sandwich, immunoassays overcome this type of cross-reactivity by incorporating two different antibodies (capture and detection) that bind to two separate epitopes on the protein. The sandwich immunoassay thus has tolerance to sample-driven cross-reactivity since a single binding event does not generate a signal, while two simultaneous binding events occur very rarely. The effects of sample-driven cross-reactivity and their effects on single-binder and dual-binder immunoassays are depicted in **Figure 2.8**.

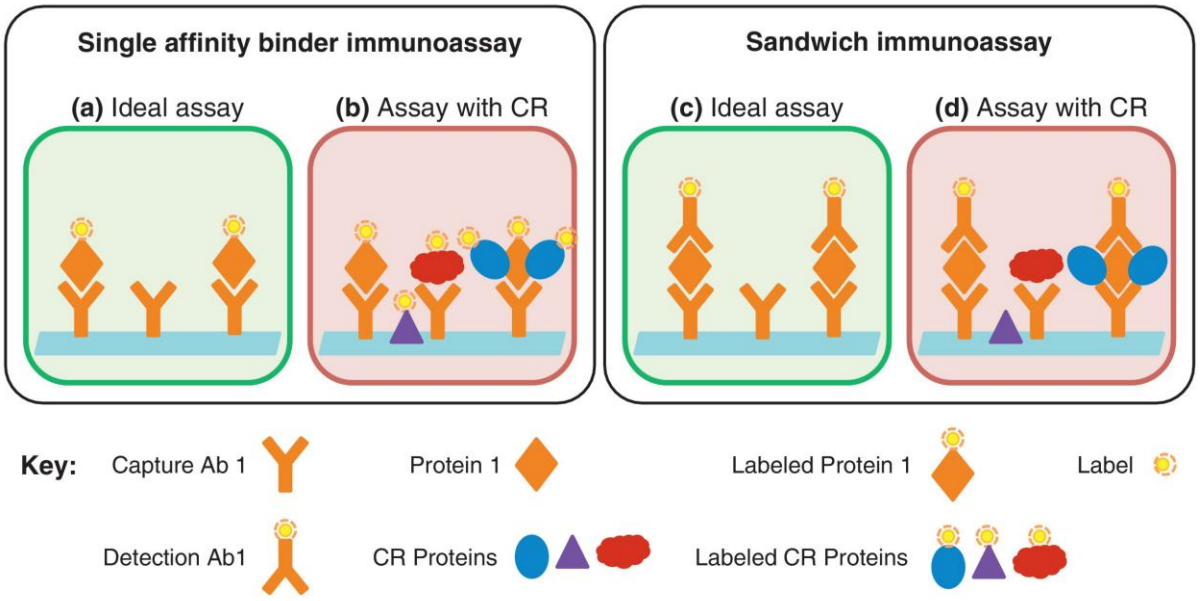

Figure 2.8 | Sample-driven cross-reactivity and its effects in singleplex single-binder vs dual-binder immunoassays. (A) The ideal case in which the capture antibodies immobilized onto a solid surface binds to their respective protein targets and generates a detectable signal. **(B)** A case of false positive signal generation via sample-driven cross-reactivity with cases of non-specific adsorption (purple), protein-protein interactions between off-target proteins (blue) to the target protein, and a cross-reacting protein to the affinity binder (red). **(C)** The same ideal singleplex assay in dual-binder conditions, in which the capture and detection antibodies bind to their target protein, completing an immunocomplex. **(D)** A higher tolerance to sample-driven cross-reactivity as the previous cases of non-specific adsorption, protein-protein interaction, and cross-reacting proteins in single-binder conditions do not generate a detectable signal in dual-binder conditions. Reproduced from ref.[57] with permission from Elsevier, copyright 2014.

On the other hand, MSAs are burdened with another type of cross-reactivity in which the number of cross-reactivity events increases exponentially with the number of targets. Conventional MSAs first incubate their immobilized capture antibodies with the sample, followed by the addition of detection antibodies to the solution. In an ideal situation, we expect the detection antibodies to bind to their specific protein target that is bound to its respective capture antibody. While thermal agitation ensures that each reagent encounters its target, it also results in combinatorial interaction of all detection antibodies with the other (1) proteins, (2) capture antibodies, and (3) detection

antibodies. We define cross-reactivity introduced from reagent mixing as *reagent-driven cross-reactivity*[57].

The concept of *liability pairs* was previously introduced encompassing the combinations of antibody-antibody, antibody-protein, and protein-protein interactions that give rise to false positive signals upon cross-reactive binding[71]. The total number of liability pairs for an assay with N targets is computed by combinatorial enumeration of each binding pair according to the scenarios in **Figure 2.9**[71]. The liability pairs are: (1) detection antibody-protein, (2) detection antibody-capture antibody, (3) detection antibody-detection antibody, (4) capture antibody-protein, and (5) protein-protein. We neglect the scenario of capture antibody - capture antibody which may occur in some assay formats, but as the assay readout is linked to the detection antibody, this scenario is not as significant.

In scenarios (1), (2), and (4), each of the N molecules can combinatorically encounter every other constituent in solution aside from its cognate protein and capture-antibody, thus corresponding to (N-1) interactions for each of the N sandwich immunocomplexes. Therefore, each of these three scenarios have N (N-1) liability pairs. For scenarios (3) and (5), the liability pairs are between the same group of molecules and thus the number of pair-wise combinations are given by $\frac{N\,(N-1)}{2}$ [71]. In MSAs, the total number of liability pairs resulting from *reagent-driven cross-reactivity* as a sum of all five scenarios is 4N (N-1), in which N represents the number of protein targets.

By minimizing reagent-driven cross-reactivity, MSAs become a more viable option to obtain disease-related data focused on patient health, while simultaneously alleviating the constraints of reagent cost, long experiment durations, and use of high sample volumes that occur with repeated ELISAs.

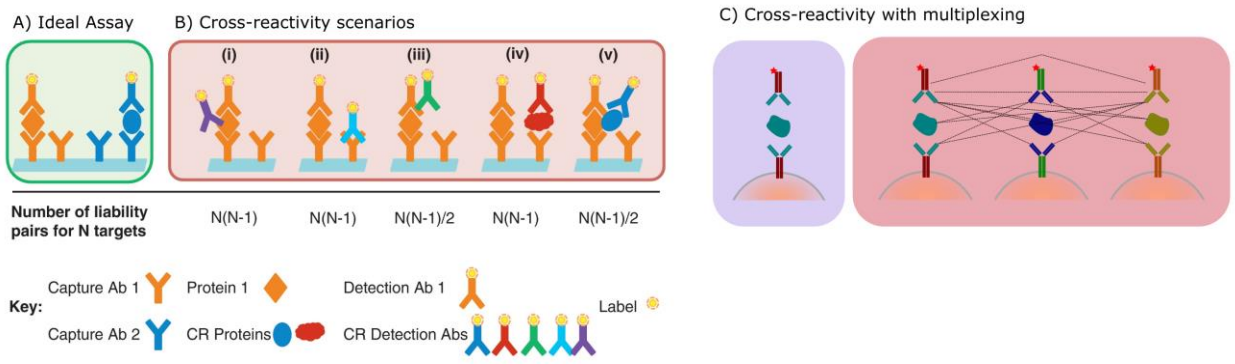

***Figure 2.9* | Scenarios of reagent-driven cross-reactivity. (A)** An ideal assay in which the correct antibodies form a sandwich with the correct protein. **(B)** The possible cross-reactivity scenarios with the number of liability pairs for N targets. Depicts the cross-reactive binding of the: (i) detection antibody to target protein, (ii) detection antibody to capture antibody, (iii) detection antibody to detection antibody, (iv) off-target protein to capture antibody, and (v) protein-protein interaction between two different protein targets. The total number of liability pairs equates from the sum of these five conditions, scaling to 4N (N-1), for N number of protein targets. **(C)** A proper sandwich immunoassay on the left contrasted with the compounding issue of cross-reactivity when scaling up multiplexing. On the right, the antibodies for different protein targets may interact with different target antibodies, or the different proteins may interact with off-target antibodies to generate false positive signals. This demonstrates the exponential increase of cross-reactivity with the number of targets being measured. A and B were reproduced from ref.[71] under CC BY-NC 3.0.

2.3.3 Buffers and Sample Types

When optimizing performance for the measurement of proteins in complex sample matrices such as blood plasma, it is crucial to establish a buffer that mimics the complexity of the matrix, *i.e.* a "mimic buffer". Unfortunately, commercial companies typically keep these buffer compositions confidential, which can potentially account for some of the unexpected results received from their services. An acceptable mimic buffer must accurately simulate the complex matrix since this buffer will be used to directly generate the standard calibration curve for the analysis of the clinical samples. The standard curve cannot be constructed from a sample of the true complex matrix itself due to its endogenous protein levels which will confound the baseline and skew the detection of those proteins in the assay. Instead, a mimic buffer is made to simulate the complexity whilst

excluding endogenous human proteins and imitates the background signal that would be observed in the complex sample itself.

The importance of a representative mimic buffer is further emphasized by its purpose in extrapolating the standard curve to calculate the concentrations of target analytes from the signal generated. Thus, if the mimic buffer does not properly simulate the complex nature of the sample, large inconsistencies and misinterpretations in the data will arise, in which the interpolated concentrations will be unrepresentative of the true concentration of the target protein in the sample. Misinterpretations of protein concentrations can become especially problematic when the calculated concentrations are used in clinical applications to diagnose patients or determine their treatment plan. Additionally, a suitable mimic buffer must be optimized for every unique complex matrix to maximize the accuracy of the interpolated concentrations.

An appropriate mimic buffer for a complex matrix is identified by comparing the background signals of the candidate mimic buffers to the diluted samples. It is important that no proteins are added to the mimic buffers to ensure that no endogenous concentration of the proteins exist to skew the results. For this purpose, many candidate mimic buffers are screened for their background level similarity to the complex sample being measured. The buffers closest in background are selected for further testing to evaluate which amongst them has the best performance using spike-and-recovery tests.

In spike-and-recovery testing, a full-range standard curve is generated in the potential mimic buffers, and several known protein concentrations are spiked into the complex sample at various dilutions (1:2, 1:4, etc.). The spiked-in concentrations are interpolated from each of the standard curves in different candidate mimic buffers and the percent recovery (% recovery) is calculated using equation (2)[72]:

$$\%\ Recovery = \frac{Observed\ Concentration - Background\ Concentration}{Expected\ Concentration} \times 100$$

The accepted range for % recovery with reasonable accuracy is between 80% and 120%[72, 73]. Percent recovery that is lower than 100% implies that the interpolated concentration is lower than the theoretical concentration, or there was an elevated background signal. Percent recovery that is

greater than 100% has the opposite meaning, where the interpolated signal is elevated compared to the theoretical, or the background is depressed.

Following mimic buffer selection, a suitable "standard diluent" buffer is also necessary for the analysis of complex samples. The standard diluent will be used to decrease the level of complexity of the sample upon dilution. For example, when reducing the complexity of neat (undiluted) blood plasma to 1:2 diluted blood plasma, the standard diluent will be used to dilute the plasma. This buffer is typically selected as a clean buffer (*i.e., PBS*) with some added constituents to maintain some complexity of the sample even with high levels of dilution.

2.5 Technological Advances in Protein Immunoassays

Since the development of the ELISA in the 1970s, there have been many technological advances in protein immunoassays. Typically, these can be categorized into two groups based on the specific constraint of protein measurement that they address. The first group includes the technologies that address the analytical sensitivity necessary to measure low abundance proteins. These technologies typically reduce LODS, LOQs, and enable a more robust method for the discovery of low abundance biomarkers. The second group of technologies target cross-reactivity and aim to scale the number of proteins that can be profiled from a single sample, ideally also pushing down the costs of testing. Although developments in single-cell technologies have recently exploded, the techniques will not be covered in this section. Comprehensive reviews on single-cell techniques and their use for proteomic analysis are referenced for more detailed information[74, 75].

2.5.1 Technologies Addressing Sensitivity

Classic sandwich immunoassays, such as ELISA, can provide considerable sensitivity in the pg/mL range for protein analytes. However, as many candidate biomarkers and proteins-of-interest are found below these concentrations, and thus below the range of most sandwich immunoassays, methods of increased sensitivity are required. Sandwich immunoassays can be hindered from achieving higher sensitivity from non-specific binding or other interactions that increase the background signal. Technologies that can offer higher sensitivity by amplifying the signal, decreasing the background signal, or otherwise providing unique methods of single-molecule counting will be described below.

2.5.1.1 Immuno-Polymerase Chain Reaction (Immuno-PCR)

First, a simple method to increase the sensitivity of the ELISA would be to alter its protocol to incorporate a PCR-based amplification of the signal. This method can significantly amplify the generated signal, attributing to $10 – 10^9$ fold increases in the signal[76]. The immuno-PCR is based on coupling DNA oligonucleotides (oligos) to antibodies and subsequently amplifying the oligos from the antibodies that have formed immunocomplexes using methods of PCR. With this method, it abolishes the need of an enzyme or fluorophore to generate a signal as with traditional ELISA formats. Immuno-PCR can be performed in all the different formats of ELISA highlighted previously depending on the measured sample and the protein types being measured. Furthermore, there are also many methods of coupling the antibody to the DNA oligo (**Fig. 2.10 A-C**), as well as methods of readout. Since many of the traditional methods to measure proteins lack the sensitivity required for biomarker discovery and validation, immuno-PCR is a relatively simple method that can overcome this issue with little deviation from the current methodology of ELISA. Currently, the most popular methods of amplification and detection include using quantitative PCR (qPCR) and digital PCR. The concept of immuno-PCR using qPCR is shown in **Figure 2.10 D**. While these methods of amplification prove the technology with a significant increase in sensitivity, it also limits its throughput. The main advantage of immuno-PCR is its ability to drastically increase the sensitivity of the ELISA, an accepted gold standard of protein measurement. Furthermore, this innovation can be easily modified to incorporate different types of affinity binders and readout methods, making it very versatile to the specific needs in the field of research. However, the biggest disadvantage to immuno-PCR is that it does not solve the major problem of reagent-driven cross-reactivity, thus limiting its scalability while relying on the ELISA format. Furthermore, since the methods of readout are very sensitive, any false-positive signals generated during the assay will also propagate to readout, complicating result analysis. Lastly, this method depends heavily on every affinity binder being conjugated to the same number of DNA oligos to generate comparable results, a feat that may be difficult in practice.

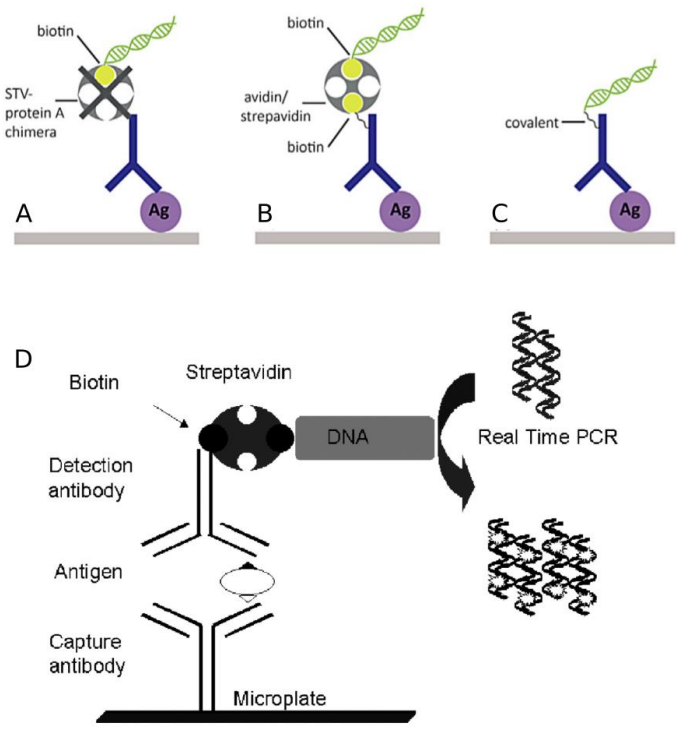

Figure 2.10 | Immuno-PCR Assay strategies and format. (A) The original immuno-PCR format of antibody-oligo conjugation, in which a streptavidin-protein A fusion protein was used to link the antibody with a DNA oligo. B) A more universal format which used a biotinylated antibody bound to either avidin or streptavidin which was then bound to the DNA oligo via a biotin-(strept)avidin interaction. (C) To avoid potential issues of heterogenous antibody-oligo conjugates from the various biotin-(strept)avidin interactions, a covalent crosslinker can be used to directly conjugate the DNA oligo to the antibody. (D) A schematic of immuno-PCR using an ELISA format with a biotin-streptavidin linkage and qPCR readout. For quantification, a series of dilution standards would be included in the assay, a regression analysis is performed, and the resulting equation is used. A-C were adapted from ref. [76] with permission from Elsevier, copyright 2016. D was reproduced from ref. [77] with permission from Clinical Chemistry, copyright 2005.

2.5.1.2 Meso Scale Discovery platform

A method of protein detection that is very advantageous due to its ability to eliminate a significant amount of the background signal observed in many fluorescent-based readout methods is the Meso Scale Discovery assay (MSD)[78]. To do this, MSD incorporates electrochemiluminescence, a technology that allows for light emission through chemical reactions, into their assay (**Fig. 2.11 A**).

The MSD assay utilizes antibodies that have ruthenium labels instead of fluorescent molecules, in which the label emits light upon a chemical oxidation reaction with an electrode (**Fig. 2.11 B**). MSD uses a dual-binder (sandwich) immunoassay format in 96-well microtiter plates to increase its throughput (**Fig. 2.11 C**). The plates used for this assay contain carbon ink electrodes on the bottom of the wells. These electrodes printed on the bottom of the plate act as both the solid phase for the antibodies to be immobilized onto, as well as the source of electrochemical energy to induce electrochemiluminescence of the ruthenium labels. The protocol for this method is very similar to a standard ELISA and differs mainly from the method of signal readout.

An initial capture antibody is immobilized onto the solid surface of the carbon electrode at the bottom of each well and the specific antigen binds to it following incubation with the sample. After multiple washing steps to remove non-specific interactions and unbound molecules, the detection antibody tagged with a ruthenium label is introduced to bind to another epitope on the target protein. The plate is subsequently washed and the signals are measured using a proprietary plate reader (**Fig. 2.11 D**)[79].

The greatest benefit of this technology is its method to reduce the background signals by eliminating the measurement of any autofluorescence from the sample. However, due to the planar nature of this technology, the MSD platform has limited potential to scale up since they require the antibodies to be immobilized onto the bottom of their plates, limiting their number of protein targets to approximately 10 per plate. Furthermore, since the MSD platform requires proprietary microtiter plates and plate readers, there are also increased costs associated with its use.

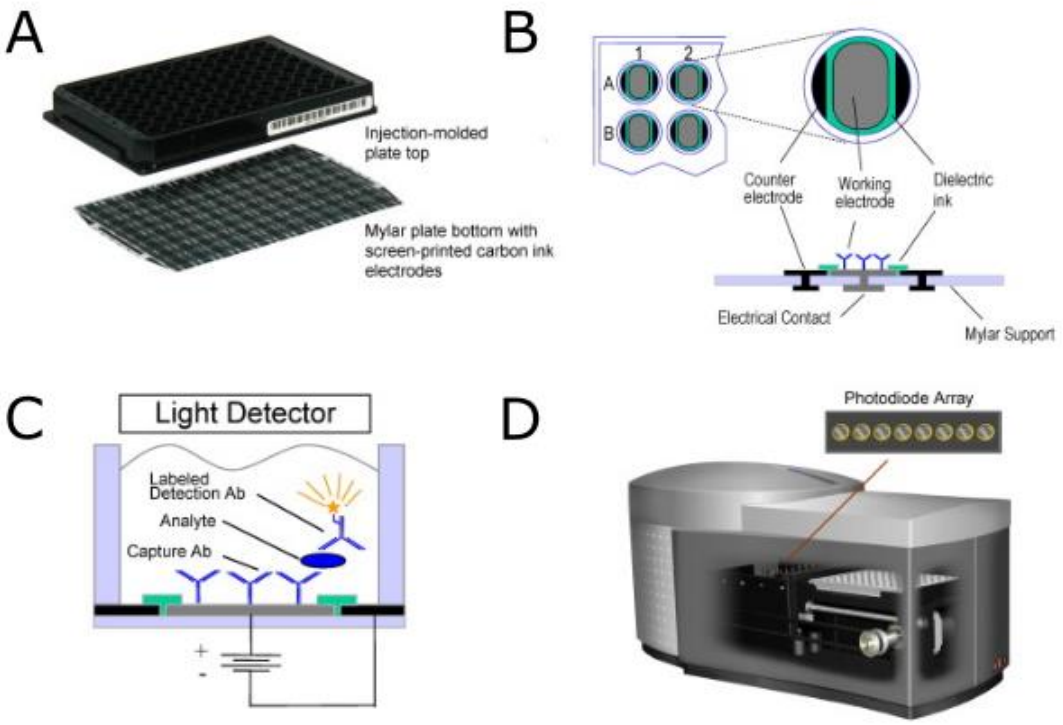

Figure 2.11 | Meso Scale Discovery Assay. (A) An exploded view of the MSD plate system that is composed of an injection molded plate top and a screen-printed Mylar plate bottom. (B) Schematic of the electrodes and the antibodies that make up a single well. (C) A schematic of a sandwich immunoassay with electrochemiluminescent detection. (D) Partially transparent view of the Sector PR 400 plate reader which can induce ECL one column at a time. Reproduced from ref. [78] with permission from Elsevier, copyright 2007.

2.5.1.3 nCounter Analysis System

Through amplifying the generated signal or incorporating ECL for measurement, one can significantly increase the sensitivity of the assay. The nCounter platform was first established in academia but later commercialized by Nanostring[80]. The nCounter platform achieves higher sensitivity by allowing single-molecule counting through means of digitally counting the occurrences of specific fluorescent barcodes in solution, as opposed to quantifying the signal generated[81]. The nCounter was first devised to precisely count RNA targets but has been adapted to permit the measurement of proteins. Like immuno-PCR, the nCounter platform measures proteins by utilizing antibody-oligo conjugates. However, these oligos differ in that they include sequences that bind specifically to a unique probe sequence for each protein target. A schematic

for the assay is shown in **Figure 2.12**. Upon antibody-binding to the protein(s) of interest, the DNA oligo probe is cleaved off and hybridized to a capture and reporter probe. The capture probe hybridizes to the cleaved probe with a universal sequence, while the reporter probe sequence is unique to each protein target. The capture probe includes a biotin at one end of its sequence which immobilizes the oligos on a solid surface, whereas the reporter probe includes a specific barcode composition at its end. Each barcode incorporates six spots which can have one of four different fluorophores at each spot to give each protein target its own unique barcode. After hybridization of the probes to the specific reporter and universal capture probes, the complex is bound onto the solid surface of the cartridge, in which an electric current is subsequently passed to align and stretch the complexes. After these steps, a picture is taken, and each specific barcode is digitally counted to permit quantification of captured proteins. The major advantage the nCounter platform achieves is its high sensitivity attributed from its ability to count single molecules. Furthermore, the majority of the nCounter technology is automated to allow for an ease of handling and workflow. However, the technology is also attributed to higher costs of reagents and equipment due to the need of such equipment. Furthermore, a big limitation is that although multiplexable in concept, nCounter technology does not use a dual-binder format, thereby having the risk of cross-reactivity to generate false-positive signals.

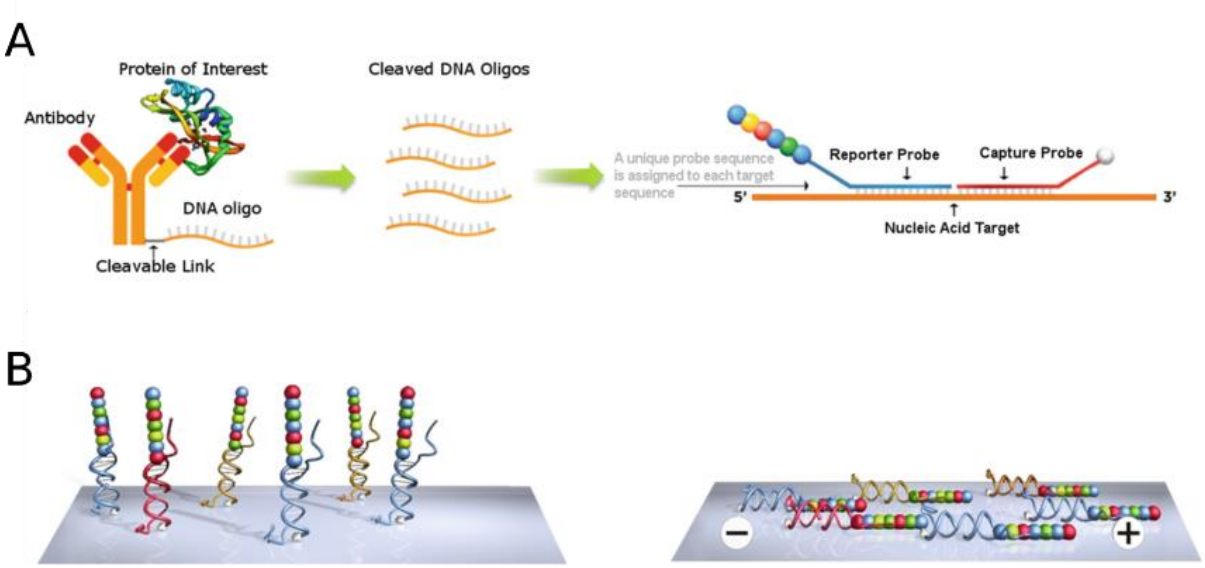

Figure 2.12 | nCounter Assay Workflow. (A) An antibody conjugated to a target-specific DNA oligo binds to its protein of interest that has been previously immobilized onto a solid surface. The unbound antibodies are removed and the cleavable link between the DNA oligo probe and the antibody is then cleaved. Afterwards, target-specific reporter probes and universal captures probes are incubated with the cleaved probes to complimentarily bind to their respective pairs. Upon hybridization, each unique DNA oligo probe has its own unique barcode from the reporter probe and a biotin from the capture probe. (B) The oligo complexes are immobilized onto a solid surface which is put into the nCounter machine. An electric current is passed across the surface to align and stretch the complexes so that a picture may be taken to clearly detect and count the unique barcodes, thereby quantifying the proteins. Adapted from ref.[81] with permission from Springer Nature, copyright 2018.

2.5.1.4 Single-Molecule Arrays (SiMoA)

The Single-Molecule Array (SiMoA) was first developed in academia and later commercialized to detect single protein molecules that had been labeled with an enzyme[82]. This technology focuses on isolating fluorescent labels in very low volume wells (~50 fL) to generate high effective fluorescent signals[2, 83]. SiMoA is ultrasensitive as each capture bead is introduced in excess into a sample with low target protein abundance. Poisson statistics dictates that the capture bead will bind to either one or zero protein molecules, making it impossible to detect the extremely low amount of enzyme labels using standard detection methods, such as a plate reader, as the fluorescence would be diluted in the larger assay volume and hundreds of thousands of enzyme labels would be required for a detectable signal above background level. Instead, the signal is

measured by acquiring time-lapsed fluorescence images of the full array using microscope optics to determine which wells in the array has a detectable signal ("on") and which wells had no associated enzyme with the bead ("off")[82]. Imaging these arrays allows for tens of thousands of immunocomplexes to be simultaneously measured.

In a SiMoA assay, the capture beads are incubated in excess into a sample with low target protein concentration to induce binding between them. The beads are then incubated with their respective detection antibodies tagged with enzymes and are loaded into an array of numerous femtolitre-sized wells that can only accommodate a single bead. Due to the spatial restriction of the array and given that each well will contain only a single or no bead, only a minority of wells will contain full sandwich immunocomplexes. Once the beads are confined in their respective wells, an enzymatic substrate is added, and each well is sealed with oil to decrease any well-to-well cross-contamination. Those with sandwich immunocomplexes generate a highly concentrated fluorescent signal in the well, while incomplete complexes do not. The array is analyzed using microscope optics to determine which wells had a detectable signal. The protein concentration is then determined by counting the number of wells containing a fluorescent product in respect to the total number of wells containing beads.

The assay workflow and signal generation are illustrated in **Figure 2.13**. Furthermore, through the use of different fluorescent dyes to barcode the beads used to capture the target, this technology also has the capability to be multiplexed[84]. The major advantage of this technology is its ultrasensitivity to detect proteins in very low concentrations which traditional sandwich immunoassays lack. However, the methods used to achieve the high level of sensitivity is not easily adaptable for multiplexed analysis, thus limiting their number of protein targets per assay.

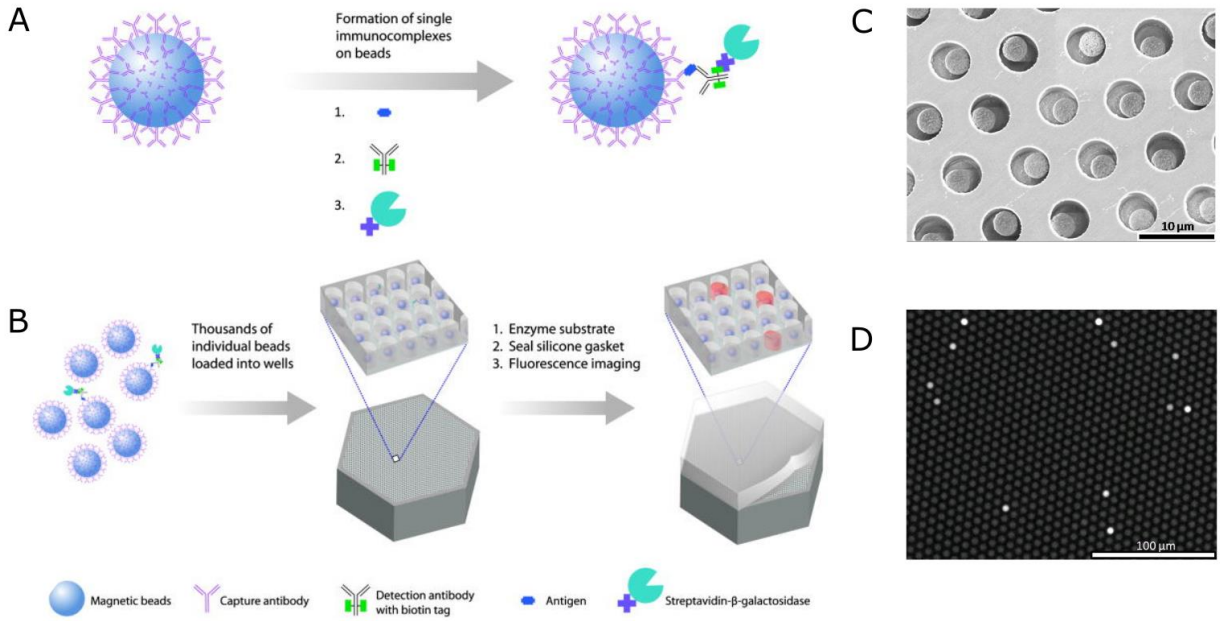

Figure 2.13 | SiMoA Assay Workflow. (A) Single target molecule (blue oval) binds to antibody-labeled beads and is subsequently bound by a biotinylated detection antibody. Streptavidin-β-galactosidase (blue plus and teal semi-circle) is incubated and binds to the detection antibody through a biotin-streptavidin interaction. (B) In assay conditions, an excess of antibody-immobilized beads are added to the sample containing very low concentration of the target protein so that only one or zero proteins will bind onto each bead. The beads are loaded into femtolitre-sized wells so that only one bead may fit into each well and is subsequently incubated with the enzyme substrate. The wells are sealed with oil and fluorescent images are taken of the array, in which the protein concentration is calculated. (C) Scanning electron micrograph image of the array containing single beads in the respective femtolitre-sized wells. (D) Fluorescent image of the array following signal generation via enzyme substrate incubation. Reproduced from ref. [82]with permission from Springer Nature, copyright 2010.

2.5.2 Overcoming Cross-Reactivity in Dual-Binding Multiplexed Assays

Potential for large numbers of proteins to be analyzed simultaneously by multiplexed sandwich assays, thus granting better cost- and time-efficiency, is a prerequisite for large-scale biomarker discovery studies. However, as discussed previously, current MSAs lack the ability to overcome the issue of cross-reactivity, preventing the potential to scale-up the number of protein targets due to the exponential generation of false positive signals. With multiplexed immunoassays, the greatest hurdle is the extensive optimization required to reduce the effects of cross-reactivity, dramatically increasing the time needed for assay development[71, 85], while still being subject to and

limited by reagent driven cross-reactivity . Technologies and strategies developed to overcome the issue of cross-reactivity include those that: (A) Developed novel affinity binders that operate as single-binder assays, (B) Use extensive antibody optimizations to create protein panels, (C) physically separated the capture and detection antibodies to prevent interaction, (D) designed DNA-assisted assays to prevent off-target interactions from generating a signal, and (E) colocalized the detection antibody onto a microparticle containing the capture antibodies. These technologies will be further detailed below.

2.5.2.1 Slow Off-rate Modified Aptamer (SOMAmers)

As a means to overcome combinatorial cross-reactivity in dual-binder multiplexed sandwich assays, an academic group led by Larry Gold replaced the use of antibodies as affinity binders with modified aptamers while reversing to a single-bainder assay and an assay protocol that minimized sample-driven cross reactivity, thereby removing the issue of extensive screening and optimization to scale-up[86]. This technology, termed the Slow Off-rate Modified Aptamers (SOMAmers), was further developed and later commercialized with SomaLogic SOMAmers minimize cross-reactivity events using aptamers that are modified to have slow off-rates in the place of conventional antibodies. As a result, any interactions with non-cognate proteins will dissociate very quickly, whereas specific target-binding events will dissociate more slowly, therefore increasing assay specificity[86].

Aptamers are short single-stranded oligos that can fold into diverse molecular structures and can bind to small molecules, peptides, and proteins[87]. By using a system called the Systematic Evolution of Ligands by EXponential enrichment (SELEX)[88], it has become possible to screen through large aptamer libraries and generate large panels of unique molecules. SOMAmers, the modified aptamers, include nucleotides that have different 5-position groups to confer unto them protein-like functional groups, increasing their specificity for the target protein of interest. The SOMAmer assay workflow is outlined in **Figure 2.14**. SOMAmers can mitigate non-specific interactions in a single-binder format by sequentially capturing, releasing, and re-capturing the bound complexes on two different sets of MPs and an anionic challenge. The main advantage of this technology is its high multiplexing capability, as well as the improved sensitivity and specificity from the slow off-rates. The use of SOMAmers in a single-binder format eliminates the need of a detection antibody, thus eliminating reagent-driven cross-reactivity. Furthermore,

SOMAmers also have sensitivities in the low-picomolar to high-femtomolar range, and with their continued development, have the capability for proteomic-level analysis[86]. However, although SOMAmers have the potential to overcome many of the inherent limitations that antibodies have, due to their DNA make-up, the modified aptamers have an overall negative net charge which complicates binding to c proteins. Furthermore, SOMAmers are also susceptible to rapid degradation via nucleases that are found in certain samples, and can thus require extensive sample-specific optimizations. Lastly, although SomaLogic claims that SOMAmers can significantly discriminate against non-specific binding interactions and thus do not require dual binders, they do not provide this validation, causing uncertainty as to what part of the protein the SOMAmers specifically bind to, as well as how they can address different protein isoforms.

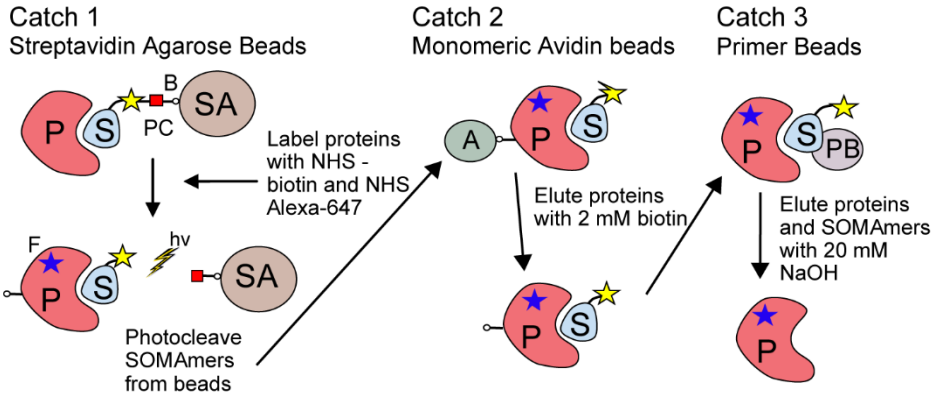

Figure 2.14 | SOMAmer Assay Workflow. SOMAmers are first incubated in the sample, and SOMAmer (S) – protein (P) complexes are formed. In Catch 1, these complexes are captured onto a streptavidin coated bead (SA) and the protein is tagged with biotin (B) and a fluorescent label (F). All unbound proteins are washed away, then S-P complexes are released from the SA bead using a photocleavable linker (PC). In Catch 2, S-P complexes are bound to a monomeric avidin bead (A), washed and released from the (A) beads with incubation of 2 mM biotin. At this stage, S-P complexes are subjected to a kinetic challenge similar to immunoassays, where specific S-P interactions will remain, and non-specific S-P interactions will dissociate. Finally, in Catch 3, specific S-P complexes are bound to primer beads (PB) through a DNA primer that is complementary to a sequence on the SOMAmer. Any dissociated complexes are washed away, and then the specific S-P complexes are dissociated from PB with 20 mM Sodium Hydroxide and the target protein is eluted for analysis by PAGE. Reproduced from ref. [86] with permission from the American Chemical Society, copyright 2007.

2.5.2.2 Luminex xMAP bead-based assay platform

The Luminex xMAP bead-based assay allows for high-throughput multiplexing through the use of microparticles (MPs) that have been internally barcoded with a unique combination of red and infrared fluorescent dyes[89, 90]. The surface of each barcoded MP is conjugated to capture antibodies that are specific to the target. Upon sample incubation and subsequent protein binding to the capture antibodies, the MPs are subjected to a series of stringent washes to remove any unbound and non-specifically bound proteins. Afterwards, biotinylated detection antibodies for all protein targets are added to the solution and bind to their protein targets that are immobilized onto the MPs. After another washing step to eliminate unbound antibodies, the streptavidin-tagged phycoerythrin reporter is incubated to generate a signal. This protocol provides fully formed sandwich immunocomplexes that have both an internal fluorescent emission to distinguish between the different target-specific MPs, and an external fluorescent emission to quantify the abundance of bound proteins.

After the sandwich complex forms, the MPs are analyzed using flow cytometers with optimized optical components for Luminex bead sets. Luminex-compatible cytometers use dual lasers to simultaneously detect the identity of each MP and measure the median fluorescence intensity (MFI) of the reporter for each specific target (**Fig. 2.15**).

This technology is currently the most popular MP-based platform and is regularly used in both academia and the clinic for various stages of drug development and biomarker discovery. The main advantage of the Luminex xMAP bead-based assay is its ability to perform multiplex experiments, significantly increasing the number of proteins that can be measured in a single sample. Furthermore, the use of MPs increases the range of detection over planar surfaces due to its higher surface area, while the use of two separate fluorescent signals to identify the target-specific MP and analyte signal allows for the MPs to be mixed a single solution.

As discussed in **Figure 2.8**, the xMAP technology can overcome sample-driven cross-reactivity using dual affinity-binders, which have higher tolerance to this form of cross-reactivity, as non-specific interactions on a single-binder do not contribute to signal generation. However, as outlined in **Figure 2.9**, scenarios of reagent-driven cross-reactivity increases with the number of antibody targets, scaling to 4N (N-1). The Luminex xMAP technology fails to address this issue, as there are no mechanisms in place to prevent these events from occuring. Instead, as the xMAP

technology relies on mixing detection antibodies in solution, extensive optimizations and screening must be performed to minimize antibody cross-reactivity in their protein panels. Hence, since each panel is extensively optimized to prevent antibody cross-reactivity, the xMAP technology cannot easily mix protein targets from different panels due to the potential of cross-reactivity without revisiting extensive optimizations. Although the xMAP technology offers extensive panels for specific areas of research, they lack the flexibility to customize these panels and add any proteins-of-interest, instead needing to measure the proteins in separate small panels. Furthermore, the use of Luminex technology can be expensive since it requires proprietary MPs, reagents, and a modified flow cytometer to measure both the internal and external fluorescence of the MPs.

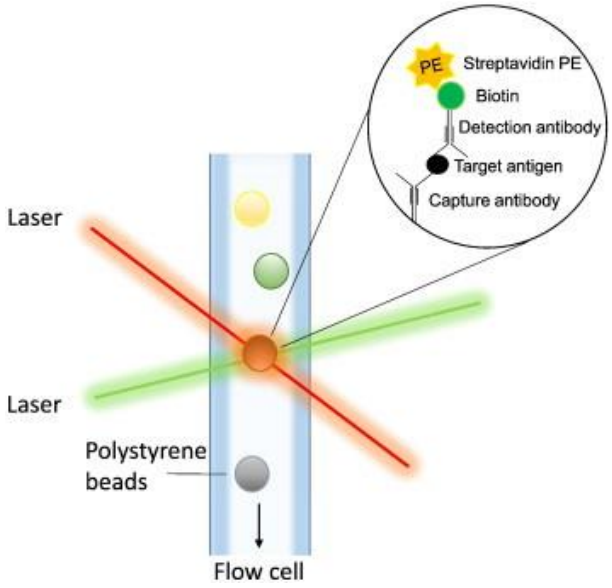

Figure 2.15 | Signal generation for Luminex xMAP System. The measured microparticle has capture antibodies attached onto the surface that are specifically bound to a target antigen. A biotin-tagged detection antibody binds to a separate epitope on the target, and with subsequent binding from the streptavidin-pycoerythrin reporter, a detectable signal is generated. Within the Luminex analyzer, two lasers are used to gather fluorescence intensity data from the microparticles. One laser is used to classify each microparticle's identity from its internal fluorescent reading, while the other laser detects the fluorescence intensity given off by the reporter fluorophore. Reproduced from ref.[91] under CC BY 3.0.

2.5.2.3 Antibody Colocalization Microarray (ACM)

Although the xMAP technology offered a method of extensive multiplexing capability, they lacked in the ability to target and add any protein of interest to a panel due to the need of extensive antibody optimizations. The need for such optimizations can be overcome by physically separating the capture and detection antibodies, so that the reagents of two different targets do not have the opportunity to interact, thereby eliminating reagent-driven cross-reactivity.

The Antibody Colocalization Microarray (ACM) was developed in our lab at McGill University and was created on the concept of reducing cross reactivity by printing the detection antibodies directly atop the corresponding capture antibodies. Since the detection antibodies are not mixed with one another as in traditional multiplexed immunoassays, the different targeted antibodies cannot mix and interact with off-target proteins and affinity binders. Due to this, the same level of specificity of ELISA can be achieved[58, 71].

First, microscope slides are printed with capture antibodies using a microarray printer. Afterwards, upon blocking and incubating the sample with the spotted slides, the slides are dried and spotted with biotin-tagged detection antibodies over the respective capture antibodies with great accuracy using the microfluidic spotter. This method allows for the measurement of many different proteins on the same microscope slide, in which each spot is specific for a certain protein. The slides are then incubated with a streptavidin-tagged reporter molecule (*i.e.*, *Alexa-Fluor 647*) and observed on a fluorescence scanner to detect its binding. The workflow of the ACM is outlined in **Figure 2.16**.

Parallex BioAssays, a spinoff company from the Juncker Lab, has further engineered this technology by greatly improving its convenience with the introduction of the SnapChip. This technology overcomes the constraint of requiring an expensive spotter on-site to spot the antibodies onto the slides. This is done by preparing the spots on the slides beforehand and transferring of reagents from spot-to-spot simply by snapping the two slides together[92]. As this method allows the arrays to be stored, it eliminates the need for extensive periods of antibody spotting during the experiment.

The major advantage of this technology is its ability to overcome the issue of reagent-driven cross-reactivity by preventing the detection antibodies from interacting to off-target proteins and

antibodies. Furthermore, unlike the xMAP platform, the ACM allows for proteins-of-interest to be easily incorporated in analysis. Also, the protocol and handling of the reagents for the ACM technology are uncomplicated, in which the experimental protocol is very similar and translatable to other immunoassays. However, since the ACM relies on a planar format, there exists a trade-off between multiplexing capability and the spotting time needed—highly multiplexable formats will require more antibody spots, thus requiring a longer duration of time for spotting. The increase in spotting time further results in a decrease in sample throughput. Furthermore, the potential issues due to the different length of time the antibodies remain on the slide (*i.e.* between the first and last spotting round), and in the case of the SnapChip, the technical requirement to transfer reagents from one slide to the other could impact its reproducibility, while the requirement of a microarray scanner and proprietary slides can increase the cost requirements. Lastly, although antibody colocalization restores ELISA-like conditions at the nanoscale, the requirements of precise fluidic delivery tools and the reliance on a planar format hinders this technology from being widely used compared to the other technologies mentioned in this section.

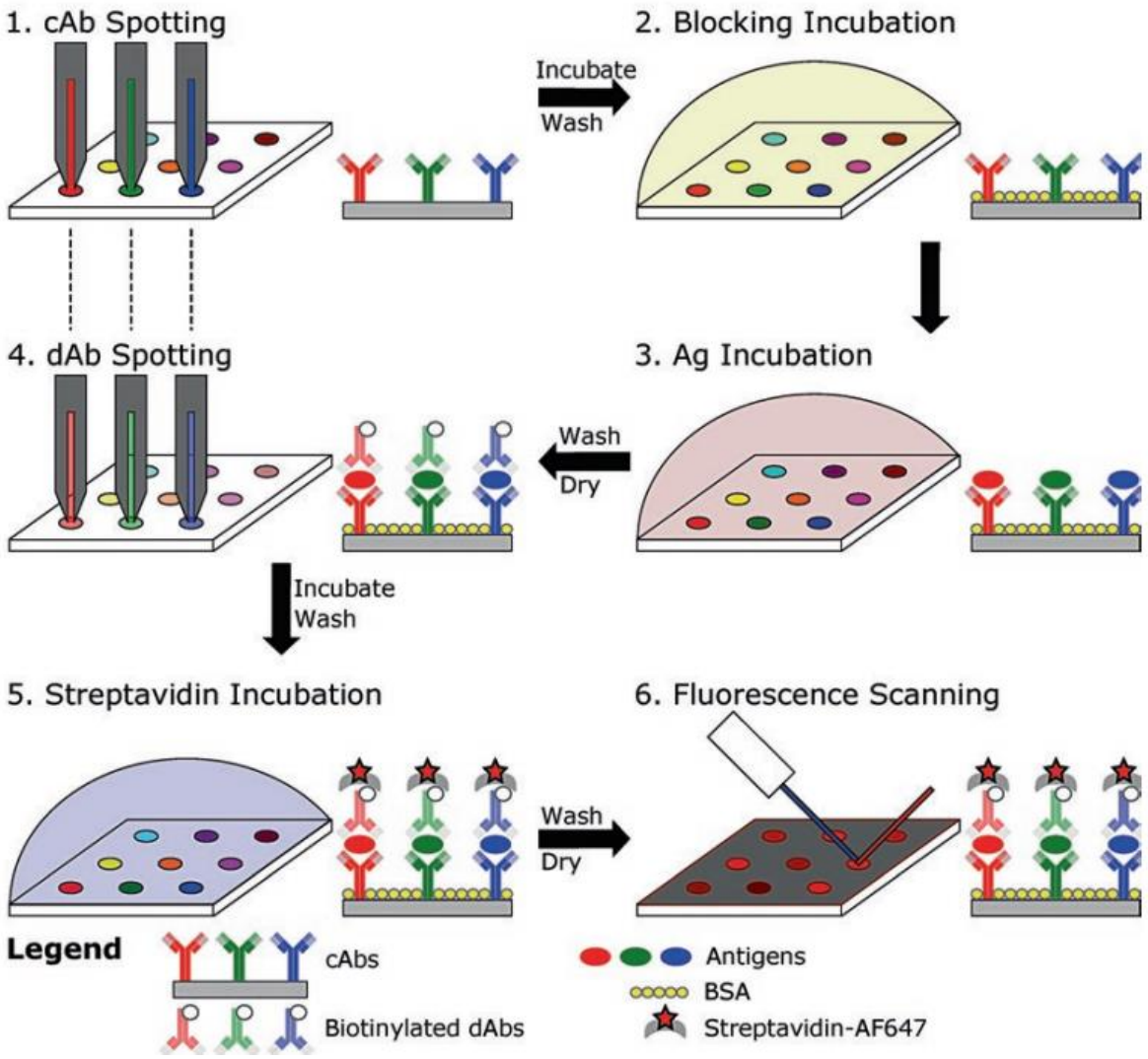

Figure 2.16 | Antibody Colocalization Microarray Assay Workflow. (1) Capture antibodies are spotted onto a glass slide using silicon quill pins and incubated for 24 h. (2) Spotted slides are then washed and blocked. (3) The slide is incubated overnight with the sample and antigen standard at 4°C. (4) Slides are washed and dried before printing the correct biotinylated detection antibodies onto the spots. (5) Slides are incubated for 16 – 24 h before washing, and then incubated with fluorescent streptavidin to bind to the biotinylated detection antibodies. (6) After washing and drying the slides, they are scanned with a fluorescence scanner to determine antigen binding and concentration. Reproduced from ref. [58] with permission from Springer Nature, copyright 2017.

2.5.2.4 Proximity Ligation Assay (PLA) and Proximity Extension Assay (PEA)

A novel method of eliminating cross-reactivity from non-specific interactions was developed incorporating DNA to increase the specificity and sensitivity of the assay. Developed in academia

by Landergren and his team, antibodies tagged with specific DNA oligos are used to form immunocomplexes that bring the attached oligos to proximity to each other. Termed the proximity ligation assay (PLA), the two oligos are ligated upon incubation of their reagents, and subsequently amplified and detected via quantitative polymerase chain reaction (qPCR)[93]. PLA, as well as the proximity extension assay (PEA), were later commercialized by Olink, offering extensive panels for protein measurement. PEA was introduced as an alternative to PLA since the proximity probes joined via DNA ligase suffered from a loss of recovery in complex samples[94].

PEA operates very similarly to PLA, relying on conjugation of complimentary oligos onto each of two separate antibodies against the protein target. These paired antibodies are analogous to capture and detection antibodies in sandwich immunoassays, in that they target two separate epitopes on the target protein. Upon both antibodies binding to the protein, the two oligos are brought in close proximity to one another. The matched oligos complementarily hybridize together, which minimizes non-specific interactions as mismatched oligo probes cannot hybridize to one another. Afterwards, DNA polymerase is added, thereby extending the sequence for amplification and analysis by qPCR. The steps of the PEA workflow are indicated in **Figure 2.17**. Upon signal readout, the analyte concentration in the sample can be determined from its direct proportionality to the number of templates measured[85, 93].

The main advantage of this method of protein analysis is that it dramatically reduces the issue of reagent-driven cross-reactivity from multiplexing by relying on matched oligos to be within proximity of each other to generate the measured signal. Although the cross-reactivity events outlined in **Figure 2.9** still occur in solution, no observable signal is generated upon only one of the antibodies binding to the target or in the case that both bind but are too far apart, in which both scenarios are more likely to occur for non-specific targets rather than the affinity-based target[95]. In the event of mismatched pairs being in proximity to one another, for example due to reagent-driven cross-reactivity to the target, an observable signal is not generated as the oligo sequences are unique for each matched pair, and mismatched oligos will not hybridize, and will not be ligated or extended, and thus not generate a signal. Other advantages of the PEA are that it has a fast and rather simple experimental protocol, can be adapted to use lower affinity antibodies without much optimizations, and has a method of signal amplification via PCR. However, while protein recognition is performed in a multiplexed format, amplification of the DNA via qPCR is performed

separately for each target. Since PCR is not designed for specific strand amplification in a multiplexed context, samples must be fractionated into isolated PCR reactions, which requires microfluidic qPCR chips, thus considerably limiting the efficiency and scalability of this technology. Additionally, in the unlikely event that false-positive signals are generated, they would also be amplified due to the extreme sensitivity of qPCR, complicating and giving false results.

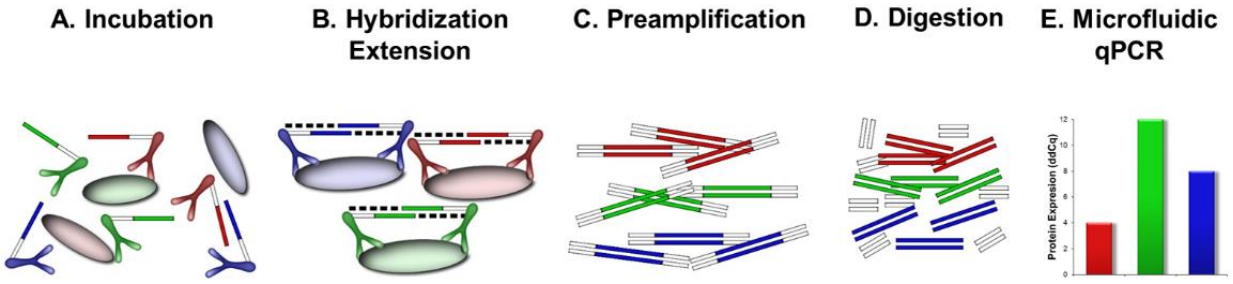

Figure 2.17 | Proximity Extension Assay Workflow. (A) Each antibody conjugated with a specific oligo sequence is incubated in the sample containing the target proteins (ovals). (B) Upon sample incubation and binding of the proximity probes onto the target proteins, the oligos of the matching probes are brought near one another and hybridize. Addition of DNA polymerase extends and joins the two oligos to form a PCR template. (C) Universal primers are used to pre-amplify the different DNA templates in parallel. (D) Incubation of uracil-DNA glycosylase partly digests the DNA templates and removes any unbound primers. (E) The individual DNA sequences are amplified, detected, and quantified with the use of specific primers with microfluidic qPCR. Reproduced from ref. [85] under CC BY 4.0.

2.5.2.5 Colocalization-by-Linkage Assay on MicroParticles (CLAMP)

Finally, the colocalization-by-linkage assay on microparticles (CLAMP) technology was developed in the Juncker Lab at McGill University and is being further developed by a spin-off company, nplex biosciences. The fundamental principles of the CLAMP technology are similar to those of the Luminex xMAP system, as both systems rely on MPs in solution and incorporate the use of two different fluorescent signals: one distinguishes between the target-specific MPs, while the other is used to quantify the abundance of the target protein bound to the MP. In contrast to Luminex's internal fluorescent barcoding, the CLAMPs are barcoded using fluorescent oligos (barcoding oligos) that are hybridized to complementary oligos (capture oligos) immobilized onto streptavidin-coated MPs via a biotin-streptavidin linkage. Additionally, the CLAMPs also have biotinylated capture antibodies on the MP surface that are specific for the target analyte.

To complete the sandwich immunocomplex, the CLAMPs incorporate a detection antibody for the target analyte that is conjugated to an oligo (hook oligo), which itself is hybridized complementarily to a section of the capture oligo on the MP surface. To regulate the density of detection antibodies tethered to the MP, delicate control of the hook oligo is crucial. For this purpose, spacer oligos, which are capture oligos that do not include a complementary sequence for hook oligo binding, serve to regulate the density of the capture oligos and, by extension, the density of detection antibodies available on the MP surface (**Figure 1.3**).

Each target-specific CLAMP is analogous to an ELISA, in which two affinity binders specifically bind to the same target protein to generate a detectable signal. In this way, the CLAMP effectively circumvents the issue of reagent-driven cross-reactivity as the affinity binders for each target are isolated onto their respective MP, eliminating the potential for different target reagents to interact with one another. After protein incubation and formation of sandwich immunocomplexes, the addition of a fluorescent displacement oligo releases the hook oligo tether from the MP surface. This occurs through toe-hold mediated displacement, in which the displacement oligo preferentially binds to the hook oligo, generating a fluorescent signal from the sandwich immunocomplex. The only interaction localizing the fluorophore to the MP is the target-specific interaction of the fluorophore-bound detection antibody with the target protein (**Figure 2.18**). The fluorescent displacement step is critical to achieve low background signals and decrease noncognate interactions as it eliminates any off-target interactions; signal will only be produced when the tethered detection antibody is bound to its specific-analyte, and any noncognate partners are washed away through vigorous washing steps.

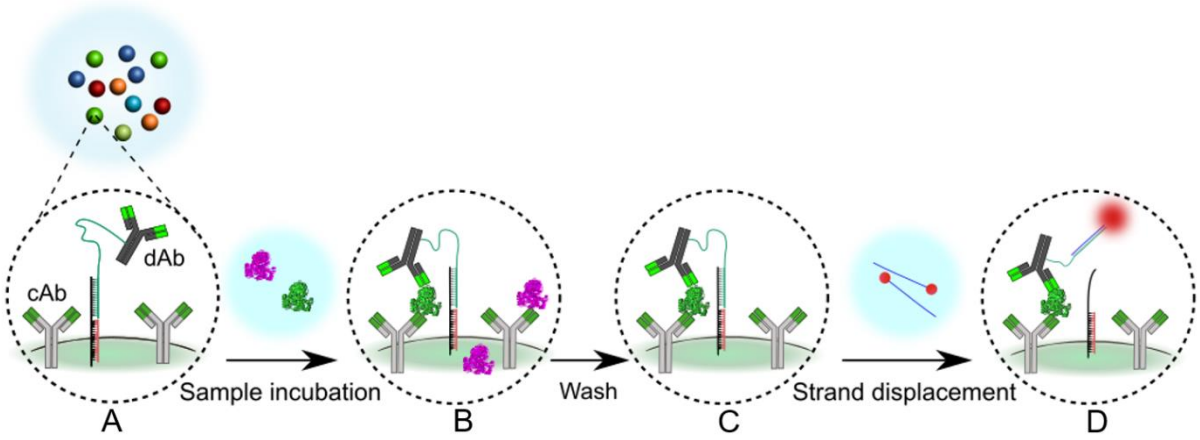

Figure 2.18 | CLAMP Assay Workflow. (A) Each colored sphere represents a CLAMP for a different target. Each CLAMP has capture antibodies, spacer oligos, and capture oligos immobilized onto its surface via biotin-streptavidin linkage. The capture oligo is complementarily hybridized to a barcoding oligo (red), to generate a unique protein-specific fluorescent emission, and a tethered hook oligo (green), to link the detection antibody onto the MP. The CLAMPs are mixed together and suspended in solution. (B) Upon blocking and incubating the sample, specific (green protein) and non-specific interactions (purple protein) between antibodies and analyte will take place. However, only the specific cognate interactions will typically form a full sandwich immunocomplex, as two non-specific interactions are unlikely. (C) After the sample is incubated, vigorous washing take place to remove non-specific interactions that may have occurred during sample incubation. (D) The displacement oligo is added and incubated in the solution, which displaces the detection antibody through toe-hold mediated displacement. The detection antibody is now tethered onto a fluorescent oligo and remains on the CLAMP only through its specific binding to the target analyte. Reproduced from ref. [20] with permission from author, copyright 2018.

2.6 Summary and Potential for CLAMP

The technologies previously mentioned can overcome the issue of low sensitivity by simply amplifying the signal, decreasing the background signal using electrochemiluminescence, or through single-molecule digital counting. Furthermore, cross-reactivity in multiplexing is overcome using aptamers with off-rate optimizations, rigorous optimizations of antibodies, use of proximity and the prerequisite of proper sandwich immunocomplexes, as well as mechanically separating the affinity binders. However, current technologies are still limited in scaling up and throughput. For example, Luminex overcomes cross-reactivity through extensive optimization of antibody pairs, theoretically allowing for high multiplexing capability. However, this not easily

met. Furthermore, more sensitive techniques such as Meso Scale Discovery, immobilizes their antibodies onto the bottom of their 96-well microtiter plates which limits their capability of scaling up.

On the other hand. the CLAMP platform has the potential for overcoming cross-reactivity by colocalizing the detection antibodies onto MPs with immobilized capture antibodies. This overcomes reagent-driven cross-reactivity similarly to ACM by physically separating the different target affinity binders and preventing them from interacting. Furthermore, due to its simple fluorescent readout via flow cytometry, the platform also has the potential to be easily scaled up with high-throughput. Additionally, as the CLAMP utilizes a suspension-based approach, the platform offers more flexibility, ease-of-handling, improved mass transport, and statistical robustness compared to the ACM platform. Although the CLAMP platform cannot yet match ultrasensitive protein assay technologies in terms of sensitivity, the CLAMP platform offers a cost-efficient method to scale-up the number of proteins measured, allowing the flexibility to easily add protein targets to the cohort being measured, unlike the xMAP platform for example. As the CLAMP relies on the use of MPs and flow cytometry for rapid signal readout, it is not limited in scalability like the proximity assays (PLA and PEA) are from their inherent requirement of a microfluidic qPCR chip. Due to these reasons, the CLAMP platform could fill the need of an MSA that is cost-efficient and highly multiplexable, while still offering gold-standard ELISA-sensitivity.

However, for the CLAMP platform to measure clinical samples accurately, optimizations of the fabrication and assay workflow are required to maximize signal generation while minimizing background signal. Moreover, an optimal mimic buffer must be found to accurately represent the complex sample matrix of blood plasma to calculate the protein concentrations from the respective standard curves. These optimizations will be highlighted in the subsequent sections.

3 | Materials and Methods

In this chapter, the step-wise process of CLAMP fabrication is detailed consisting of the following steps: (1) the conjugation of antibodies to oligos, (2) the functionalization of MPs with biotinylated oligos and antibodies, and (3) the pulldown of the antibody conjugates onto the functionalized MPs. The current CLAMP assay protocol is outlined and is followed by a detailed account of several key optimization experiments that were necessary for its development. Early stages of optimization focused on minimizing false-positive signals that emerged from the released DNA constituents binding non-specifically to the MP surface. Subsequent optimizations to the CLAMP assay modified factors such as capture oligo density, antibody conjugation valency, and sample incubation periods. Following the optimizations of the CLAMP assay, this chapter concludes with the optimization and selection of a mimic buffer to produce reliable and meaningful protein standard curves. Of note, selecting an appropriate mimic buffer is critical for the accurate measurement of clinical blood plasma samples, which will be required to transition the CLAMP platform from the laboratory to practical applications in the future.

3.1 CLAMP Procedures

This section discusses the CLAMP fabrication protocol and encompasses all of the steps required to create functional CLAMPs from DNA oligos, antibodies, and streptavidin-coated MPs. Furthermore, this section details the steps to perform the CLAMP assay.

3.1.1 Formation of the CLAMP: Antibody-oligo conjugation, purification, and characterization

CLAMP fabrication is a multi-step process that begins by conjugating monoclonal detection antibodies to an oligo tether (hook oligo), and subsequently purifying the antibody-oligo (Ab-O) conjugates from the non-reacted hook oligos. The thiol-terminated hook oligos were selected to facilitate conjugation through a cross-linking reaction that leverages a thiol-reactive heterobifunctional linker to target oligo conjugation to a primary amine on the antibody. Finally, the Ab-O conjugates were purified using Protein G beads to remove any free-DNA remaining in the solution, a critical step to prevent unreacted hook oligos from binding to the capture oligo during CLAMP fabrication.

These protocols were previously established in the Juncker lab[20], and are described in detail below.

For Ab-O conjugation, 40 µL of 30 µM thiol-modified hook oligos were reduced at 37°C for 1 h in phosphate buffered saline (PBS) with 0.05% Tween20 (PBST0.05) supplemented with 200 mM DTT. The reduced hook oligos were then buffer exchanged into pH 7.0 PBS using a Zeba desalting spin-column (7K MWCO, Thermo Scientific) and activated for ten minutes using 8 µL of 9 mM sulfosuccinimidyl 4-(N-maleimidomethyl) cyclohexane-1-carboxylate (sulfo-SMCC) dissolved in a solution of pH 7.0 PBS (80%) and anhydrous dimethyl sulfoxide (20%). Following activation, the buffer was exchanged to pH 7.0 PBS to remove excess sulfo-SMCC, in which 90 pmol of activated hook oligos were combined with 10 µL of 1 mg/mL monoclonal antibodies. This reaction was incubated at room temperature (RT) for 1 h, then at 4˚C overnight. Following completion of Ab-O conjugation, the solution was incubated with Protein G-coated MPs (Dynabeads™ Protein G, Invitrogen) to isolate both the conjugated and unreacted antibodies from the unreacted hook oligos, according to the manufacturer's protocol. The purified antibody mixture was then evaluated using SDS-PAGE and subsequent silver staining to estimate the concentration of the Ab-O conjugates. For this purpose, samples were first heated to 80°C for 10 minutes in LDS-containing sample buffer (NuPAGE™, Novex), then loaded in a 3-8% NuPAGE Tris-acetate gel. The gel was left to run at 150 V for 1 h in 1X NuPAGE™ Tris-acetate SDS running buffer. Upon completion of the gel, both the proteins and nucleic acids were visualized with silver staining (Pierce™ Silver Stain, Thermo Scientific) according to the manufacturer's protocol. Band intensities were measured and compared using the Fiji distribution of ImageJ (Rasband W., NIH[96, 97]), and then used to estimate the concentration of the Ab-O conjugates, in addition to their average conjugation valency.

3.1.2 Formation of the CLAMP: Barcoding and Assembly of Antibody-Oligo conjugates on MPs

Once Ab-O conjugation was completed, streptavidin-coated MPs were functionalized with DNA-based constituents and antibodies to prepare them for the pulldown of the Ab-O conjugates, thereby completing the fabrication process to generate CLAMPs for a specific protein target.

First, streptavidin-coated MPs were spectrally barcoded by binding fluorescently labeled oligos (barcoding oligos). Four different fluorophores were incorporated in the spectral barcoding and were used in combination to generate unique barcodes for each batch of protein-specific CLAMPs.

The four fluorophores used were: Atto-488, Cy3, Cy5, and Cy5.5. The ratios of fluorophores for barcoding were selected in coordination with a spectral fluorescence arrangement to avoid signal overlap between barcodes; this a crucial consideration to avoid confounding effects of overlapping excitation/emission spectra and unfavorable interactions such as Förster resonance energy transfer (FRET)[20, 98]. Following the determination of barcode ratios, the barcoding oligos were annealed to the biotinylated capture and spacer oligos by heating them in solution to 70°C for 10 min and subsequently cooling the solution to RT for at least 20 min. The proportion of capture oligo to spacer oligo used allowed for the fine-tuning of Ab-O conjugates that would be pulled down onto the surface of the CLAMP. After annealing the DNA for barcoding, 25 µl of a barcoding solution was prepared by mixing the following biotinylated reagents together: (1) 6.7 pmol of IgG antibody, and (2) 90 pmol of barcoding oligos (*i.e.*, 20 pmol Atto-488, 20 pmol Cy3, 50 pmol unlabeled) annealed to biotinylated spacer and capture oligos in PBST0.05 + 300 mM NaCl. The biotinylated solution was added to 3.25 x 10^6 streptavidin-coated MPs (M270-Streptavidin, Life Technologies) suspended in 25 µl PBST0.05 + 300 mM NaCl, at which point the mixture was incubated for 1 h at RT, rotating vertically to ensure constant agitation. Following the incubation, the barcoded MPs were washed three times with PBST0.1 and stored at 4°C in the dark. These barcoded MPs were stored at 4°C until needed, in which 1.0 x 10^5 of the barcoded MPs were mixed with its corresponding Ab-O conjugate for 1 h at RT, rotating vertically. After pulling down the Ab-O conjugates, the fully-formed CLAMPs were washed three times in PBST0.05 and stored at 4°C for use.

3.1.3 Optimized Assay Protocol

The current optimized protocol is detailed below. All other protocols used in this work are also included in this chapter, however only the deviations from the optimal protocol are highlighted.

The amount of each respective CLAMP required for the experiment were aliquoted from their stock solutions stored at 4˚C. The CLAMPs were subsequently blocked in PBST0.05 + 150 mM NaCl + 0.5% BSA for 1 h at RT, rotating vertically. 25 µl of the blocked CLAMPs were added to their appropriate wells in a 96-well microtitre plate and mixed with 25µl of sample (*i.e.*, diluted antigens for standard curve generation) for a final well volume of 50 µl. The plate was then covered with aluminum sealing tape and incubated overnight at 4˚C, shaking at 950 rpm. The following day, the plate was removed and washed four times with PBST0.1. Afterwards, 32µl of PBST0.05

+ 450 mM NaCl was then added to resuspend the CLAMPs in each of the occupied wells. Each of these wells were mixed with 8 µl of 5 µM displacement oligo to facilitate toe-hold mediated displacement of the hook oligo. The plate was incubated for 1.5 h at RT, shaking at 950rpm. After displacement, the plate was washed four times with PBST0.1 and reconstituted with 60 µl of PBST0.1 for signal readout via flow cytometry. Using flow cytometry, the median fluorescence intensities (MFI) for each barcode was measured for further analysis. The spectral barcode of each CLAMP was decoded in MATLAB (Mathworks) to acquire their target protein identity, and the associated sample MFI data was analyzed using MATLAB and PRISM (Graphpad) to generate graphical representations for data interpretation.

3.2 Optimization of CLAMP parameters

Several optimizations were performed to minimize the nonspecific binding events of the DNA and antibody CLAMP constituents to the MP surface. These events could contribute to higher background signals due to false positive signals, thereby decreasing the sensitivity of the assay. To investigate any such nonspecific binding, MPs were specially functionalized to identify the steps of CLAMP fabrication that may introduce such interactions. Furthermore, the effect that cold storage could have on CLAMP viability was also a concern; additional experiments were designed to investigate whether long-term cold storage would be detrimental to CLAMP signal generation. Additionally, the possibility that such storage conditions could impair antibody viability or otherwise contribute to increased non-specific binding events of CLAMP constituents to the MP surface were investigated. Lastly, remaining assay parameters to be optimized included the ratio of capture oligos to spacer oligos on the MP surface, Ab-O conjugate valency, and the duration of sample incubation to maximize signal whilst minimizing background.

3.2.1 Fabrication of functionalized MPs

To test for nonspecific binding of antibody and DNA CLAMP constituents to the MP surface, five quality control-specific MPs (QC-MPs) were created. The five QC-MPs are detailed below, and consisted of: (1) bare streptavidin-coated MPs, (2) DNA-only MPs lacking any capture antibodies, (3) antibody-only MPs lacking any DNA components, (4) DNA and antibody (Combination) MPs, and (5) DNA-only MPs lacking a docking domain (see figure. 4.1 for more details).

Bare streptavidin MPs (QC-MP-1) consist of the stock streptavidin dynabeads, which are then washed and blocked using identical protocols to those used to fabricate CLAMPS. These MPs served as a negative control and were used to assess the impact of nonspecific-binding of both antibodies and DNA on the streptavidin-conjugated and BSA/tween-blocked bead surface.

The DNA-only MPs (QC-MP-2) were coated in pre-annealed capture and barcoding oligos, thus making available single-stranded sequences for hook oligo binding. These MPs served as a positive control for DNA binding, in which the hook oligo could hybridize onto the capture oligo to produce a fluorescent signal. These QC-MPs were produced by first annealing 10 µM of biotinylated capture oligos to an excess of barcoding oligos by incubating the mixture at 84°C for 10 min, followed by a 20 min cooldown step at RT. Afterwards, a 25µL volume of annealed oligos was pulled down onto approximately 1.6 x 10^7 streptavidin-coated MPs by incubating the mixture for 1 h at RT, rotating vertically.

The antibody-only MPs (QC-MP-3) were coated solely with anti-rat IgGs, presenting no available binding sites for DNA. These MPs served as a negative control for DNA binding, as there were no DNA binding sites available for hook oligo binding. These QC-MPs were created by pulling down 1 µg of biotinylated anti-rat IgGs onto the surface of approximately 1.6 x 10^7 streptavidin-coated MPs by incubating the mixture for 1 h at RT, rotating vertically.

The Combination MPs (QC-MP-4) were coated in equal amounts of DNA and antibody, a hybrid of the above DNA-only MPs and antibody-only MPs. These MPs served to test nonspecific binding of DNA and antibody constituents on a surface that closely resembled that of a functionalized CLAMP. These QC-MPs were functionalized by pulling down 1 µg of biotinylated anti-rat IgG, in addition to 10 µM of the previously described annealed DNA mixture onto the surface of approximately 1.6 x 10^7 streptavidin-coated MPs by incubating the mixture for 1 h at RT with vertical rotation.

Lastly, the DNA-only MPs that lacked a docking domain (QC-MP-5) were coated in DNA comprised of shortened capture oligos (spacer oligos) annealed to barcoding oligos. Using these shortened DNA oligos should prevent hook oligos from binding due to the lack of a complementary docking sequence normally found in the capture oligo. Thus, these MPs served as an additional negative control as they did not have the single-stranded sequences available for hybridization of the hook oligo. Furthermore, these MPs can be compared to QC-MP-1 to

determine whether the presence of the DNA can promote increased nonspecific rebinding of CLAMP constituents. These QC-MPs were produced by first annealing 10 µM of biotinylated spacer oligos to an excess of barcoding oligos by incubating the mixture at 84°C for 10 min, followed by a 20 min cooldown step at RT. Afterwards, a 25 µL volume of annealed oligos were immobilized onto approximately 1.6 x 10^7 streptavidin-coated MPs by incubating the mixture for 1 h at RT, rotating vertically.

3.2.2 Quantifying DNA and Antibody Non-Specific Binding

To determine if the effects of nonspecific sticking can be observed in the CLAMPs, both DNA and antibodies were tested against the five QC-MPs mentioned previously.

Five different experimental conditions were investigated to quality control any nonspecific binding effects (QC-NSBs). The QC-NSBs varied in terms of the amount and type of DNA and/or antibody added in solution. All conditions used PBST0.05 + 300 mM NaCl as the buffer. The 5 conditions further consisted of: (1) 1 µM of displacement oligos (QC-NSB-1), (2) 1.8 µM of annealed hook and fluorescent labeling oligos (QC-NSB-2), (3) 1.8 µM of annealed hook and displacer oligos (QC-NSB-3), (4) 1 µg/ml Goat-Anti-Mouse-AF647 (QC-NSB-4), and (5) buffer only (QC-NSB-5).

The fluorescent labeling oligo introduced in QC-NSB-2 is an oligo that was designed to bind to a portion of the hook oligo sequence in which its binding did not disrupt either the tethering of the hook oligo to the antibody or the hook oligo's complementary binding to the capture oligo. This oligo was designed primarily to quality control the binding of the Ab-O conjugate onto the functionalized MP surface.

To test for nonspecific interactions, each of the five functionalized bead types were aliquoted from their stock solutions stored at 4°C and subsequently blocked in PBST0.05 + 150 mM NaCl + 0.5% BSA for 1 h at RT, rotating vertically. Next, 25µl of blocked, functionalized MPs were incubated with 25µL of each test condition in duplicate for a total of 25 different combinations in 50 separate wells. The mixture was incubated for 1 h, shaking at 950rpm in RT. After incubation, the respective wells were washed three times with PBST0.1 and resuspended in a final volume of 150 µl for readout via flow cytometry.

3.2.3 Effects of Cold Storage

A 27-day time-course series of four experiments were conducted to determine if prolonged 4°C cold storage of the CLAMPs negatively affected their viability and accuracy of protein measurement. In each of the four experiments (termed Expt. Storage-1 to Storage-4), a standard calibration curve was generated and several quality controls were used to determine the fluorescent signal and structural integrity of the CLAMPs, which ensured that the DNA and antibody constituents were not dissociating from the CLAMPs. These experimental conditions will be detailed further below.

First, CLAMPs targeting EpCAM were created following the fabrication protocol detailed previously. The experiments were then conducted on days 1, 4, 12, and 27 post-fabrication. An increasing amount of days between each timepoint was applied in order to observe any large changes in the fluorescent signal without excessively repeating the experiments, wasting the fabricated CLAMPs and reagents.

For these experiments, the EpCAM CLAMPs were first aliquoted from their stocks stored at 4°C and subsequently blocked in PBST0.05 + 150 mM NaCl + 0.5% BSA for 1 h, rotating vertically. After blocking, 25 µl of the CLAMPs were loaded into a 96-well microtiter plate, in which 25 µl of serially diluted antigen (EpCAM) in PBST0.05 + 150 mM NaCl + 0.25% BSA was mixed with the CLAMPs to generate a 10-point standard curve ranging from 1.00 x 10^3 fg/ml to 1.95 x 10^9 fg/ml in a 5x dilution series. Additionally, five negative control wells consisting only of the CLAMPs and PBST0.05 + 150 mM NaCl + 0.25% BSA were included to represent the background signal. The plate was then incubated for 1 h at RT, shaking at 950 rpm. Following incubation, the CLAMPs were washed four times with PBST0.1 and resuspended in 40 µl of PBST0.05 + 300 mM NaCl + 0.25% BSA. A volume of 10 µl of 5 µM displacement oligo in PBST0.05 + 450 mM NaCl was then mixed into the wells, in which each well had an effective displacement oligo concentration of 1 µM. Upon adding the displacement oligos, 25 µl of previously blocked CLAMPs in PBST0.05 + 300mM NaCl were added to three additional wells, and 50 µl of blocked CLAMPs was added to another single well. One of four quality controls were added to each of the four wells. In the three wells containing 25 µl of blocked CLAMPs, 25 µl of: (1) 5 µM displacement oligo (QC-Storage-1), (2) 4 µM donkey anti-goat-AF647 (QC-Storage-3), and (3) 4 µM goat-anti-mouse-Cy5 (QC-Storage-4) were added, respectively. In the well containing 50 µl

of CLAMPs, 50 µl of 2 µM labeling oligo (QC-Storage-2) was added. The quality controls were included to determine the integrity of the CLAMPs at a given timepoint. First, effectively 1 µM of the displacement oligo was used to ensure that there was no elevated background signal upon only displacing the tethered antibody. Furthermore, to determine the presence of the hook oligo, tethered antibody, and capture antibody on the CLAMPs, 1 µM of the labeling oligo, 2 µg/ml of goat anti-mouse-AF647, or donkey anti-goat-Cy5 were used to label them, respectively.

Following the addition of the displacement oligo and the quality controls, the plate was incubated for 1 h at RT, shaking at 950 rpm to facilitate fluorescent displacement and quality control labeling of CLAMP constituents. Following this incubation, the plate was washed three times with PBST0.1 and resuspended in 60 µl of the same buffer to be read out via flow cytometry. For the analysis of these time-course experiments, signal-to-background ratios (SBRs) were calculated to compare the results across different experimental days using equation (3):

$$SBR(target) = \frac{Mean\ of\ replicate\ sample\ MFI}{Mean\ of\ replicate\ blank\ MFI}$$

3.2.4 Assay Parameter Optimizations

The CLAMP assay was further optimized in order to determine an optimal CLAMP composition and experimental workflow that yielded maximum assay signal whilst still retaining minimal background signal. This optimization sweep was performed by first deducing the optimal capture oligo density on the MP surface. Next, an optimal Ab-O conjugate ratio was determined that minimized the proportion of multivalent Ab-Os. Finally, the duration of antigen incubation with the CLAMPs was established to maximize antigen binding whilst minimizing nonspecific binding from other constituents in the sample.

First, CLAMPs for IL-8 were fabricated using varying conditions to generate different barcoded CLAMPs for each experimental condition. The CLAMPs were created by first barcoding and functionalizing streptavidin-coated MPs with either 20 pmol, 40 pmol, or 80 pmol of capture oligos. The mixture was supplemented with spacer oligos to achieve 90 pmols of total DNA content on the MP surface, as well as 1 µg of biotinylated antibodies. During the conjugation step to fabricate the Ab-O conjugates for IL-8, an increasing amount of hook oligos were added to 10 µg of IL-8 antibody to create Ab-O conjugates of low, medium, and high oligo valency. The ratio of oligo:antibody was 0.35, 0.7, and 1.4 for low, medium, and high oligo valencies, respectively.

The higher oligo valencies had multiple hook oligos tethered to a single antibody, whereas the low oligo valency focused on maintaining a 1:1 ratio.

Upon functionalizing the surface of MPs and conjugating three groups of Ab-O conjugates, each of the three MP-groups with varying levels of capture oligo densities were mixed with each of the Ab-O valencies for hybridization onto the capture oligos. The three groups of Ab-O conjugates were combined with a proportional number of MPs; for instance, more MPs were required to hybridize the higher valency group than for the lower Ab-O valencies, as the higher valency group was more concentrated. The low and medium oligo valencies were pulled down onto 1.72×10^6 barcoded MPs of each capture oligo density, while the high oligo valency was pulled down onto 2.58×10^6 barcoded MPs. The pull-down mixture was incubated at RT for 1 h, rotating vertically.

After CLAMP fabrication, to determine the best combination of capture oligo surface density, Ab-O valency, and sample incubation duration, triplicate 10-point standard curves ranging from 2.56×10^2 fg/ml - 5.0×10^8 fg/ml following a 5x dilution series were generated. These standard curves were generated by first aliquoting the CLAMPs from cold storage and blocking them for 1 h at RT in PBST0.05 + 150 mM NaCl + 0.5% BSA, rotating vertically. Afterwards, 25 µl of the blocked CLAMPs were loaded into a 96-well microtiter plate and mixed with 25 µl of pre-diluted antigen. The plate was then incubated overnight (~12 h) at 4°C, shaking at 950 rpm. This plate included each of the three capture oligo surface densities, Ab-O valencies, and represented the overnight sample incubation condition.

Two other plates were prepared on the following day to test other durations of sample incubation. Briefly, another set of CLAMPs were blocked for 1 h, added to a separate 96-well microtiter plate, and subsequently incubated with antigen for 3 h at RT, shaking at 950 rpm. Lastly, 1 h into the second plate's antigen incubation, a third set of CLAMPs were blocked for 1 h and subsequently added to another plate to be incubated with antigen for 1 h, shaking at 950rpm in RT. Upon finishing their incubations, the three plates were washed four times with PBST0.1 and resuspended in 32 µl of PBST0.05 + 300 mM NaCl + 0.25% BSA. 8 µl of 5 µM displacement oligo was then added to each of the wells creating an effective displacement oligo concentration of 1 µM per well. The displacement oligo mixture was incubated for 1 h at RT, shaking at 950 rpm. These three plates contained each of the three capture oligo surface densities and Ab-O valencies, and also represented the three durations of sample incubation: 1 h, 3 h, and overnight. After incubation, the

plates were washed three times with PBST0.1 and resuspended in 60 µl of the buffer to be read out via flow cytometry.

3.3 Optimizing for Complex Sample Analysis

To begin mimic buffer optimization, the background signals of 12 different proteins were first measured in human pooled normal blood plasma (plasma from human, Sigma-Aldrich, cat. P9523), and several candidate mimic buffers were subsequently compared to the diluted normal blood plasma. Afterwards, once the candidate mimic buffers that most represented the background of the diluted blood plasma were selected, spike-in and recovery tests were performed to further evaluate how representative they were of the complex sample matrix. Furthermore, to dilute complex samples such as human blood plasma, PBST0.05 + 0.5% BSA was used as a "standard diluent", or the diluting buffer to simplify the matrix.

3.3.1 Measurement of Sample Backgrounds

First, the endogenous concentrations of the proteins must be established for the human blood plasma that was to be analyzed. For this purpose, CLAMPs for the following 12 targets were generated, following the fabrication protocol previously mentioned: IFN-γ, IL-8, IL-2, IL-12, GM-CSF, IL-10, IL-13, IL-17, IL-23, IL-4, TNF-α, and IL-1β. These CLAMPs were then aliquoted from cold storage and subsequently blocked in PBST0.05 + 150 mM NaCl + 0.5% BSA for 1 h at RT, rotating vertically. After blocking, the CLAMPs were buffer exchanged by pelleting the CLAMPs with a magnet, removing the buffer, and resuspending them in PBST0.05 + 0.5% BSA. Afterwards, 25 µl of the CLAMPs were added in multiplex into 12 wells of a 96-well microtiter plate and incubated with 25 µl of neat pooled human plasma (undiluted), effectively producing 1:2 diluted human blood plasma in each of the 12-replicate wells. The plate was incubated overnight at 4°C, shaking at 950 rpm. The following day, the plate was washed four times with PBST0.1, and then resuspended in 32 µl of PBST0.05 + 300 mM NaCl + 0.25% BSA. 8 µl of 5 µM displacement oligo was then added to each of the wells creating an effective displacement oligo concentration of 1 µM per well. The displacement oligo mixture was incubated for 1 h at RT, shaking at 950 rpm. After incubation, the plate was washed three times with PBST0.1 and resuspended in 80 µl of PBST0.1 to acquire its fluorescent intensity data via flow cytometry.

3.3.2 Measurement of Mimic Buffer Backgrounds

Following the detection of the endogenous level of proteins in the pooled human blood plasma, the background signals of 17 different buffer compositions were compared to PBST0.05 + 0.5% BSA, as well as to 1:2, 1:4, 1:6, and 1:8 diluted pooled human blood plasma. Furthermore, CLAMPs for TNF-α were used in further mimic buffer optimizations as the protein was found to have very low endogenous concentrations in the blood plasma that was being measured.

CLAMPs for TNF-α were aliquoted and blocked in PBST0.05 + 150 mM NaCl + 0.5% BSA for 1 h at RT, rotating vertically. After blocking, the CLAMPs were buffer exchanged to PBST0.05 + 0.5% BSA. 25µl of the CLAMPs were then added to a 96-well microtiter plate in triplicate and mixed with the complex portion of the respective mimic buffers, based on the mimic buffer compositions found in **Table 3.1**. For example, mimic buffer 1 consisted of 25 µl of CLAMPs in PBST0.05 + 0.5% BSA mixed with 20% mouse serum in PBST0.05 + 0.5% BSA to effectively make 10% mouse serum in PBST0.05 + 0.5% BSA. The plate was then incubated overnight at 4°C, shaking at 950 rpm. The following day, the plate was removed and washed four times with PBST0.1, and the wells subsequently resuspended in 32 µl of PBST0.05 + 300 mM NaCl + 0.25% BSA. 8µl of 5µM displacement oligo was added to each well and incubated for 1 h at RT, shaking at 950rpm. Following incubation, the plate was washed three times in PBST0.1 and resuspended in 60µl of the buffer for readout via flow cytometry.

Table 3. 1 | A summary of the 17 different candidate mimic buffer compositions.

Mimic No.	Mimic Composition
Mimic-1	10% mouse serum in PBST0.05 + 0.5% BSA
2	25% mouse serum in PBST0.05 + 0.5% BSA
3	50% mouse serum in PBST0.05 + 0.5% BSA
4	10% Fetal Bovine Serum (FBS) in PBST0.05 + 0.5% BSA
5	25% FBS in PBST0.05 + 0.5% BSA
6	50% FBS in PBST0.05 + 0.5% BSA
7	10% mouse plasma in PBST0.05 + 0.5% BSA
8	25% mouse plasma in PBST0.05 + 0.5% BSA
9	50% mouse plasma in PBST0.05 + 0.5% BSA
10	10% mouse serum + 10% FBS in PBST0.05 + 0.5% BSA
11	10% mouse plasma + 10% FBS in PBST0.05 + 0.5% BSA
12	25% mouse serum + 10% FBS in PBST0.05 + 0.5% BSA
13	25% mouse plasma + 10% FBS in PBST0.05 + 0.5% BSA
14	25% FBS + 10% mouse serum in PBST0.05 + 0.5% BSA
15	25% FBS + 10% mouse plasma in PBST0.05 + 0.5% BSA
16	10% mouse serum + 10% FBS + 10% mouse plasma in PBST0.05 + 0.5% BSA
17	50% mouse serum in PBS + 0.5% BSA

3.3.3 Validation of Mimic Buffer

Upon selecting two mimic buffers that closely represented the background of diluted blood plasma, they were further validated through spike-in and recovery tests (**Chapter 4.3** for more details) to select the one that better represented the complex sample matrix. The two candidate mimic buffer compositions being tested were: (1) 25% fetal bovine serum (FBS) in PBST0.05 + 0.5% BSA, and (2) 25% mouse plasma in PBST0.05 + 0.5% BSA.

First, standard curves were generated in each of the two candidate mimic buffers. Additionally, CLAMPs for TNF-α were incubated with known concentrations of the TNF-α antigen spiked into the diluted human blood plasma. The standard curve was fitted and graphically represented using

PRISM, and the spiked-in concentrations were calculated for each of the two mimic buffers. Furthermore, the percent recovery (% recovery) was calculated to determine how close the mimic buffer was to the expected spike-in concentrations. The % recovery was calculated using equation (2) from **Chapter 2.3.3**:

$$\%\ Recovery = \frac{Observed\ Concentration - Background\ Concentration}{Expected\ Concentration} \times 100$$

To generate the standard curves, CLAMPs for TNF-α were aliquoted and blocked in PBST0.05 + 150mM NaCl + 0.5% BSA for 1 h at RT, rotating vertically. After blocking, the CLAMPs were buffer exchanged into PBST0.05 + 0.5% BSA. 25 µl of the CLAMPs were added to the 96-well microtiter plate and mixed with 25 µl of the diluted antigens for the triplicate 12-point standard curve. The standard curves were generated in PBST0.05 + 0.5% BSA, as well as in the two mimic conditions: (1) 25% FBS in PBST0.05 + 0.5% BSA and (2) 25% mouse serum in PBST0.05 + 0.5% BSA. For these standard curves, double the amount of the antigen was added to the CLAMPs in double the concentration of each candidate mimic buffer. For example, 50% FBS in PBST0.05 + 0.5% BSA was used to add double the amount of the antigen to the CLAMPs to effectively incubate the proper antigen concentration and the correct mimic condition of 25% FBS in PBST0.05 + 0.5% BSA. The standard curves ranged from 20.5 fg/ml to 1.0 x 10^9 fg/ml in a 5x dilution series. Following the addition of each standard curve, 12 replicates of blanks (no antigen) were added for each of the three buffers to generate an accurate representation of the background signals from the three standard curves.

Following standard curve generation, six concentration spike-ins were added in triplicate to both 1:2 and 1:8 diluted pooled human blood plasma. The spike-in concentrations for TNF-α ranged from 3.13 x 10^4 fg/ml to 1.00 x 10^6 fg/ml in a 2x dilution series. After addition of the spike-ins, six replicate blanks in 1:2 and 1:8 diluted pooled human blood plasma were also added. The plates containing the three standard curves and spike-ins were then incubated overnight at 4°C, shaking at 950 rpm. The following day, the plates were removed and washed four times with PBST0.1. Subsequently, the wells were resuspended in 32 µl of PBST0.05 + 300 mM NaCl + 0.25% BSA, and mixed with 8 µl of 5 µM displacement oligo to facilitate fluorescent displacement. The plate was then incubated for 1 h at RT, shaking at 950 rpm. After incubation, the plates were washed

three times with PBST0.1 and resuspended in 60 µl of the buffer for readout via flow cytometry. The % recovery data was then calculated using equation (2).

To determine if the % recoveries would improve when utilizing a decreased fold-dilution in the standard curve and spike-in concentrations, the previous experimental protocol was repeated with small variations to accommodate a smaller fold-of-dilution. For the retesting and validation of the % recoveries in candidate mimic buffers, TNF-α and IFN-γ, which both had very low endogenous antigen concentrations, were used.

The background signals of both TNF-α and IFN-γ in the two mimic buffers were first retested and compared to PBST0.05 + 0.5% BSA, as well as to 1:2 and 1:4 diluted blood plasma following the same procedure to measure sample background. Afterwards, standard curves were generated only in the 25% FBS mimic buffer for both TNF-α and IFN-γ in a multiplexed format. These 12-point standard curves implemented a 3x fold dilution instead of a 5x fold dilution. Furthermore, the initial concentration of the standard curves differed for the two proteins to maximize the linear quantifiable region in each of the two targets. The starting concentrations were determined by reviewing previous standard curves that were generated for the targets and estimating the linear concentration range. With these estimations, a starting concentration was back-calculated incorporating the new lower fold-dilution. The concentration range of the standard curve for TNF-α was from 2.26 x 10^2 fg/ml to 4.00 x 10^7 fg/ml, and the standard curve for IFN-γ was from 90.3 fg/ml to 1.60 x 10^7 fg/ml.

Afterward, triplicate spike-in and recovery tests were performed with three spike-in concentrations in a 4x-fold dilution following the procedure previously stated. The three spike-in concentrations for TNF-α were 9.26 x 10^4 fg/ml, 3.70 x 10^5 fg/ml, and 1.48 x 10^6 fg/ml, and the spike-in concentrations for IFN-γ were 3.70 x 10^4 fg/ml, 1.48 x 10^5 fg/ml, and 5.93 x 10^5 fg/ml. Finally, the % recoveries were calculated for the three spike-in concentrations in each buffer.

4 | Results

The CLAMP platform was optimized to enable the accurate measurement of human blood plasma for the discovery and validation of neurological biomarkers. First, it was optimized to minimize nonspecific binding events from the DNA and antibody constituents, as well as to determine their viability when placed in 4°C cold storage. Afterwards, several parameters of the CLAMP fabrication were optimized to maximize signal generation, while maintaining minimal background signal. Lastly, a mimic buffer was optimized to enable the accurate detection and measurement of proteins in human blood plasma.

4.1 Essential Optimizations

The several optimizations performed during the initial stages of the project focused on minimizing any nonspecific binding events of the CLAMP constituents. The nonspecific binding of CLAMP constituents onto the MP surface could generate false positive signals, complicating interpretation of any data generated.

4.1.1 DNA and Antibody Sticking

The DNA components of the CLAMP assay following fluorescent displacement was the first group of constituents investigated for nonspecific binding. To investigate these potential occurrences, five different functionalized MPs were created to pinpoint the stage of CLAMP fabrication that was attributed to nonspecific binding (**Fig. 4.1 A-E**). Additionally, three different DNA oligomers and an antibody were prepared and employed to determine their potential for nonspecific binding for all five bead types (**Fig. 4.1 F-I**). Additionally, a blank was included as a negative control to establish the background signal (**Fig. 4.1 J**). To readily detect the increases in signal due to nonspecific binding, an excess of the DNA groups was incubated with the bead groups to maximize any such interactions.

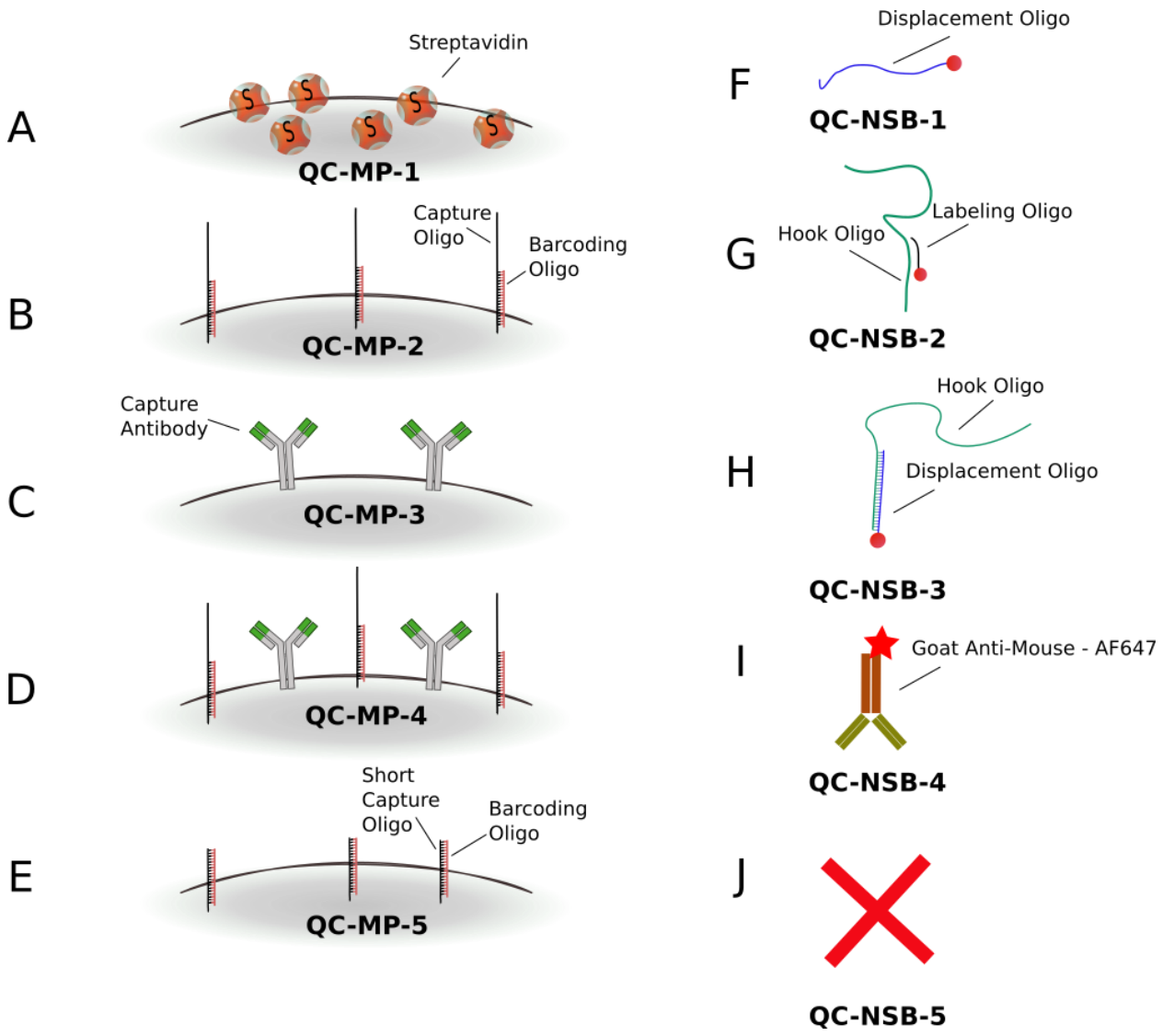

Figure 4.1 | Functionalized MPs and DNA groups used to evaluate DNA and antibody sticking in CLAMP assays. Combinations of A-E with F-J were used to identify confounding nonspecific binding events. **(A)** Streptavidin-coated MPs (QC-MP-1) served as a negative control due to a lack of binding sites for the DNA. **(B)** MPs coated with biotinylated capture oligos annealed to barcoding oligos (QC-MP-2). DNA-coated MPs were designed to give a positive signal in the presence of hook oligos due to their sequence complementarity to the capture oligos. **(C)** MPs coated with biotinylated anti-rat IgGs (QC-MP-3). As they have no DNA-binding sites, antibody-coated MPs was not expected to generate a significant signal. **(D)** MPs coated with both biotinylated DNA and antibodies (QC-MP-4). The dual MP was expected to generate a positive signal, but lower signal, compared to the DNA-coated MPs due to having fewer capture oligos on the surface available for binding. **(E)** MPs coated with shortened capture oligos annealed to barcoding oligos (QC-MP-5). This template served as an additional negative control as it lacked available binding sites. It also offers insight into the effect of increased negative charge on nonspecific sticking. **(F)** Fluorescently labeled (red circle) displacement oligo used in fluorescent displacement of

the hook oligo (QC-NSB-1). The displacement oligo was not expected to bind to any of the functionalized beads as it is only complementary to the hook oligo. **(G)** The hook oligo annealed to a fluorescently labeled (red circle) labeling oligo (QC-NSB-2). This was expected to generate a signal with any of the non-shortened capture oligos as the hook oligo will bind complementarily to the capture oligo. **(H)** The hook oligo annealed to a displacement oligo (QC-NSB-3). This DNA group was expected not to generate a signal since the displacement oligo occupied the capture oligo binding sequence. **(I)** The goat anti-mouse-Alexa Fluor 647 (QC-NSB-4). This antibody group was not expected to bind to any of the five QC-MPs as there are no mouse antibodies on any of the surfaces. **(J)** The blank buffer, PBST0.05 + 300mM NaCl (QC-NSB-5). This group served as a negative control and demonstrates the background signal.

Through testing the 15 possible MP:DNA combinations, the stages of CLAMP fabrication that were susceptible to nonspecific binding were identified (**Fig. 4.2**). QC-MP-1, QC-MP-3, and QC-MP-5 did not exhibit any nonspecific binding events. In these conditions, the fluorescent signal was approximately equal to background, which was established as the level produced by QC-MPs incubated with QC-NSB-5. A positive signal was observed from QC-NSB-2 for QC-MP-2 and QC-MP-4, as QC-NSB-2 had been designed as a positive control, in which the hook oligos could complementarily hybridize to the capture oligos on the MP surface, labeling the MPs.

However, it was also observed that the QC-NSB-3 still bound onto the surface of QC-MP-2 and QC-MP-4. This was unexpected as the capture oligo-binding sequence in the hook oligo should have been occupied by the displacement oligo and thus unable to bind onto the capture oligo on the MP surface. The signal generated by this group was equivalent to approximately 20% of the positive signal generated by QC-NSB-2.

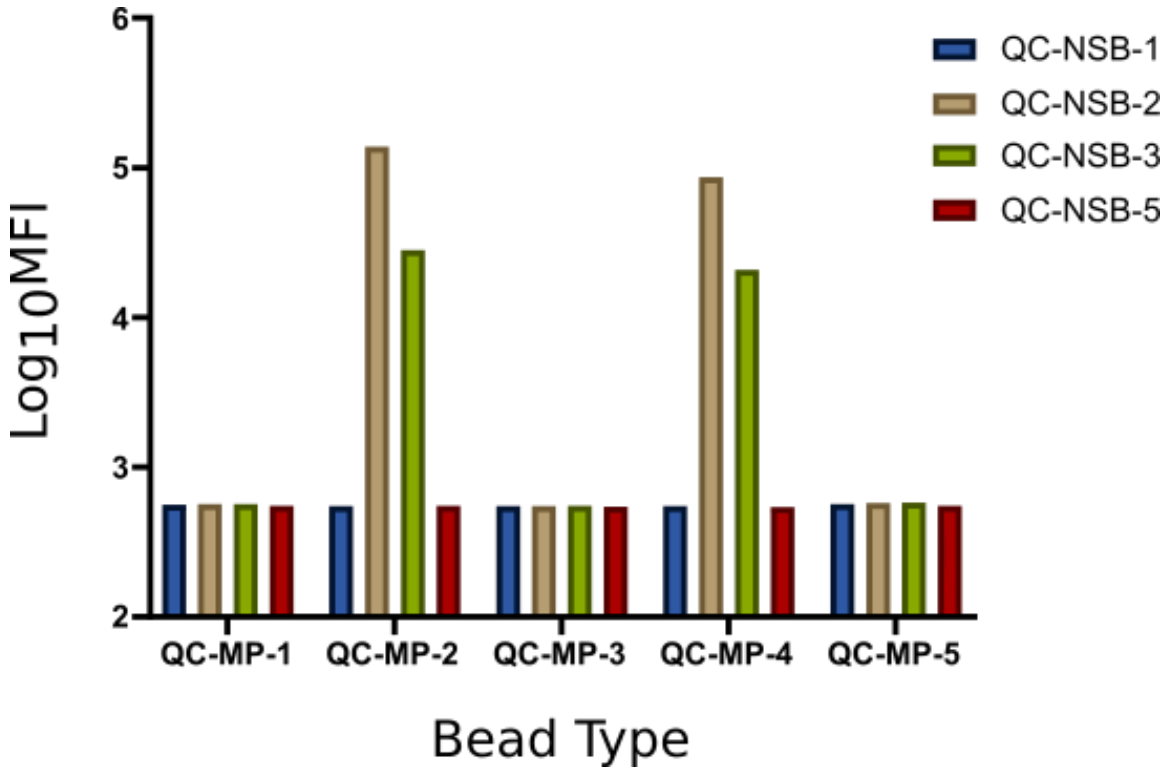

Figure 4.2 | Bar graph of quality controls in the DNA sticking experiments. In the x-axis, the five different functionalized MPs are arranged (left to right): streptavidin-coated MPs (QC-MP-1), DNA-coated MPs (QC-MP-2), antibody-coated MPs (QC-MP-3), combination MPs (QC-MP-4), and short-DNA MPs (QC-MP-5). The y-axis is Log_{10} transformed MFI. Displacement oligo (QC-NSB-1, dark blue) and the buffer control (QC-NSB-5, light blue) are all at background level of approximately 550 MFI across the five different QC-MPs. Next, we observe that the annealed hook and labeling oligo (QC-NSB-2, beige) show a high fluorescent signal at approximately 138 500 MFI for the DNA-coated MPs and 86 500 MFI for the dual MPs. Lastly, we see a fluorescent signal from the annealed hook oligo with the displacement oligo (QC-NSB-3, green) at 28 000 MFI for the DNA-coated MPs and 21 000 for the dual MPs.

From these findings, it was concluded that the hook oligo had the capacity to nonspecifically bind to the MPs. Upon examination of the hook oligo sequence, a 15-basepair (bp) repeated region was discovered, which effectively repeated the entire toehold sequence along with 6 bp of the displacement oligo binding region. The detailed designs of the different oligos can be seen in **Figure 4.3**, with the repeated region highlighted in red. This repetition could account for QC-NSB-3 nonspecifically binding to the MPs, thereby generating false-positive signals. To eliminate this artifact, we randomized the 15-bp repeat sequence and subsequently repeated the experiment.

In the repeated experiment, QC-NSB-1 and QC-NSB-5 maintained their background signal levels at approximately 550 MFI across the five different bead types. QC-NSB-2 had the highest signal at approximately 115 500 MFI for QC-MP-2 and 81 000 MFI for QC-MP-4. With the new hook oligo sequence, QC-NSB-3 produced signals of approximately 550 MFI and 2500 MFI for QC-MP-2 and QC-MP-4, respectively. The hook oligo sequence optimization greatly reduced the signal to only 2% of the positive control for the DNA-only MPs (~background), and 12% of control for the dual MPs (**Fig. 4.4**).

Figure 4.3 | Detailed design of the CLAMP oligos. (A) The sequences of the old (v1) and new (v2) hook oligos are shown with the changed 15-bp sequence highlighted in red. The 16-bp sequence highlighted pink represents the complementary binding sequence of the labeling oligo, the 9-bp sequence in purple represents the toe-hold sequence for the displacement oligo, and the 21-bp sequence in green represents the common sequence which complementarily binds to either the capture or displacement oligo. Furthermore, the hook oligos contain a thiol group on the 5' end of the sequence for antibody conjugation. **(B)** The sequences of the displacement and labeling oligo are shown here with the complementary sequences to the hook oligo highlighted. The displacement oligo has a Cy5 fluorophore conjugated onto its 3' end, while the labeling oligo has a Cy5 fluorophore on its 5' end. **(C)** The sequences of the barcoding, capture, and spacer oligos are shown with their complementary binding sequences highlighted in blue. The barcoding oligo has one of many different fluorophores used for barcoding the CLAMP on the 3' end of the sequence, here denoted with Cy3. The capture and spacer oligos are functionalized with a biotin group on the 5' end of the sequence for it to bind onto the streptavidin-coated MP. The 21-bp sequence in the capture oligo (highlighted in green) complementarily binds to the hook oligo, in which with incubation of the displacement oligo, is displaced via toe-hold mediated displacement.

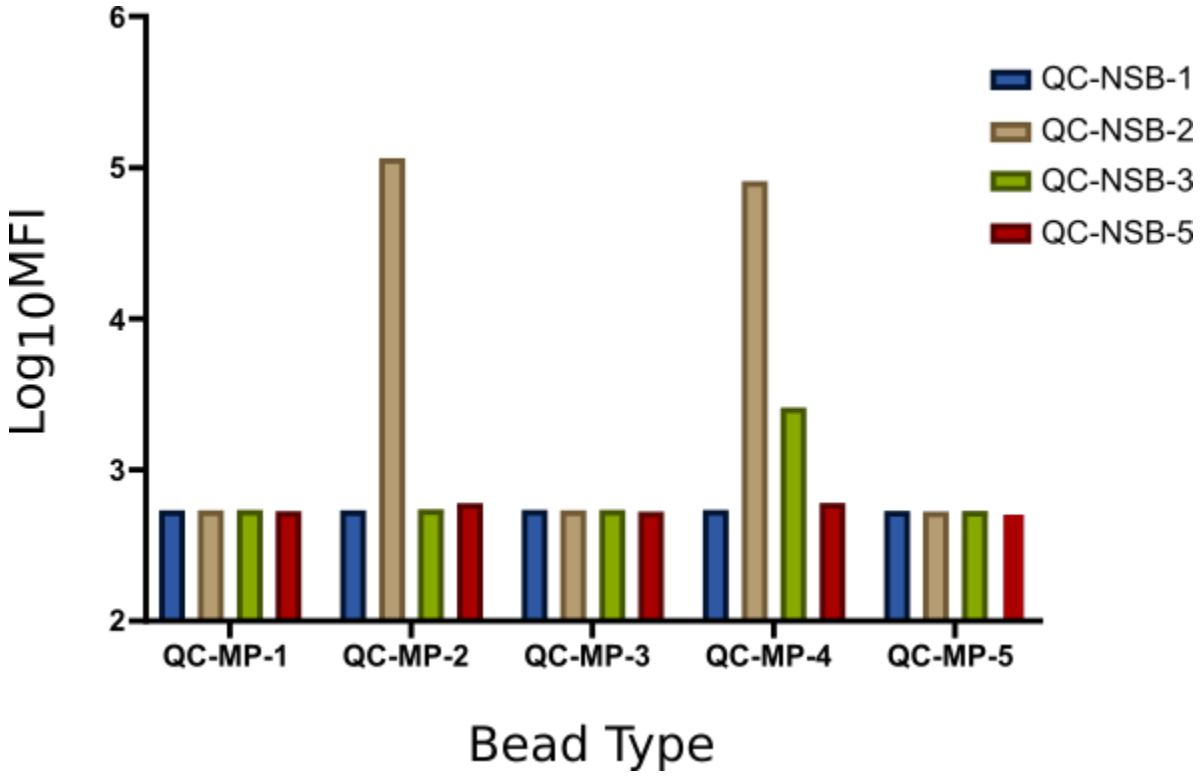

Figure 4.4 | Bar graph of hook oligo optimization. Here, the background signal is shown at approximately 550 MFI depicted by QC-NSB-1 and QC-NSB-5. QC-NSB-2 was observed to have the highest signal at approximately 115 500 MFI for QC-MP-2 and 81 000 MFI for QC-MP-4. Upon changing the sequence of the hook oligo to remove the 15-bp repeat, it was observed that the signal drastically decreased for QC-NSB-3 to background signal at around 550 MFI for QC-MP-2 and to approximately 2500 MFI for QC-MP-4.

Following a similar line of investigation, it was questioned whether the antibodies in the CLAMP assay could also nonspecifically bind back onto the MPs, thereby generating a false positive signal. For this purpose, goat-anti-mouse antibodies labeled with Alexa Fluorophore-647 (GAM-AF647, QC-NSB-4) were incubated with the QC-MPs. The fluorescent signals produced by QC-NSB-4 were at background level across all of the QC-MPs, indicating that no antibody sticking had occurred (**Fig 4.5**).

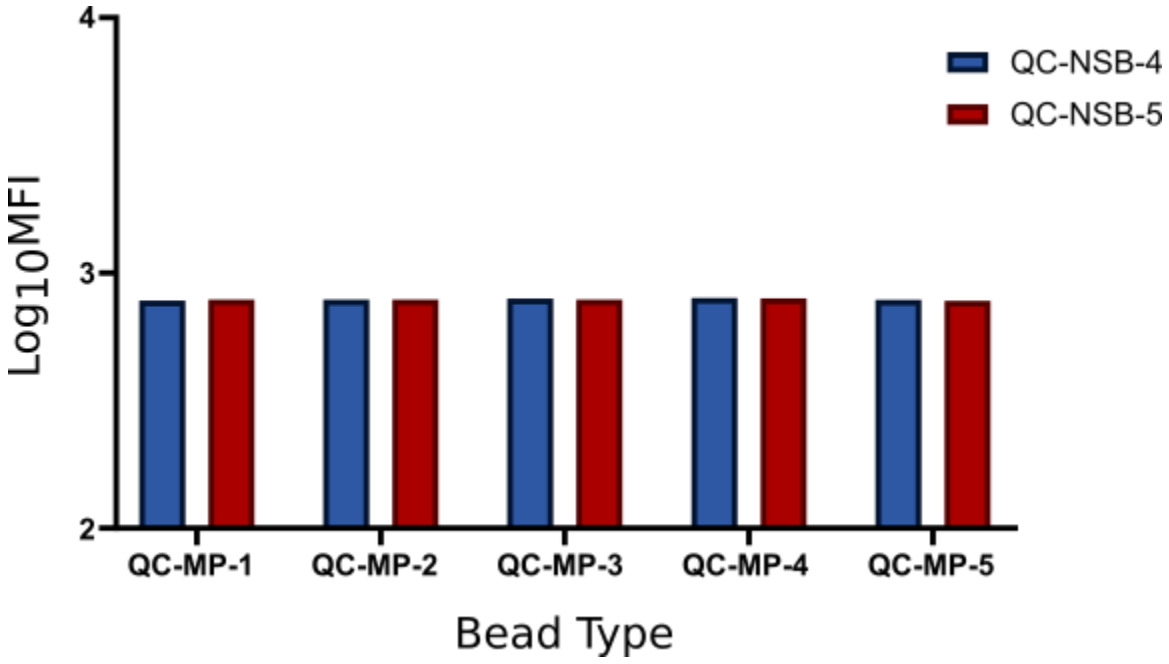

Figure 4.5 | Bar graph of antibody sticking experiment. Here, the background signal is shown in red (QC-NSB-5). Incubation of the GAM-AF647 (QC-NSB-4, dark blue) had no effect in increasing the background signal through nonspecific sticking, in which the background signal remained at approximately 800 MFI.

4.1.2 Effects of Prolonged Cold Storage

To determine if prolonged 4°C cold storage had a detrimental effect on CLAMP integrity and performance, CLAMPs for EpCAM were tested in four timepoints over 27-days. Standard curves were generated on days 1, 4, 12, and 27 after CLAMP fabrication to determine if the signal would decline over time due to the cold storage. As shown in **Figure 4.6**, the 10-point standard curves demonstrated a gradual decline in signal-to-background-ratio (SBR). SBR allows for comparison of the timepoints since it accounts for the differences in calibration of the flow cytometer across different experiment days. From timepoints 2 (Day 4) to 4 (Day 27), there was a 20-30% decline in signal for each point in the quantitative linear region and high-end of the curve. Furthermore, the highest concentration point had a decline in SBR from 6.8 on Day 1 to 4.9 on Day 27.

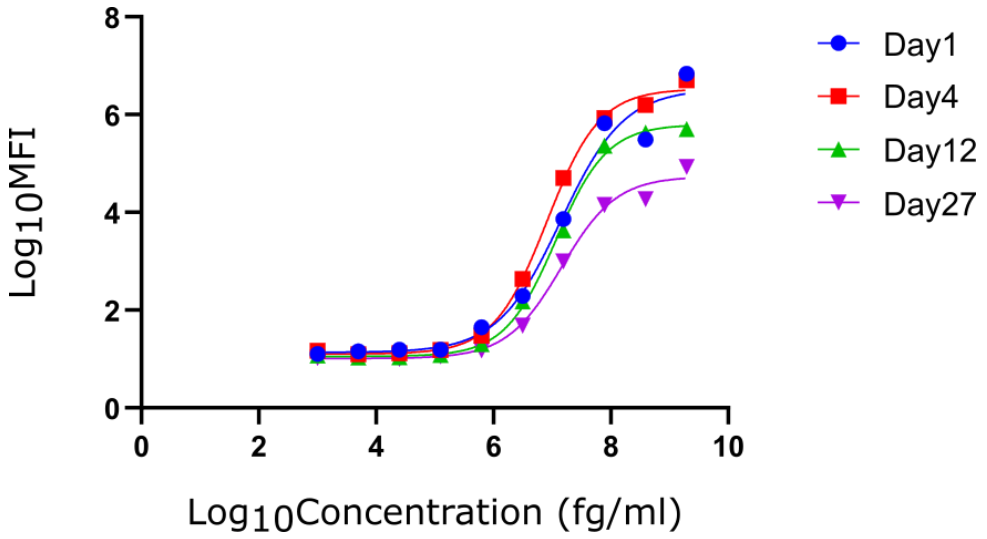

Figure 4.6 | Standard curves for EpCAM obtained at day 1, 4, 12 and 27 reveal effect of cold storage. Four 10-point triplicate standard curves of the EpCAM protein at a 5x dilution series over the course of 27-days post fabrication. A decline in maximum signal is observed the longer the CLAMPs are kept in cold storage. Big changes in MFI are not observed between timepoint 1 (Day 1) and 2 (Day 4); however, the differences in MFI become more significant at timepoint 3 (Day 12), in which timepoint 4 (Day 27) having the lowest maximum signal.

To determine what factors may have contributed to the decreased signal from cold storage, four quality controls were also included in the experimental design and were implemented in parallel with standard curve generation. The following quality controls were introduced to fluorescently label certain CLAMP components: (1) 2.5 µM of the displacement oligo (QC-Storage-1), (2) 1 µM of the labeling oligo (QC-Storage-2), (3) 2 µM of donkey anti-goat-Cy5 (QC-Storage-3), and (4) 2 µM of goat-anti-mouse-AF647 (QC-Storage-4). QC-Storage-1 was expected not to generate a fluorescent signal, as it would displace all of the hook oligos, in which the signal could not be propagated due to lack of an antigen. QC-Storage-2 was a positive control that bound to the hook oligo to confirm their presence. QC-Storage-3 served to label the antibodies on the CLAMP surface, while QC-Storage-4 labelled the tethered antibodies that were conjugated to hook oligos. With the inclusion of these four quality controls, precise determination of the CLAMP surface integrity was possible. As seen in **Figure 4.7**, the differences in the signal generated from each quality control condition were negligible across the four timepoints.

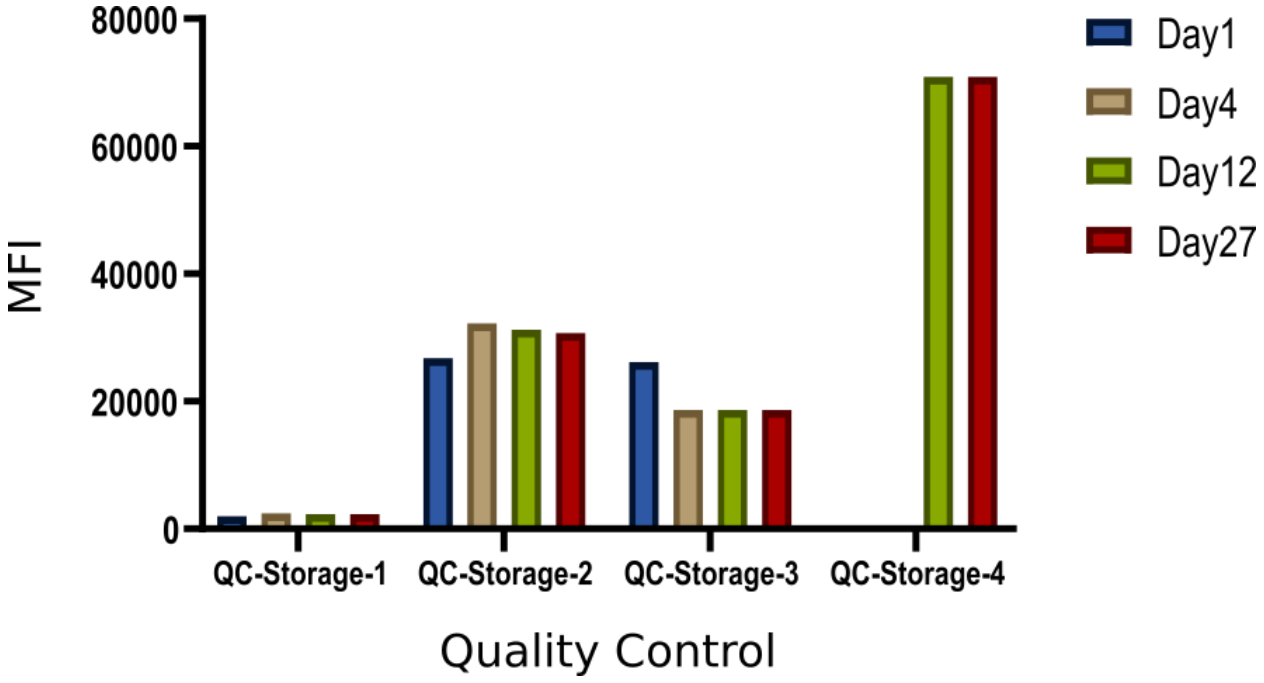

Figure 4.7 | Bar graph of quality controls for the cold storage experiments. QC-Storage-1 (displacement) oligo showed very similar background signals across the four different timepoints. QC-Storage-2 (labeling oligo) showed only small differences between the different timepoints, demonstrating that the hook oligos did not un-attach from the capture oligos due to prolonged cold storage. QC-Storage-3 (donkey anti-goat-Cy5) also did not demonstrate large deviations, labeling the goat antibodies immobilized on the surface. This validated that the surface antibodies did not un-attach from the MP surface. Finally, QC-Storage-4 (goat anti-mouse-AF647) also did not show any large difference between the two timepoints, depicting that the detection antibodies are still tethered onto the CLAMPs. QC-Storage-4 was missing its first two timepoints due to the antibody not being available during those experiments.

4.2 Assay Parameter Optimizations

To further improve CLAMP performance, the optimal capture oligo density on the MP surface, antibody-hook oligo (Ab-O) conjugate ratio, and the duration of antigen-CLAMP incubation were determined to maximize fluorescent signal generation, whilst maintaining minimal background signal.

First, to determine the ideal capture oligo density, MPs with varying amounts of capture oligos were fabricated and subsequently evaluated to determine the effects it had on assay signal, specificity, and sensitivity. The amount capture oligos on the MP surface were: (1) 20 pmol, (2)

40 pmol, and (3) 80 pmol. The amount of capture oligos were supplemented with spacer oligos summing to a total of 90 pmol of DNA on the MP surface. Triplicate standard curves for IL-8 were generated to determine which of the three amounts of capture oligo had the strongest fluorescent signal, while preserving minimal background signal. The standard curves ranged from 2.56 x 10^2 fg/ml - 5.0 x 10^8 fg/ml in a 5x dilution series. As depicted in **Figure 4.8**, the 20 pmol capture oligo density exhibited both the lowest background and maximum signal, whereas the 80 pmol capture oligo density had the highest background signal and a comparable maximum signal to the 40 pmol condition. Since the CLAMP assay was intended to measure proteins in very low abundance as candidate biomarkers in complex samples, 20 pmol was selected to be most optimal amongst the three conditions due to its superior analytical sensitivity.

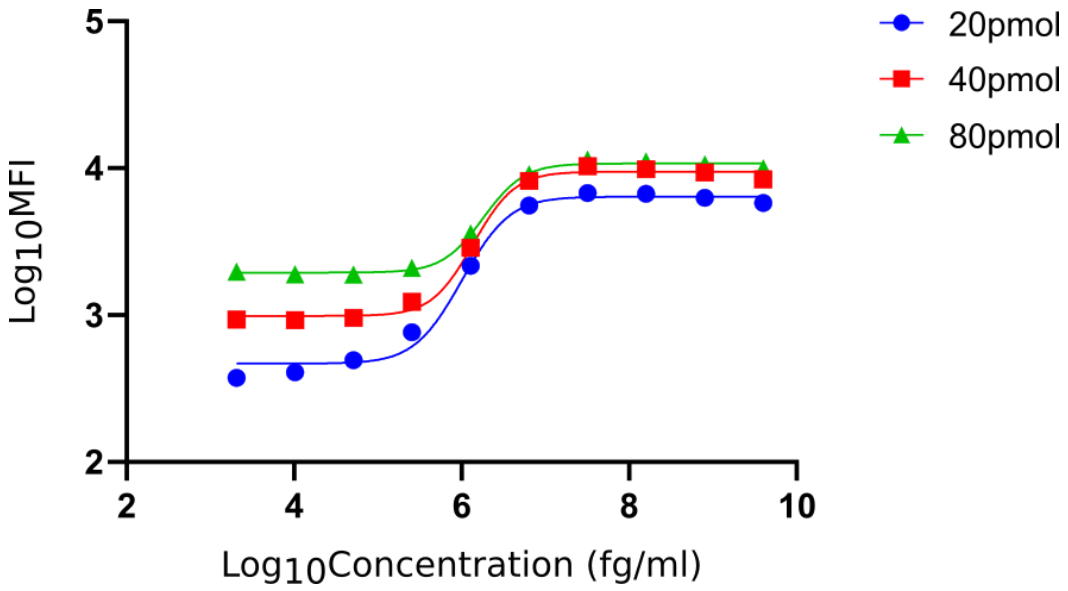

Figure 4.8 | Standard curves for IL-8 of varying capture oligo densities. The graph depicts triplicate standard curves. The blue curve shows the 20 pmol capture oligo density condition, while the red and green depict the 40 pmol and 80 pmol condition, respectively. Here, the 20 pmol capture oligo condition was observed to have the lowest background signal as well as the lowest maximum signal. The 80 pmol capture oligo condition depicted the highest background and maximum signal, while the 40 pmol condition was in between. The 20 pmol condition was selected to be most optimal for the CLAMP due to its superior analytical sensitivity for the measurement of proteins in low abundance.

Second, the effect of Ab-O conjugate valency on CLAMP performance was determined. When the amount of antibody was kept constant and increasing amounts of hook oligo were added during conjugation, increasing populations of multivalent Ab-O conjugates (more than one oligo per antibody) were established (data not shown). CLAMPs were fabricated using populations characterized to have low, medium, or high Ab-O conjugate valencies to determine the relative amount of hook oligo that can be added before the presence of multivalent conjugates significantly increased the background signal. As depicted in **Figure 4.9**, the low valency condition had the lowest background signal compared to the medium and high valency conditions, while also providing a high maximum signal falling just below that of the medium valency condition, which had the highest maximum signal of all. For this reason, the low valency was selected as it minimized the background signal, while still providing high maximum signal.

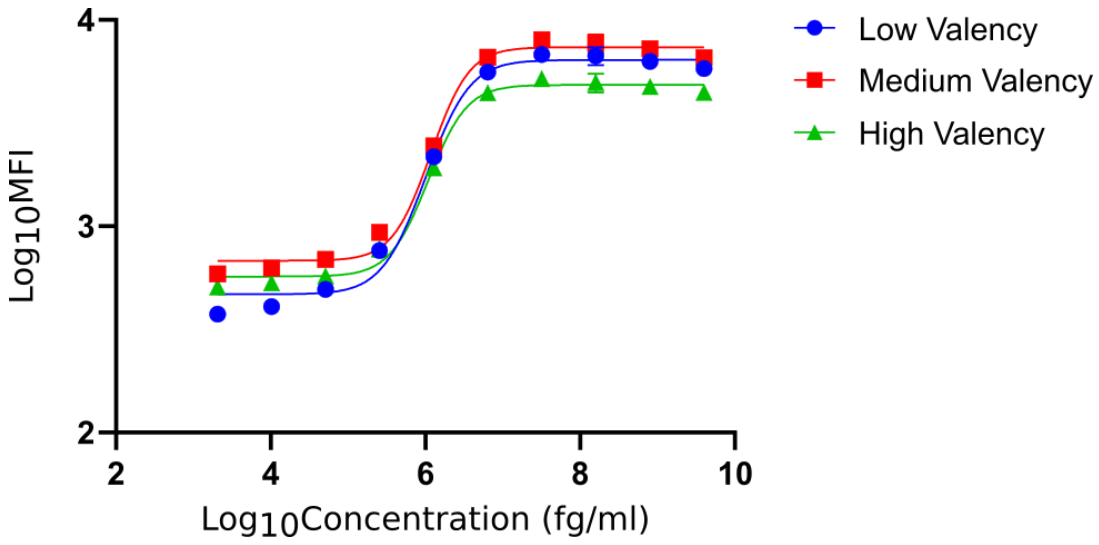

Figure 4.9 | Standard curves for IL-8 of varying antibody conjugate valencies. The graph depicts triplicate standard curves. The blue curve shows the low valency condition, the red curve shows the medium valency, and the green curve shows the high valency condition. Here, the low valency condition was observed to have the lowest background signal while maintaining a high maximum signal for the higher concentrations and was thus deemed most optimal for the CLAMP assay.

The last fabrication parameter optimized was the duration of CLAMP-antigen incubation to maximize antigen binding while minimizing any nonspecific binding events. As depicted in **Figure 4.10,** the following three different durations of antigen incubation were tested: 1 h, 3 h, and overnight (~14 h). The 1 h incubation produced the lowest fluorescent signals compared to the other two conditions, which had comparable results. Although the 3 h and overnight incubations had nearly identical results, the overnight incubation condition was selected to maximize any antigen binding and provide the CLAMPs a great amount of time to bind to the low concentration proteins. Furthermore, since the background level remained relatively constant between the three conditions, it was established that there were very minimal effects of nonspecific binding.

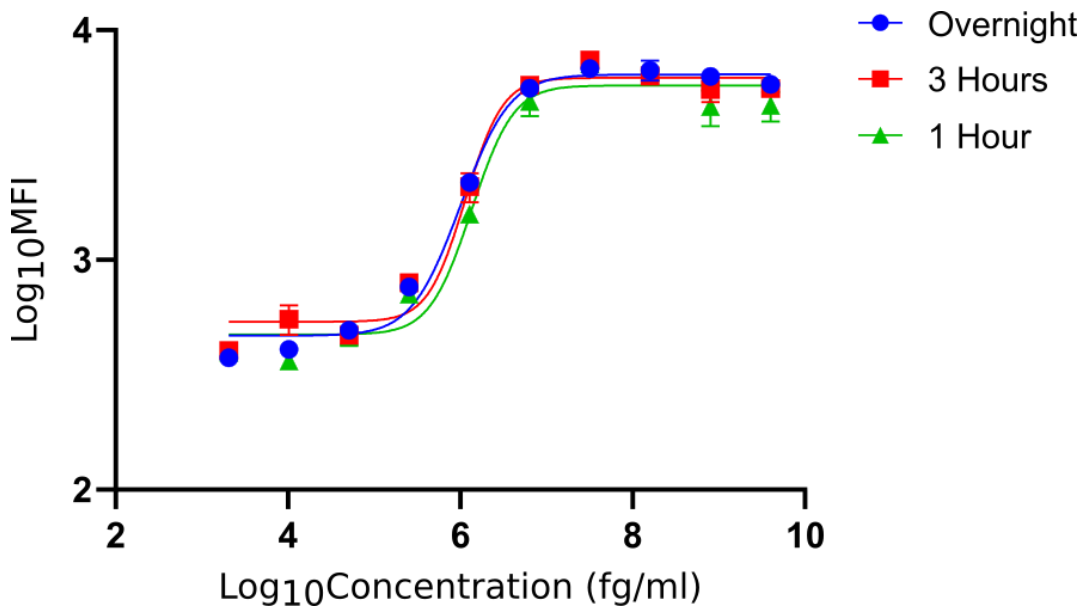

Figure 4.10 | Standard curves for IL-8 of varying antigen incubation durations. The graph depicts triplicate standard curves. The blue, red, and green curves represent the overnight, 3 h, and 1 h incubation conditions, respectively. The blue and red curves were almost overlapping, while the green curve showed a decreased signal in the linear region of the curve. The blue curve was deemed most appropriate for the CLAMP assay to guarantee the maximum amount of time for low abundance antigen binding.

4.3 Optimizing Analysis of Complex Samples

To accurately measure proteins in complex samples such as blood or cerebral spinal fluid, an appropriate mimic buffer is necessary to produce a standard curve that is representative of the

sample. However, since analyte-free blood human plasma was not available to guide the optimization of a mimic buffer for human blood plasma, the endogenous levels of 12 different proteins in pooled normal human blood plasma was acquired (**Fig 4.11**). TNF-α and IFN-γ was observed to have the lowest MFI signals and were thus attributed with the lowest endogenous concentration. Therefore, to alleviate the need for analyte-free human blood plasma, TNF-α or IFN-γ were used as the protein targets in all future mimic buffer optimizations, in which the endogenous concentration was assumed to be negligible.

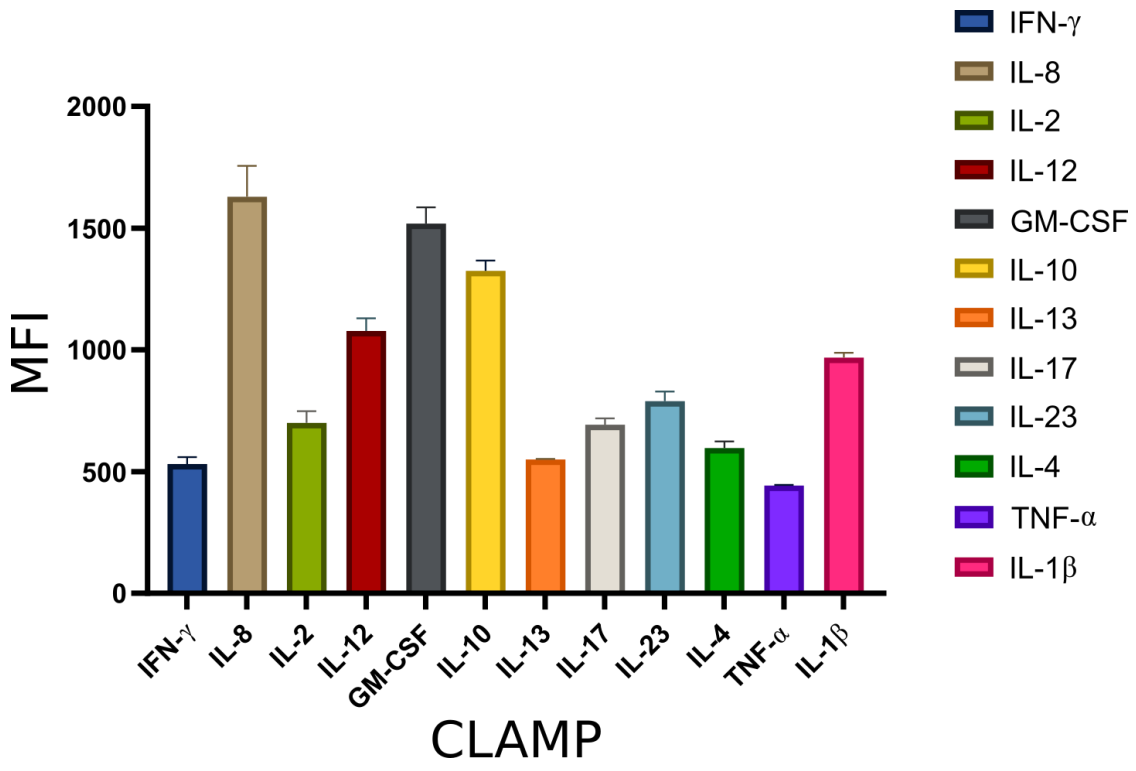

Figure 4.11 | Bar graph depicting the background signals of 12 different proteins in pooled normal human blood plasma. Background signals of the 12 different protein targets performed in triplicate are shown. The two lowest observed signals were IFN-γ and TNF-α at 531 MFI and 443 MFI, respectively. Error bars represent the standard deviation of the data.

The goal was to find a mimic buffer composition to closely reflect the background levels of diluted human blood plasma. Using TNF-α as the protein target, the background signals of 17 different mimic buffers were extensively screened (**Table 3.1** in **Section 3.3.2**) and compared to diluted blood plasma. These buffer compositions contained low to progressively higher levels of a single

complex matrix, while some of them contained a combination of several different complex matrices to try to closely represent the diluted human blood plasma. **Figure 4.12** illustrates that mimic buffers 5, 6, 8, and 9 have background signals closest to those of the human blood plasma dilutions. The two mimic buffers selected for further testing were compositions 5 (25% fetal bovine serum (FBS) in PBST0.05 + 0.5% BSA) and 8 (25% mouse plasma in PBST0.05 + 0.5% BSA). Although other mimic buffer compositions such as buffer 6 and 9 also had viable background signal, it was decided to proceed first with the simplest buffer compositions that could achieve a background near the desired range to reduce the complexity of preliminary optimization experiments.

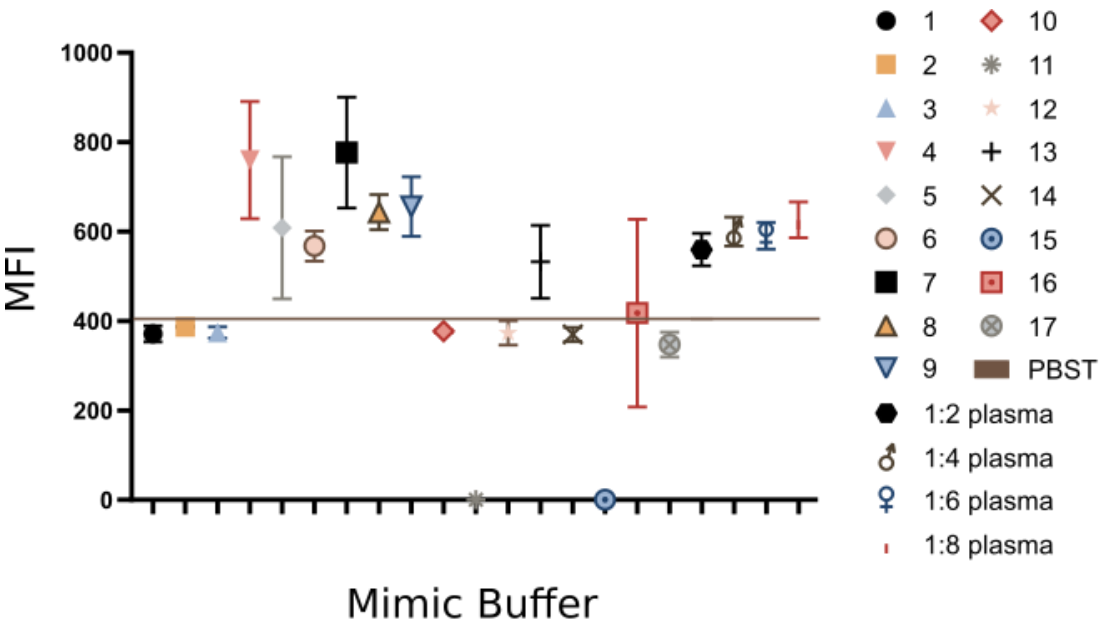

Mimic No.	Composition added to PBST0.05 + 0.5% BSA	Mimic No.	Composition added to PBST0.05 + 0.5% BSA
1	10% mouse serum	10	10% mouse serum + 10% FBS
2	25% mouse serum	11	10% mouse plasma + 10% FBS
3	50% mouse serum	12	25% mouse serum + 10% FBS
4	10% FBS	13	25% mouse plasma + 10% FBS
5	25% FBS	14	25% FBS + 10% mouse serum
6	50% FBS	15	25% FBS + 10% mouse plasma
7	10% mouse plasma	16	10% mouse serum + 10% FBS + 10% mouse plasma
8	25% mouse plasma	17	50% mouse serum (in PBS + 0.5% BSA)
9	50% mouse plasma	-	-

Figure 4.12 | Scatterplot of the background signals of 17 different buffer compositions for TNF-α. The graph shows the MFI on the y-axis, and the mimic buffer identity on the x-axis, while the points on the graph depicts the

average MFI of triplicate datapoints. The brown line across the plot depicts the PBST0.05 + 0.5% BSA background. The four rightmost points on the graph depicts the different human blood plasma dilutions at 1:2, 1:4, 1:6, and 1:8. Samples 11 and 15 depict 0 readings likely due to inefficient washing during the experiment, resulting in insufficient CLAMPs being able to be measured via flow cytometry. Below the scatterplot is an abbreviated version of Table 3.1 to show the identity of each candidate mimic buffer.

Moving forward with the two most promising simplistic mimic buffers from the initial screening, these candidates were investigated more thoroughly to identify which of the two would be most representative of the complex matrix in human blood plasma. For this purpose, spike-in and recovery experiments were performed. Replicate standard curves for each mimic buffer and a PBST control were generated for TNF-α using 12-points with a 5x dilution series (**Fig. 4.13**). Furthermore, six known concentrations of TNF-α were spiked into 1:2 and 1:8 diluted human blood plasma in triplicate. The spiked-in concentrations ranged from 1.0 x 10^6 fg/ml to 3.1 x 10^4 fg/ml, in a 2x dilution (**Fig 4.14**). The average % recoveries for 25% FBS (MB-1), 25% mouse plasma (MB-2), and PBST0.05 (PBST) were 67%, 94%, and 95%, respectively, in the 1:2 diluted plasma; and 90%, 101%, and 99% in 1:4 diluted plasma. The % recovery data was calculated using equation (2).

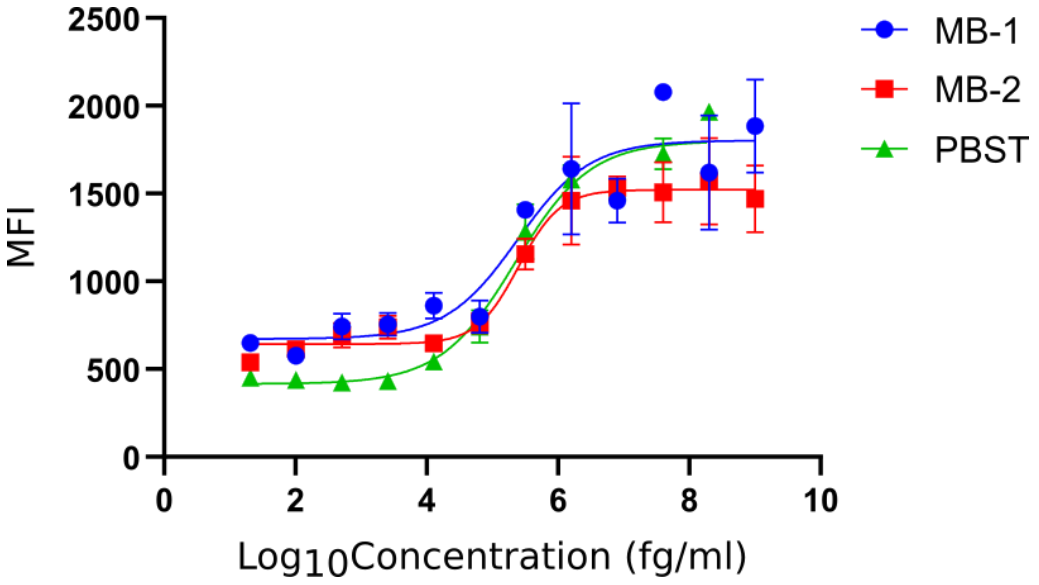

Figure 4.13 | 12-point Standard curves for TNF-α of two mimic buffers compared to PBST0.05 + 0.5% BSA. Triplicate standard curves performed in PBST0.05 + 0.5% BSA (PBST, green) and in the two candidate mimic buffers: (1) 25% FBS in PBST0.05 + 0.5% BSA (MB-1, blue), and (2) 25% mouse plasma in PBST0.05 + 0.5% BSA (MB-2, red). MB-1 and MB-2 both show higher background signals than PBST. However, MB-1 was observed to have a higher maximum signal compared to MB-2, being more similar to PBST. The graph is depicted with a linear y-axis to compensate for the low dynamic range of the standard curves. Error bars represent the standard deviation of the data.

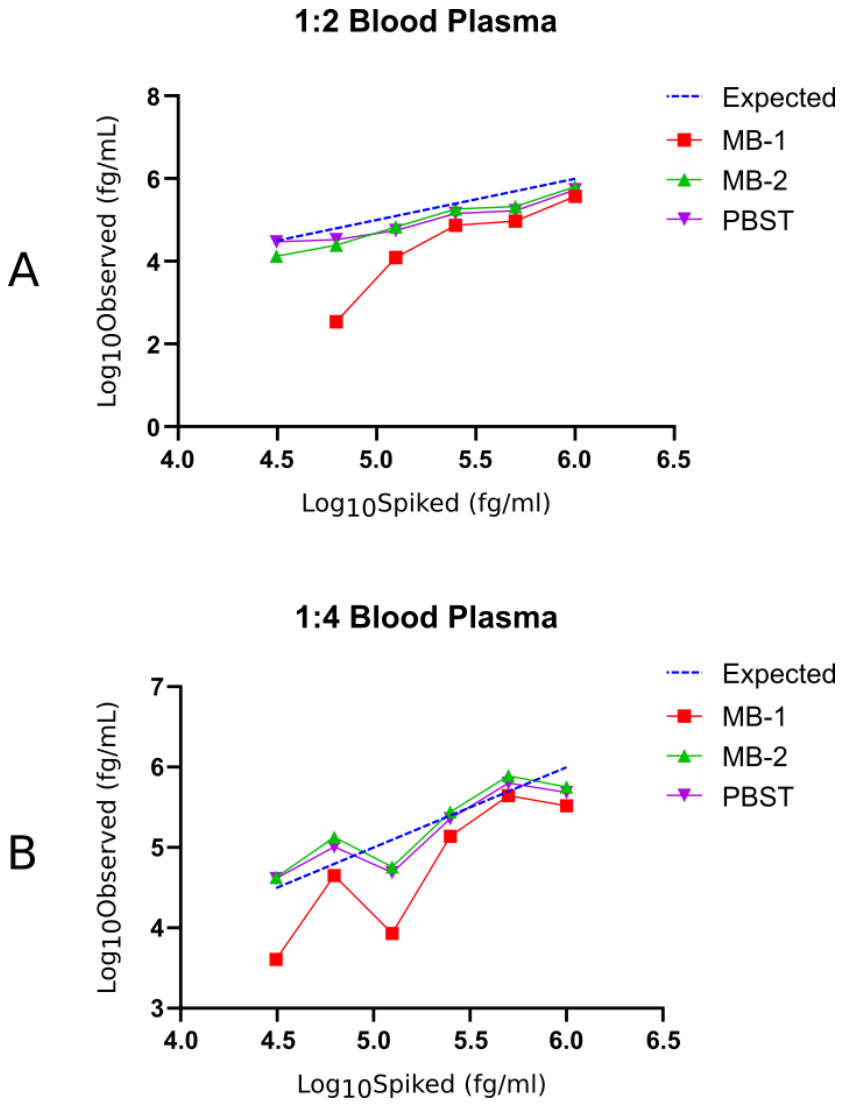

Figure 4.14 | % Recovery plots in log-log scale from spike-in and recovery experiments in 1:2 and 1:4 diluted blood plasma. The graph depicts the % recovery calculated from 25% FBS in PBST + 0.5% BSA (MB-1, red), 25% mouse plasma in PBST0.05 + 0.5% BSA (MB-2, green), and PBST0.05 + 0.5% BSA (PBST, purple). Furthermore,

the expected concentration at 100% recovery is highlighted as a hashed line in blue. Each plot depicts the $\log_{10}$ transformed observed concentration (fg/ml) that was calculated from the standard curve on the y-axis, while the x-axis depicts the $\log_{10}$ transformed spiked-in concentration (fg/ml). **(A)** In the 1:2 diluted human blood plasma, MB-2 and PBST were observed to be very close to the expected value with an average % recovery of 94% and 95%, respectively. On the other hand, MB-1 was missing its first datapoint due to low bead count during flow cytometry and had a comparably lower % recovery of 67%. **(B)** In the 1:4 diluted human blood plasma, a general trend in the data of a drop in the first, third, and last point was observed. Furthermore, MB-2 and PBST were observed to be very close to the expected value with % recoveries of 101% and 99%, respectively. In the case of 1:4 diluted human blood plasma, MB-1 also demonstrated an acceptable % recovery value of 90%.

Although the % recoveries calculated for the two mimic buffers were both within an acceptable range, another similar set of experiments was performed to determine the reproducibility of the result, as well as to determine if the % recoveries could be further improved by implementing a lower fold of dilution to expand the linear and quantitative region of the standard curves. First, the background signals of MB-1 and MB-2 were re-established and compared to 1:2 and 1:4 diluted human blood plasma. The same outcome was achieved, in which the MB-2 had a higher background signal compared to MB-1 and the diluted human plasma (**Fig. 4.15**). Due to its lower and more comparable background signal, MB-1 was selected to proceed with further the spike-in and recovery tests.

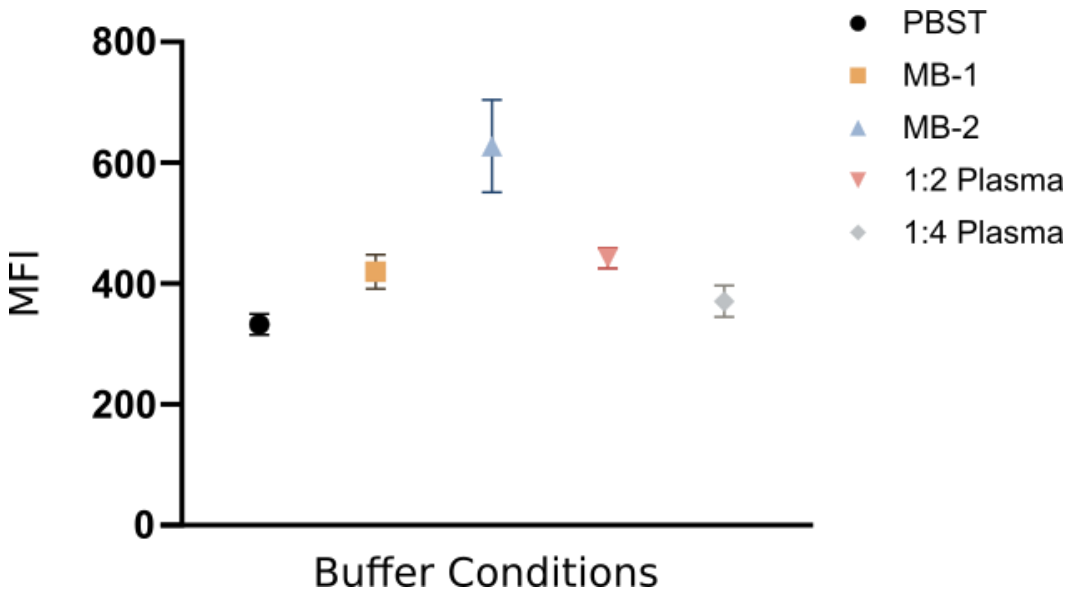

Figure 4.15 | Scatterplot of the mimic buffer backgrounds. This graph depicts the background signals from triplicate measurements of MB-1 (yellow) and MB-2 mimic buffers compared to PBST0.05 + 0.5% BSA (PBST, black), and to 1:2 (red), and 1:4 (gray) diluted human blood plasma. MB-1 was observed to be much closer to the 1:2 and 1:4 diluted blood plasma than MB-2. The background signal for MB-1 was 420 MFI compared to 442 and 370 MFI of the 1:2 and 1:4 diluted human blood plasma, respectively. MB-2 had a much higher background signal at 628 MFI. The PBST background signal had an MFI of 333, which was lower than the complex samples. MB-1 was selected for further optimization as it had both a lower background signal, as well as more closely resembled the background of the diluted human blood plasma. Error bars represent the standard deviation of the data.

In the following validation experiments, 12-point standard curves for each TNF-α and IFN-γ were generated, utilizing a lower 3x fold of dilution, while also incorporating protein-specific initial concentrations of 4.00 x 10^7 fg/ml and 1.60 x 10^7 fg/ml to maximize the linear quantitative region of each standard curve, respectively. The IFN-γ standard curve ranged from approximately 950 to 10 150 MFI; comparatively, the TNF-α curve had a much shorter dynamic range of 1 800 to 3 200 MFI (**Fig. 4.16**). Subsequently, spike-in and recovery experiments were performed to gauge the performance of the MB-1 relative to 1:3 and 1:9 diluted human blood plasma (**Fig. 4.17**). The three spiked-in concentrations applied 4x dilutions and ranged from 9.26 x 10^4 - 1.48 x 10^6 fg/ml for TNF-α, and from 3.7 x 10^4 - 5.93 x 10^5 fg/ml for IFN-γ. The average % recovery for TNF-α was 101% for the 1:3 dilution and 93% for the 1:9 dilution, while the average % recovery for IFN-γ was 91% for both the 1:3 and 1:9 dilutions. As the background of MB-1 was very similar to that of the diluted human blood plasma, and its average % recoveries ranged from an acceptable range of 91-101%, this mimic buffer was demonstrated to be a suitable candidate for future neurological biomarker discovery and validation in human blood plasma.

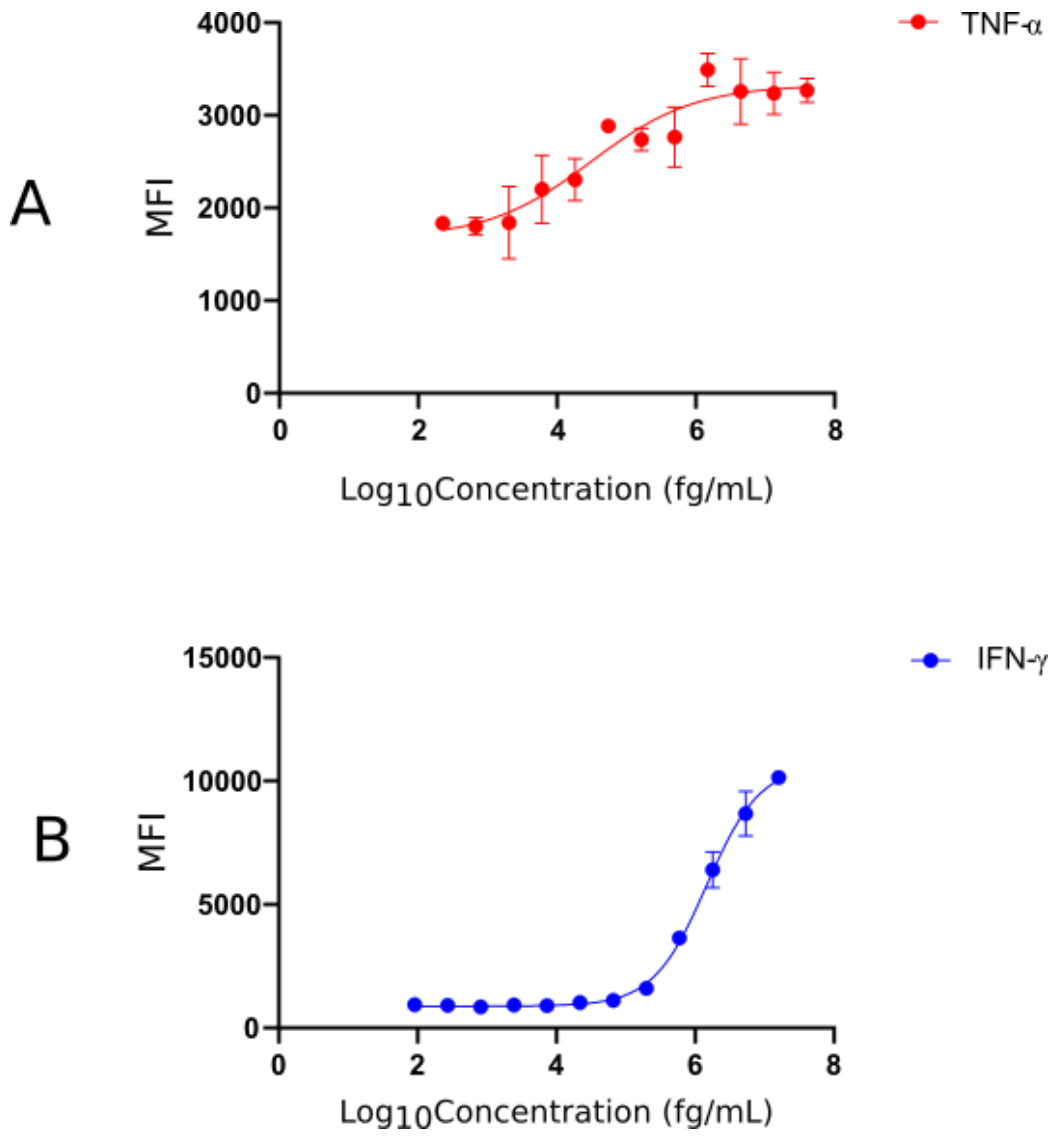

Figure 4.16 | Standard curves for TNF-α and IFN-γ in MB-1 with protein-specific initial concentrations. (A) The triplicate standard curve for TNF-α with a 3x fold dilution is depicted in red. The concentration ranged from 226 fg/ml to 4.0 x 10^7 fg/ml which generated MFI signals between 1 800 to 3 200. The TNF-α standard curve was observed to have a small dynamic range with a lower maximum signal compared to IFN- γ. **(B)** The triplicate standard curve for IFN-γ with a 3x fold dilution is depicted in blue. The concentration ranged from 90.3 fg/ml to 1.60 x 10^7 fg/ml which generated MFI signals between 950 to 10 150, respectively. This curve was observed not to fully saturate on the high-end of the curve, and thus had the potential to increase its signal further. Error bars represent the standard deviation of the data.

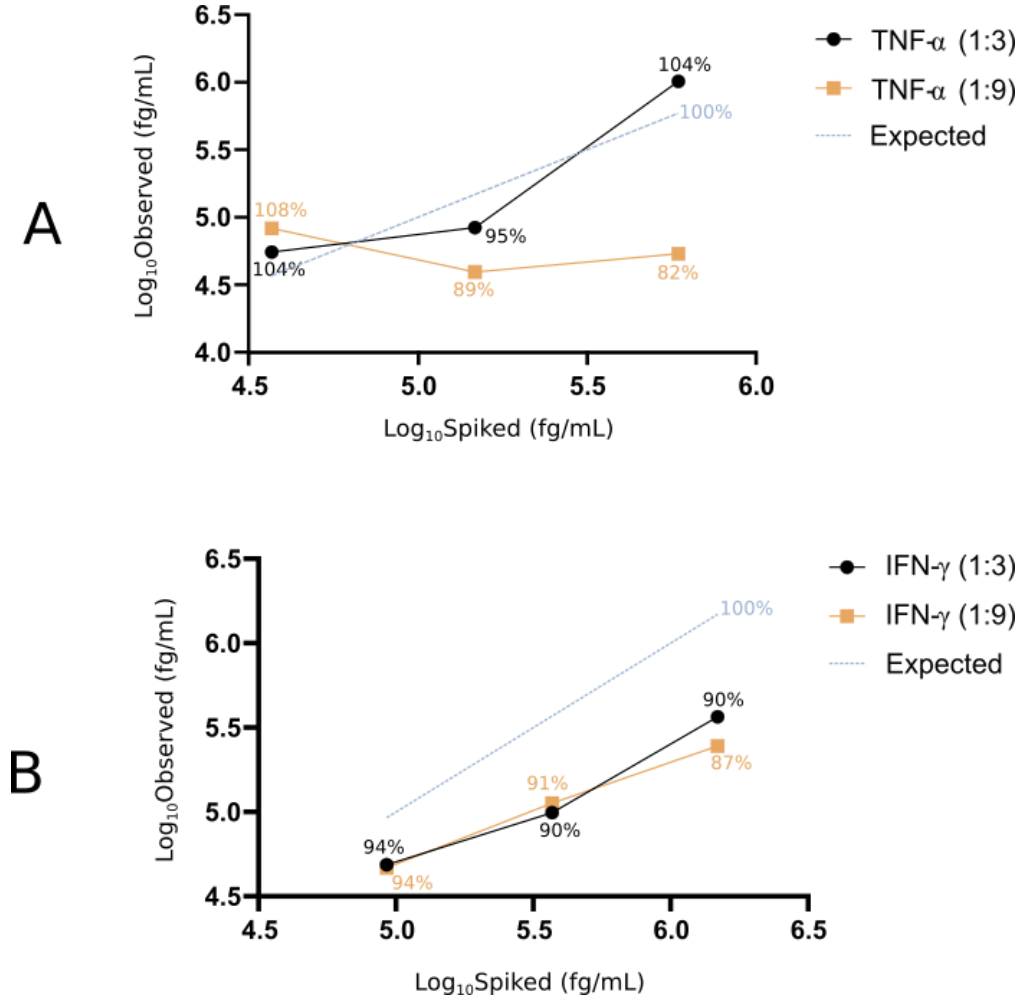

Figure 4.17 | % Recovery plots for TNF-α and IFN-γ in 1:3 and 1:9 diluted blood plasma. The two plots depict the % recovery data for both TNF-α and IFN-γ in 1:3 and 1:9 diluted human blood plasma. Each plot depicts the Log_{10} transformed observed concentration (fg/ml) that was calculated from the standard curve on the y-axis, while the x-axis depicts the Log_{10} transformed spiked-in concentration (fg/ml). **(A)** TNF-α was observed to have good % recoveries in 1:3 human blood plasma (black) compared to the expected recoveries of 100% (blue). The average % recovery in 1:3 human blood plasma for TNF-α was approximately 101%. In the 1:9 dilution of human blood plasma, TNF-α performed less ideally (yellow) with greater discrepancy from the expected curve, generating an average % recovery of 93%. **(B)** IFN-γ was observed to have similar recoveries both in the 1:3 (black) and 1:9 (yellow) dilution of human blood plasma. The average % recoveries were 91% for both 1:3 and 1:9 diluted human blood plasma.

5 | Discussion

High-throughput multiplexed immunoassays are highly valuable as they confer the ability to measure many proteins simultaneously from low sample volumes, while also significantly reducing the cost and time associated with such measurements. Currently, many immunoassay formats have a capacity for analytical sensitivity comparable to the ELISA, and certain others possess multiplex capabilities. However, most immunoassay technologies lack the ability to perform simultaneously in both analytical sensitivity and multiplexing. In particular, they fail to sufficiently minimize cross-reactivity, a significant issue that thereby limits the maximum number of protein targets that can be measured simultaneously. The CLAMP platform uniquely addresses this issue by colocalizing the detection antibody to the MP surface, which is functionalized with biotinylated DNA and antibodies in advance. Since additional incubation of the mixed detection antibodies is not necessary, reagent-driven cross-reactivity is circumvented.

For accurate protein measurements in complex sample matrices, immunoassays require a sample-specific mimic buffer to accurately imitate the complexity of the sample matrix. This mimic buffer is necessary for the generation of standard calibration curves, which are crucial for accurate quantification of protein in the sample. In the event of a poor mimic buffer, estimates of protein concentration will be subject to considerable error. In the optimizations reported herein, the candidate mimic buffers were evaluated using spike-in and recovery experiments in which the % recovery reports the accuracy with which the chosen mimic buffer could represent the complexity of human blood plasma, a common patient sample in biomarker research.

5.1 CLAMPs optimized for negligible nonspecific binding artifacts

CLAMPs were optimized to minimize artifacts of nonspecific binding by first incubating specially made functionalized MPs (QC-MPs) with annealed DNA or antibodies to exacerbate any underlying issues. The main advantage of the QC-MPs was the opportunity to efficiently detect nonspecific binding events in a combinatorial way, requiring very few experiments for expedient resolution of any issues. These experiments revealed that the hook oligos could nonspecifically bind onto the capture oligos on the MP surface. Revisiting the hook oligo nucleotide sequence revealed an unintended 15-bp segment that repeated the entire toehold

sequence and part of the displacement oligo binding sequence. Upon randomizing this 15-bp repeat, the nonspecific binding signal was greatly minimized, resolving the issue.

Following correction of the hook oligo sequence, an elevated signal was detected from the optimized hook oligo annealed to the displacement oligo (QC-NSB-3, **Fig. 4.1**) on the combination MPs (QC-MP-4). This result was not observed in the DNA-coated MPs (QC-MP-2), nor the antibody-coated MPs (QC-MP-3); therefore, it stands to reason that the optimized hook oligo does not bind to the capture oligo, nor to the surface antibodies. Yet, the results suggest that the optimized hook oligo is somehow binding to the combination MPs (QC-MP-4), despite the lack of binding to either group in spatially distinct contexts. A proposal to accommodate this unexpected observation is that a negative signal groups (QC-NSB-1 or -5) was mistakenly added instead of QC-NSB-3 to QC-MP-2, thus producing a false negative signal, and that the optimized hook oligo is still binding inappropriately to the capture oligo. This could be validated through replication of the experiment.

Furthermore, when incubating the QC-MPs with GAM-AF647 (QC-NSB-4), the negative control buffer (QC-NSB-5) generated a signal similar to the background. However, since the GAM-AF647 antibody was incubated in solution, it did not represent the high local concentration of a tethered detection antibody on a typical CLAMP. Thus, a better experimental design to determine nonspecific binding of antibodies would be to incubate CLAMPs themselves for different lengths of time and then fluorescently displace the tethered antibodies with the displacement oligo (QC-NSB-1) to determine if nonspecific binding increased with incubation time. Another experiment to determine if antibody constituents re-attached themselves onto the MP surface could be to first incubate the displacement oligos with CLAMPs to facilitate fluorescent displacement, and then subsequently determine if nonspecific binding increases with incubation time. These experiments together could reveal whether the nonspecific binding occurs before or after fluorescent displacement via toehold mediated displacement.

Additionally, replicating this experiment would give more confidence in the previous findings. Although, ~10 000 CLAMPs were measured in each well to generate the MFI, the well could have potentially been loaded improperly, thereby skewing the results generated. Thus, to be fully confident in the lack of nonspecific binding on the CLAMPs, as well as validate the result of

nonspecific binding only being observed for the combination MPs (QC-NSB-4), repetition of the experiments in triplicate wells are necessary.

Lastly, the focus of optimizing non-specific binding on the CLAMP surface was limited to the potential causes after fabricating the CLAMPs, and thus failed to consider any non-specific binding events that could have occurred during the fabrication procedure. During fabrication, non-specific binding could occur when the antibodies conjugated to the hook oligos (AbOs) are incubated with the functionalized MP surface. Both during the immobilization step, and during the storage prior to the assay, the AbOs could adsorb onto the MP surface which would result in an increased background signal, and thus should be tested and optimized alongside the other conditions post-fabrication.

5.2 Antibody viability, but not CLAMP integrity, decreases with cold storage

Prolonged cold storage of the CLAMPs was detrimental, as demonstrated by a depreciation of the signal generated from the standard curves over time. However, since the quality controls implemented in the experimental design did not reveal any significant issues with the CLAMP fabrication, the loss of signal observed over time can only be attributed to the loss of antibody affinity.

Although the experiment generated a full standard curve to observe the effect of cold storage, as well as including quality controls to verify the integrity of each CLAMP, the experiment had a few shortcomings. The major weakness was the lack of technical replicates for the standard curves and quality controls, which was a consequence of preserving as many CLAMPs as possible for future timepoints to limit CLAMP usage and prioritize qualitative observations over the quantitative in this pilot experiment. Another weakness was the utilization of a high 5-fold dilution in the curve; the purpose of a high-fold dilution was to achieve complete coverage of the standard curve.

This series of experiments was first proposed to determine the effect of cold storage of the CLAMPs without consuming many CLAMPs. A follow-up experiment would be to generate triplicate 10-point standard curves utilizing a smaller 2- or 3-fold dilution with variable starting concentrations for five targets to maximize the linear quantitative region of each target, as well as identify if cold storage effects vary between CLAMPs for different targets. Furthermore, such

an experiment must include the same quality controls as this pilot, of which labeling the hook oligo is most important on account of the potential of Ab-Os nonspecific binding onto the MP surface due to their high local concentration. This proposed experiment could be performed utilizing a similar premise of increasing intervals between timepoints since it is advantageous to first observe any broad effects over a large timescale of 2+ months, then concentrate further on timepoints where problems were noted. Inclusion of another experiment focused on a specific timepoint to generate day-to-day datapoints could overcome the inherent weakness of the broad sweep, as there is a lack of resolution between the distant timepoints (*i.e.*, Day 12 and Day 27, **Fig. 4.6**).

5.3 Multi-pronged optimization approach improved assay sensitivity

Capture oligo density, Ab-O conjugate valency, and the duration of sample incubation were optimized to maximize analyte signal whilst maintaining minimal background signal. The capture oligo density was correlated with the total signal generated because it tethers the detection antibody to the MP. Excessive MP surface density of capture oligos produced a higher background signal, suspected to be due to loss of fluorescent displacement efficacy. Higher capture oligo densities would introduce steric hindrance; a fluorescent displacement oligo could not as easily access the binding region of the hook oligo as compared to MP surfaces with lower capture oligo density.

In terms of the optimal capture oligo density, the 20 pmol condition was selected because it had the greatest sensitivity. Biomarkers for disease are typically present in very low concentrations, and therefore high assay sensitivity is critical.

With the potential for multivalent Ab-O conjugates on the CLAMPs, incomplete displacement is a significant issue. Multivalent conjugates have the potential to increase the background signal by reporting a fluorescently labeled displacement oligo while it is still maintained on the MP surface by a secondary or tertiary hook oligo. This can generate a false positive signal, thereby increasing the background signal and decreasing the assay's dynamic range and limit of detection. Although monovalent conjugates are desired, the efficiency of their conjugation is very low; to maximize monovalency, a minimal amount of activated hook oligos are introduced an excess of detection antibodies for conjugation.

In this case, the Ab-O conjugation valency optimization sought to improve the yield of monovalent conjugates, thus minimizing wasted antibodies. This investigation determined the amount of activated hook oligos that can be added during conjugation while avoiding multivalency. Furthermore, this optimization investigated the degree to which multivalent Ab-O conjugates could be tolerated—if the signal increase was minimal, inclusion of a small population of multivalent conjugates may have been acceptable to save reagent costs. However, inclusion of multivalent Ab-O conjugates ultimately led to a significant increase in background signal, which was not acceptable as the higher background signal decreased the platform's sensitivity.

Depicted in **Figure 4.9**, the medium valency condition had higher background and maximum signals than the high valency condition. It was anticipated that the high valency condition would have the highest concentration of multivalent conjugates, but this is not supported by the data. This unexpected result could be attributed to a mislabeling of the medium and high valency conditions. However, although the high valency condition had a higher background signal than the low valency condition, it also had the lowest maximum signal. Although this effect would typically be interpreted as an indication that fluorescent displacement may have been more effective, this is more likely to be caused by a technical error during fabrication of the high valency CLAMPs. The low valency condition had the greatest proportion of monovalent conjugates and was selected as the optimal condition to minimize background signal. Furthermore, although the low valency condition had the lowest conjugation efficiency, it had the best analytical sensitivity for detection of low concentration proteins presumably thanks to its monovalency. Additional repetition of this experiment is needed along with optimization of the incubation conditions to validate these results.

Lastly, different durations of sample incubation were tested. When incubating samples for a longer time, the maximum signal increases as more CLAMPs bind the target protein, until equilibrium is reached; however, longer incubation times also risk increasing the background signal due to elevated nonspecific binding. As seen in **Figure 4.10**, the overnight and 3 h conditions had very similar standard curves, whereas the 1 h incubation had lower MFI in the linear region and was the least sensitive of the three conditions. Ultimately, the overnight condition was selected to maximize MFI signal and to give the reaction excess time to reach

equilibrium. Reaching equilibrium is important because protein biomarkers are typically at very low concentration, and any method to maximize the signal generated is essential.

5.4 Mimic Buffer and Standard Diluent Optimization

The purpose of the mimic buffer is to replicate the complexity of a sample matrix such as blood plasma. Each complex sample has its own unique composition, which confers varying background signals. Therefore, when generating a standard curve to calculate the concentrations of targeted proteins, an appropriate mimic buffer is required that can represent the complexity of the sample. If an unsuitable mimic buffer is used, substantial errors in the calculation of the concentration can arise. Misrepresentation of protein concentration in the sample can be devastating, especially when the data is used to evaluate clinical outcomes or drug efficacy. In the mimic buffer optimizations reported herein, an optimal mimic buffer was selected by measuring the background signals of several candidate buffers and comparing them to diluted human blood plasma, then selecting the buffers that most closely imitated the elevated background of this particular sample matrix. However, a possible weakness of the methods used during the mimic optimization was the reliance of a single pooled human blood plasma sample for all optimizations. Although pooled human blood plasma contains the blood plasma from many different donors, it would also be valuable to generate more datapoints for optimization. Hence, including pooled human blood plasma from different lots or different suppliers, assuming the methods of preparation are identical, would be beneficial to ensure that the results observed are not just a consequence of using a single pooled sample provided by one supplier. Additionally, using blood plasma extracted from individual humans could also be used as a replacement of the pooled blood plasma, so long as the method of sample preparation is the same amongst the different individuals. However, this method introduces more possibility of error as mistakes could be made during sample preparation, potentially skewing the results during optimization. Furthermore, ethical approval and testing to ensure that the samples represent a normal human population may be required, potentially lengthening the optimization process.

First, the endogenous protein in pooled human blood plasma was measured and the proteins with the lowest concentration were selected to use for mimic buffer optimizations. Selecting targets with minimal endogenous concentration facilitated the assumption that the endogenous

concentration was negligible or close to zero. This was important as unknown endogenous protein concentration can skew the results of spike-in and recovery calculations, reducing the reliability of the mimic buffer.

The mimic buffer selected to represent 1:2 diluted human blood plasma was ultimately 25% FBS in PBST0.05 + 0.5% BSA (MB-1). To this end, the background signals of 17 different mimic buffer compositions were screened and compared to PBST0.05 + 0.5% BSA and diluted human blood plasma. MB-1 was selected over other compositions with similar background levels to diluted human blood plasma due on account of the simplicity of its composition. Consequently, due to this buffer's low complexity, optimizations to further complicate the buffer could be easily performed. Furthermore, MB-1 had a more similar background to the diluted human blood plasma than the other mimic buffer candidate (MB-2), and thus was more representative of the sample complexity. The higher background from MB-2 could be problematic because it can obscure small changes in protein concentration. Furthermore, since there is a maximum MFI signal that the flow cytometer used in these experiments can measure, an increase in the background signal can limit the fluorescent range.

In **Figure 4.13**, MB-1 and MB-2 standard curves for TNF-α are compared to the PBST control curve. In the MB-1 curve, there was greater variability of the high concentration points that can be attributed to experimental variability. One of the three replicates was inconsistent with the others, although such variation was indeed replicated when the standard curves were repeated in **Figure 4.16**. Furthermore, CLAMPs for TNF-α demonstrated a small dynamic range, suggesting that the antibodies used to generate the CLAMPs had poor affinity. Additionally, the antibodies for TNF-α could have conjugated poorly, resulting in their suboptimal performance. There was an increase in variability of the % recovery calculation generated from the 1:4 dilution of human blood plasma in **Figure 4.14B**. In the 1:4 human blood plasma dilution, there were large fluctuations in the data points for each of the three buffer conditions, most prominently shown by MB-1. An explanation for this variability could be that there was an error in the antigen spike-in dilutions that skewed the measured concentrations.

Due to the unacceptable variability in the % recovery calculations, the experiment was repeated and improved by implementing a lower fold dilution for the standard curves and varying initial concentrations of the two targets (TNF-α and IFN-γ) to maximize their respective quantitative

linear regions. The main purpose of these transformations was to optimize the four-parameter logistic regression curve fitting (4-PL). By distributing the majority of datapoints along the linear region of the curve, while maintaining some points on the extremes of the curve, the curve-fitting algorithm could better represent the curve. Although these considerations were taken for the two targets, IFN-γ did not completely saturate on the upper limit of its curve (**Fig. 4.16**). In contrast, TNF-α had a limited dynamic range, which made it difficult to detect small deviations in protein concentration as they only result in small changes in MFI readout. Thus, due to its small dynamic range, TNF-α may not have been an optimal target for the first round of spike-in and recovery experiments. However, average % recovery of 101% from the repeated experiment was very similar to the 91% average % recovery from IFN-γ, demonstrating that although the standard curve for TNF-α may not have been optimal due to its low dynamic range, its purpose for back-calculating the concentrations was acceptable.

6 | Conclusion

The goal of this project was to optimize the CLAMP platform to render it capable of measuring proteins in complex clinical samples such as human blood plasma. By minimizing nonspecific binding, optimizing assay parameters, and identifying a representative mimic buffer, accurate analysis of complex samples is now feasible. This platform can thus be used to measure protein levels in human blood plasma samples for key biomarkers for neuroinflammatory diseases and determine differences in protein levels between control and patient conditions. Furthermore, this platform has the capability to perform such analyses in multiplex, reducing the cost, time and sample volume associated with protein measurement.

Future work that would be useful for the CLAMP would be to implement amplification of the fluorescent signal so that protein binding events could be more easily recognized. Furthermore, mimic buffers for other complex matrices could be similarly optimized, making the platform more translational to many types of research where other samples may be used.

References

1. Aslam, B., Basit, M., Nisar, M.A., Khurshid, M. & Rasool, M.H. Proteomics: Technologies and Their Applications. *Journal of Chromatographic Science* **55**, 182-196 (2017).
2. Cohen, L. & Walt, D.R. Highly Sensitive and Multiplexed Protein Measurements. *Chemical reviews* **119**, 293-321 (2019).
3. Gam, L.-H. Breast cancer and protein biomarkers. *World J Exp Med* **2**, 86-91 (2012).
4. Seydel, C. (2019).
5. Robeson, R.H., Siegel, A.M. & Dunckley, T. Genomic and Proteomic Biomarker Discovery in Neurological Disease. *Biomark Insights* **3**, 73-86 (2008).
6. Olsson, B. et al. CSF and blood biomarkers for the diagnosis of Alzheimer's disease: a systematic review and meta-analysis. *The Lancet Neurology* **15**, 673-684 (2016).
7. National Academies of Sciences, E. & Medicine Biomarkers of Neuroinflammation: Proceedings of a Workshop. (The National Academies Press, Washington, DC; 2018).
8. Ross, C.A. & Poirier, M.A. Protein aggregation and neurodegenerative disease. *Nature Medicine* **10**, S10 (2004).
9. Verstegen, R.H.J. & Ito, S. The Future of Precision Medicine. *Clinical Pharmacology & Therapeutics* **106**, 903-906 (2019).
10. Serretti, A. The Present and Future of Precision Medicine in Psychiatry: Focus on Clinical Psychopharmacology of Antidepressants. *Clin Psychopharmacol Neurosci* **16**, 1-6 (2018).
11. Strafella, C. et al. Application of Precision Medicine in Neurodegenerative Diseases. *Frontiers in Neurology* **9** (2018).
12. Füzéry, A.K., Levin, J., Chan, M.M. & Chan, D.W. Translation of proteomic biomarkers into FDA approved cancer diagnostics: issues and challenges. *Clinical proteomics* **10**, 13-13 (2013).
13. Diamandis, E.P. The failure of protein cancer biomarkers to reach the clinic: why, and what can be done to address the problem? *BMC Med* **10**, 87-87 (2012).
14. Anderson, L., Razavi, M., Skates, S., Anderson, N.G. & Pearson, T.W. Squeezing more value from the analytes we have: personal baselines for multiple analytes in serial DBS. *Bioanalysis* **8**, 1539-1542 (2016).
15. Anderson, N.L., Ptolemy, A.S. & Rifai, N. The Riddle of Protein Diagnostics: Future Bleak or Bright? *Clinical chemistry* **59**, 194-197 (2013).
16. Graves, P.R. & Haystead, T.A.J. Molecular biologist's guide to proteomics. *Microbiology and molecular biology reviews : MMBR* **66**, 39-63 (2002).
17. Schmid, A., Kortmann, H., Dittrich, P.S. & Blank, L.M. Chemical and biological single cell analysis. *Current opinion in biotechnology* **21**, 12-20 (2010).
18. Aebersold, R. et al. How many human proteoforms are there? *Nat Chem Biol* **14**, 206-214 (2018).
19. Ponomarenko, E.A. et al. The Size of the Human Proteome: The Width and Depth. *International Journal of Analytical Chemistry* **2016**, 6 (2016).
20. Dagher, M. Scalable Affinity-Proteomics on Microparticles. *Department of Biomedical Engineering, McGill University* (2019).

21. Singh, S., Gupta, S.K. & Seth, P.K. Biomarkers for detection, prognosis and therapeutic assessment of neurological disorders. *Rev Neurosci* **29**, 771-789 (2018).
22. Singh, S., Gupta, S.K. & Seth, P.K. Biomarkers for detection, prognosis and therapeutic assessment of neurological disorders. *Reviews in the Neurosciences* **29**, 771-789 (2018).
23. Polivka, J., Polivka, J., Jr., Krakorova, K., Peterka, M. & Topolcan, O. Current status of biomarker research in neurology. *EPMA J* **7**, 14-14 (2016).
24. Qiu, C., Kivipelto, M. & von Strauss, E. Epidemiology of Alzheimer's disease: occurrence, determinants, and strategies toward intervention. *Dialogues in clinical neuroscience* **11**, 111 (2009).
25. Ritter, A. & Cummings, J. Fluid Biomarkers in Clinical Trials of Alzheimer's Disease Therapeutics. *Frontiers in neurology* **6**, 186-186 (2015).
26. Forester, B.P. & Oxman, T.E. Measures to Assess the Noncognitive Symptoms of Dementia in the Primary Care Setting. *Prim Care Companion J Clin Psychiatry* **5**, 158-163 (2003).
27. Masters, M.C., Morris, J.C. & Roe, C.M. "Noncognitive" symptoms of early Alzheimer disease: a longitudinal analysis. *Neurology* **84**, 617-622 (2015).
28. Burns, A. & Iliffe, S. Alzheimer's disease. *BMJ* **338**, b158 (2009).
29. Xia, R. & Mao, Z.-H. Progression of motor symptoms in Parkinson's disease. *Neuroscience Bulletin* **28**, 39-48 (2012).
30. Ferrer, I. et al. Neurochemistry and the non-motor aspects of PD. *Neurobiology of disease* **46**, 508-526 (2012).
31. Blennow, K. A Review of Fluid Biomarkers for Alzheimer's Disease: Moving from CSF to Blood. *Neurology and therapy* **6**, 15-24 (2017).
32. Blennow, K. & Zetterberg, H. The past and the future of Alzheimer's disease CSF biomarkers—a journey toward validated biochemical tests covering the whole spectrum of molecular events. *Frontiers in neuroscience* **9**, 345 (2015).
33. Blennow, K., Hampel, H., Weiner, M. & Zetterberg, H. Cerebrospinal fluid and plasma biomarkers in Alzheimer disease. *Nature Reviews Neurology* **6**, 131 (2010).
34. Zetterberg, H. & Burnham, S.C. Blood-based molecular biomarkers for Alzheimer's disease. *Mol Brain* **12**, 26-26 (2019).
35. Schapira, A.H. Recent developments in biomarkers in Parkinson disease. *Curr Opin Neurol* **26**, 395-400 (2013).
36. Emamzadeh, F.N. Alpha-synuclein structure, functions, and interactions. *J Res Med Sci* **21**, 29 (2016).
37. Fronczek, R. et al. Hypocretin (orexin) loss in Parkinson's disease. *Brain* **130**, 1577-1585 (2007).
38. Bentea, E., Verbruggen, L. & Massie, A. The Proteasome Inhibition Model of Parkinson's Disease. *J Parkinsons Dis* **7**, 31-63 (2017).
39. Arndt, C., Koristka, S., Bartsch, H. & Bachmann, M. in Protein Electrophoresis: Methods and Protocols. (eds. B.T. Kurien & R.H. Scofield) 49-53 (Humana Press, Totowa, NJ; 2012).
40. Büyükköroğlu, G., Dora, D.D., Özdemir, F. & Hızel, C. in Omics Technologies and Bio-Engineering. (eds. D. Barh & V. Azevedo) 317-351 (Academic Press, 2018).
41. Magdeldin, S. et al. Basics and recent advances of two dimensional- polyacrylamide gel electrophoresis. *Clinical proteomics* **11**, 16-16 (2014).

42. Rabilloud, T. & Lelong, C. Two-dimensional gel electrophoresis in proteomics: A tutorial. *Journal of Proteomics* **74**, 1829-1841 (2011).
43. Mahmood, T. & Yang, P.-C. Western blot: technique, theory, and trouble shooting. *N Am J Med Sci* **4**, 429-434 (2012).
44. Bass, J.J. et al. An overview of technical considerations for Western blotting applications to physiological research. *Scand J Med Sci Sports* **27**, 4-25 (2017).
45. Ghosh, R., Gilda, J.E. & Gomes, A.V. The necessity of and strategies for improving confidence in the accuracy of western blots. *Expert Rev Proteomics* **11**, 549-560 (2014).
46. Glish, G.L. & Vachet, R.W. The basics of mass spectrometry in the twenty-first century. *Nature Reviews Drug Discovery* **2**, 140-150 (2003).
47. Wysocki, V.H., Resing, K.A., Zhang, Q. & Cheng, G. Mass spectrometry of peptides and proteins. *Methods (San Diego, Calif.)* **35**, 211-222 (2005).
48. Zhang, Y., Fonslow, B.R., Shan, B., Baek, M.-C. & Yates, J.R., 3rd Protein analysis by shotgun/bottom-up proteomics. *Chemical reviews* **113**, 2343-2394 (2013).
49. Singhal, N., Kumar, M., Kanaujia, P.K. & Virdi, J.S. MALDI-TOF mass spectrometry: an emerging technology for microbial identification and diagnosis. *Front Microbiol* **6**, 791-791 (2015).
50. Ho, C.S. et al. Electrospray ionisation mass spectrometry: principles and clinical applications. *The Clinical biochemist. Reviews* **24**, 3-12 (2003).
51. Aebersold, R. & Mann, M. Mass-spectrometric exploration of proteome structure and function. *Nature* **537**, 347 (2016).
52. Mardamshina, M. & Geiger, T. Next-Generation Proteomics and Its Application to Clinical Breast Cancer Research. *Am J Pathol* **187**, 2175-2184 (2017).
53. Keshishian, H. et al. Quantitative, multiplexed workflow for deep analysis of human blood plasma and biomarker discovery by mass spectrometry. *Nature protocols* **12**, 1683-1701 (2017).
54. Karpievitch, Y.V., Polpitiya, A.D., Anderson, G.A., Smith, R.D. & Dabney, A.R. Liquid Chromatography Mass Spectrometry-Based Proteomics: Biological and Technological Aspects. *Ann Appl Stat* **4**, 1797-1823 (2010).
55. Byström, S. (KTH Royal Institute of Technology, 2017).
56. Aydin, S. A short history, principles, and types of ELISA, and our laboratory experience with peptide/protein analyses using ELISA. *Peptides* **72**, 4-15 (2015).
57. Juncker, D., Bergeron, S., Laforte, V. & Li, H. Cross-reactivity in antibody microarrays and multiplexed sandwich assays: shedding light on the dark side of multiplexing. *Current opinion in chemical biology* **18**, 29-37 (2014).
58. Laforte, V., Lo, P.-S., Li, H. & Juncker, D. in Serum/Plasma Proteomics: Methods and Protocols. (eds. D.W. Greening & R.J. Simpson) 239-261 (Springer New York, New York, NY; 2017).
59. Wu, A.H.B. A selected history and future of immunoassay development and applications in clinical chemistry. *Clinica Chimica Acta* **369**, 119-124 (2006).
60. Hosseini, S., Vázquez-Villegas, P., Rito-Palomares, M. & Martinez-Chapa, S.O. in Enzyme-linked Immunosorbent Assay (ELISA): From A to Z 1-18 (Springer Singapore, Singapore; 2018).
61. Romanov, V. et al. A critical comparison of protein microarray fabrication technologies. *Analyst* **139**, 1303-1326 (2014).

62. Sutandy, F.X.R., Qian, J., Chen, C.-S. & Zhu, H. Overview of protein microarrays. *Current protocols in protein science* **Chapter 27**, Unit-27.21 (2013).
63. Hall, D.A., Ptacek, J. & Snyder, M. Protein microarray technology. *Mech Ageing Dev* **128**, 161-167 (2007).
64. Poetz, O. et al. Protein microarrays: catching the proteome. *Mech Ageing Dev* **126**, 161-170 (2005).
65. Boellner, S. & Becker, K.-F. Reverse Phase Protein Arrays-Quantitative Assessment of Multiple Biomarkers in Biopsies for Clinical Use. *Microarrays (Basel)* **4**, 98-114 (2015).
66. Davies, C. in The Immunoassay Handbook (Fourth Edition). (ed. D. Wild) 11-26 (Elsevier, Oxford; 2013).
67. Sheehan, C., He, J. & Smith, M. in The Immunoassay Handbook (Fourth Edition). (ed. D. Wild) 395-402 (Elsevier, Oxford; 2013).
68. Armbruster, D.A. & Pry, T. Limit of blank, limit of detection and limit of quantitation. *The Clinical biochemist. Reviews* **29 Suppl 1**, S49-S52 (2008).
69. Vashist, S.K. & Luong, J.H.T. in Handbook of Immunoassay Technologies. (eds. S.K. Vashist & J.H.T. Luong) 81-95 (Academic Press, 2018).
70. Kristjansdottir, K., Takahashi, S., Volchenboum, S. & Kron, S. (2012).
71. Pla-Roca, M. et al. Antibody colocalization microarray: a scalable technology for multiplex protein analysis in complex samples. *Molecular & cellular proteomics : MCP* **11**, M111.011460 (2012).
72. Andreasson, U. et al. A Practical Guide to Immunoassay Method Validation. *Frontiers in Neurology* **6** (2015).
73. Cox KL, D.V., Kriauciunas A, et al. Assay Guidance Manual: Immunoassay Methods. *Eli Lilly & Company and the National Center for Advancing Translational Sciences* (2012).
74. Labib, M. & Kelley, S.O. Single-cell analysis targeting the proteome. *Nature Reviews Chemistry* **4**, 143-158 (2020).
75. Klepárník, K. & Foret, F. Recent advances in the development of single cell analysis—A review. *Analytica Chimica Acta* **800**, 12-21 (2013).
76. Chang, L., Li, J. & Wang, L. Immuno-PCR: An ultrasensitive immunoassay for biomolecular detection. *Anal Chim Acta* **910**, 12-24 (2016).
77. Gofflot, S. et al. Immunoquantitative PCR for Prion Protein Detection in Sporadic Creutzfeldt–Jakob Disease. *Clinical chemistry* **51**, 1605 (2005).
78. Guglielmo-Viret, V. & Thullier, P. Comparison of an electrochemiluminescence assay in plate format over a colorimetric ELISA, for the detection of ricin B chain (RCA-B). *Journal of Immunological Methods* **328**, 70-78 (2007).
79. Chowdhury, F., Williams, A. & Johnson, P. Validation and comparison of two multiplex technologies, Luminex® and Mesoscale Discovery, for human cytokine profiling. *Journal of Immunological Methods* **340**, 55-64 (2009).
80. Geiss, G.K. et al. Direct multiplexed measurement of gene expression with color-coded probe pairs. *Nat Biotechnol* **26**, 317-325 (2008).
81. Warren, S. in Gene Expression Analysis: Methods and Protocols. (eds. N. Raghavachari & N. Garcia-Reyero) 105-120 (Springer New York, New York, NY; 2018).
82. Rissin, D.M. et al. Single-molecule enzyme-linked immunosorbent assay detects serum proteins at subfemtomolar concentrations. *Nat Biotechnol* **28**, 595-599 (2010).

83. Cohen, L. & Walt, D.R. Single-Molecule Arrays for Protein and Nucleic Acid Analysis. *Annual Review of Analytical Chemistry* **10**, 345-363 (2017).
84. Rivnak, A.J. et al. A fully-automated, six-plex single molecule immunoassay for measuring cytokines in blood. *Journal of Immunological Methods* **424**, 20-27 (2015).
85. Assarsson, E. et al. Homogenous 96-plex PEA immunoassay exhibiting high sensitivity, specificity, and excellent scalability. *PLoS One* **9**, e95192 (2014).
86. Gold, L. et al. Aptamer-Based Multiplexed Proteomic Technology for Biomarker Discovery. *PLOS ONE* **5**, e15004 (2010).
87. Famulok, M., Hartig, J.S. & Mayer, G. Functional aptamers and aptazymes in biotechnology, diagnostics, and therapy. *Chemical reviews* **107**, 3715-3743 (2007).
88. Tuerk, C. & Gold, L. Systematic evolution of ligands by exponential enrichment: RNA ligands to bacteriophage T4 DNA polymerase. *Science* **249**, 505-510 (1990).
89. Tighe, P., Negm, O., Todd, I. & Fairclough, L. Utility, reliability and reproducibility of immunoassay multiplex kits. *Methods (San Diego, Calif.)* **61**, 23-29 (2013).
90. Khalifian, S., Raimondi, G. & Brandacher, G. The use of luminex assays to measure cytokines. *The Journal of investigative dermatology* **135**, 1-5 (2015).
91. Biggar, K.K. & Storey, K.B. New Approaches to Comparative and Animal Stress Biology Research in the Post-genomic Era: A Contextual Overview. *Comput Struct Biotechnol J* **11**, 138-146 (2014).
92. Au - Li, H., Au - Bergeron, S., Au - Larkin, H. & Au - Juncker, D. Snap Chip for Cross-reactivity-free and Spotter-free Multiplexed Sandwich Immunoassays. *JoVE*, e56230 (2017).
93. Gullberg, M. et al. Cytokine detection by antibody-based proximity ligation. *Proceedings of the National Academy of Sciences of the United States of America* **101**, 8420-8424 (2004).
94. Greenwood, C. et al. Proximity assays for sensitive quantification of proteins. *Biomol Detect Quantif* **4**, 10-16 (2015).
95. Fredriksson, S. et al. Multiplexed protein detection by proximity ligation for cancer biomarker validation. *Nature methods* **4**, 327-329 (2007).
96. Schneider, C.A., Rasband, W.S. & Eliceiri, K.W. NIH Image to ImageJ: 25 years of image analysis. *Nature methods* **9**, 671-675 (2012).
97. Schindelin, J. et al. Fiji: an open-source platform for biological-image analysis. *Nature methods* **9**, 676-682 (2012).
98. Dagher, M., Kleinman, M., Ng, A. & Juncker, D. Ensemble multicolour FRET model enables barcoding at extreme FRET levels. *Nature Nanotechnology* (2018).